Solar-Terrestrial Centre of Excellence

Annual Report 2016

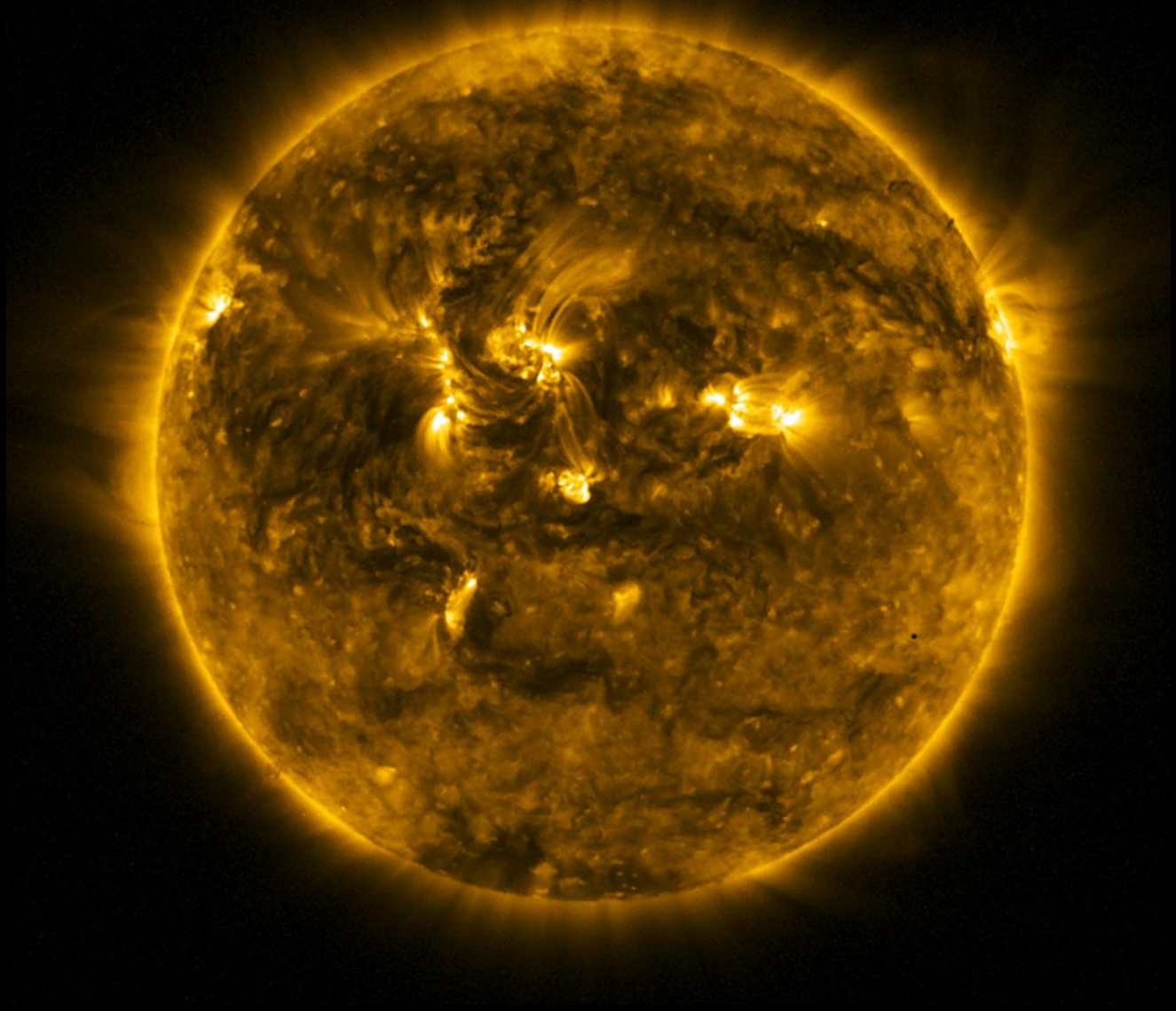

Belgian Science Policy Office belspo

Royal Observatory of Belgium

RMI

BIRA·IASB

.be

STCE

Solar-**T**errestrial **C**entre of **E**xcellence

http://stce.be/

Ringlaan 3

B-1180 Brussels

Tel.: +32 2 373 0211

Fax: + 32 2 374 9822

Front-page: *The Sun seen in extreme ultraviolet by the PROBA2/SWAP instrument on 9 May 2016. The tiny black dot near the Sun's southwest limb (lower right) is the planet Mercury.*

Table of Contents

A word from the STCE coordinator: the STCE's 10th anniversary!

On 22 March 2006, the Minister of Science Policy announced in a press release the creation of the Solar-Terrestrial Centre of Excellence. Its purpose would be twofold. First, the STCE would lift the Sun-Space-Earth research to a higher level by uniting experts working in different scientific institutes. Second, the STCE had to become an effective service centre for the government, citizens, and industries vulnerable to the impact of the physical processes triggered by solar activity. At that time, most people were not even aware of the Sun's variability, which changes on timescales from minutes and hours to several years. The short-term changes are the topic of study in the so-called "space weather" domain, while the long-term changes relate more to the "space climate" near and on Earth. Ten years later, the STCE has indeed a leading role in this very specific knowledge-based economy, in space technology, and in all related services.

Probably the biggest realization of the STCE is that it allowed maintaining healthy research groups and stabilizing people and expertise in between short-term external contracts that come and go in unpredictable ways. Hence, this plurennial funding view allowed e.g. the sustainability of permanent services such as the space weather forecast center (Regional Warning Center) and the SILSO World Data Center, as well as the creation of the STCL laboratories, and the revival of the Humain radio astronomy site. It also assured the survival of the ionosphere/cosmic radiation team in Dourbes, and of the Total Solar Irradiance space radiometer group. The STCE played an important role in the creation of the BRAMS network (radio meteors), the development of the Simba CubeSat project, as well as in the development and building of the SLP Langmuir probes for the PICASSO CubeSat. STCE also initiated a close collaboration between RMI and ROB on the exploitation of GNSS water vapour observations and its comparison with other measurement techniques. Another major realization was the continued support to the RMI's time series of ozone profile measurements with the balloon sounding, and the development of a LIDAR network. There was also the network implementation of 4 ceilometers to measure the cloud base height and aerosol backscatter profiles on a continuous basis. The instruments help to monitor/detect layers with high aerosol (and volcanic ash) concentrations over the Belgian territory.

A huge birthday cake to celebrate the STCE's 10th anniversary!

A big milestone was the November 2, 2009 launch of the PROBA2 satellite and the creation of the PROBA2 Science Center (P2SC). The latter was set up with PRODEX funding and operated with ESA funding, but all of this would have been insufficient if there wasn't an STCE stem on which to grow new branches. The STCE also provided the background to participate in ESA's Space Situational Awareness (SSA) programme by having two (of only five) Expert Service Centres (ESC) at the Space Pole: The Solar Weather ESC led by ROB, and the Space Radiation ESC led by BISA. Under the driving force of the STCE, the European Space Weather Week (ESWW) has become one of the main international space weather conferences of the year.

From the highlights above, it is clear that the STCE has more than attained the objectives put forward 10 years ago. At the same time, these examples show that the STCE cannot lower its guard and must stay vigilant. Indeed, in these times of endless budgetary restraints, the continuous pursuit of excellence and the emphasis on national and international collaboration remain the key factors to the STCE's success story. Fortunately, the aforementioned results clearly indicate that the STCE is up to the task!

*The Geophysical Center at Dourbes was the scenery for the workshop **Cosmic Rays and Space Weather** on May 17, 2016. An international gathering of scientists and institutes discussing and collaborating on not so easy scientific topics (cosmic rays, high-energy particles, and their SWx impacts) and instruments (neutron monitors), it reflected the true spirit of the STCE.*

I invite you to read about some of this year's achievements of the STCE in the following pages. Happy reading!

Ronald Van der Linden
General Coordinator of the Solar-Terrestrial Centre of Excellence
Director General of the Royal Observatory of Belgium

Structure of the STCE

The Solar-Terrestrial Centre of Excellence is a project of scientific collaboration that focuses on the Sun, through interplanetary space, up to the Earth and its atmosphere.

The solid base of the STCE is the expertise that exists in the 3 Federal Scientific Institutes of the Brussels Space Pole: the Royal Observatory of Belgium, the Royal Meteorological Institute and the Belgian Institute for Space Aeronomy. The STCE supports fundamental solar, terrestrial and atmospheric physics research, is involved in earth-based observations and space missions, offers a broad variety of services (mainly linked to space weather and space climate) and operates a fully established space weather application centre. The scientists act at different levels within the frame of local, national and international collaborations of scientific and industrial partners.

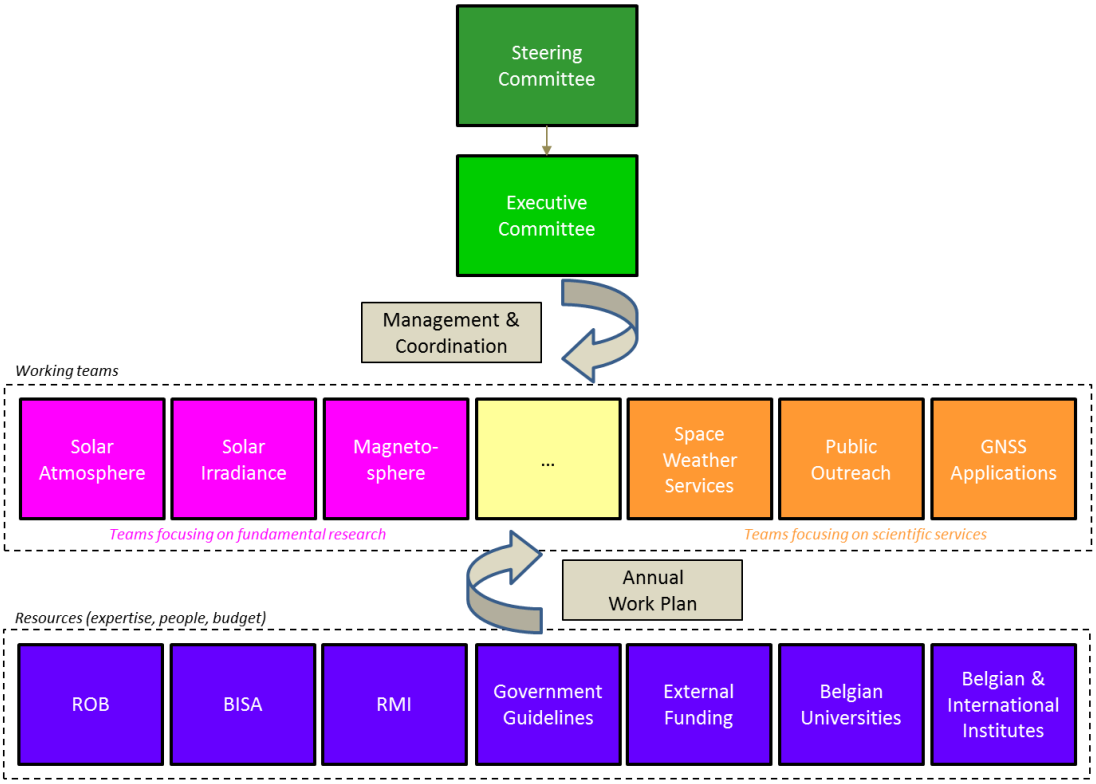

Figure 1: The STCE management structure

The STCE's strengths are based on sharing know-how, manpower, and infrastructure.

In order to optimize the coordination between the various working groups and institutions, as well as the available resources such as ICT, personnel and budget, a management structure for the STCE was put into place, consisting of a steering committee and an executive committee.

The ***steering committee*** takes all the final decisions on critical matters with regard to the STCE. It assures the integration of the STCE into the 3 institutions and the execution of the strategic plans. It is composed of:

- BELSPO Director General "Research Programmes and Applications"

  Dr. Frank Monteny (BELSPO)

- Director General of each of the 3 institutions at the Space Pole

  Dr. Ronald Van der Linden (ROB)
  Dr. Daniel Gellens (RMI)
  Dr. Martine De Mazière (BISA)

The ***executive committee*** assures the global coordination between the working groups and the correct use of the budgetary means for the various projects. It also identifies new opportunities and is the advisory body to the Steering Committee. It is composed of:

- STCE Coordinator

  Dr. Ronald Van der Linden

- Representatives of the research teams in the 3 institutes

  Dr. David Berghmans (ROB)
  Dr. Carine Bruyninx (ROB)
  Dr. Johan De Keyser (BISA)
  Dr. Norma Crosby (BISA)
  Dr. Stanimir Stankov (RMI)
  Dr. Steven Dewitte (RMI)
  Dr. Hugo De Backer (RMI)

A promotional movie giving a flavor of the STCE's tasks, interactions and various research programmes can be found via the STCE website (in English, and subtitled in French and Dutch).

Figure 2: The pleasures of working at the Space Pole: Enjoying your lunch on the freshly mowed lawn near the ROB Director's building in the shadow of a leafy tree on a warm summer day.

Monitoring Space Weather: Solar-Terrestrial Highlights in 2016

The official annual sunspot number (SN) for 2016, as determined by the WDC-SILSO (World Data Center - Sunspot Index and Long-term Solar Observations), was 39.8. This is a 43% decrease compared to 2015, when it was 69.8.

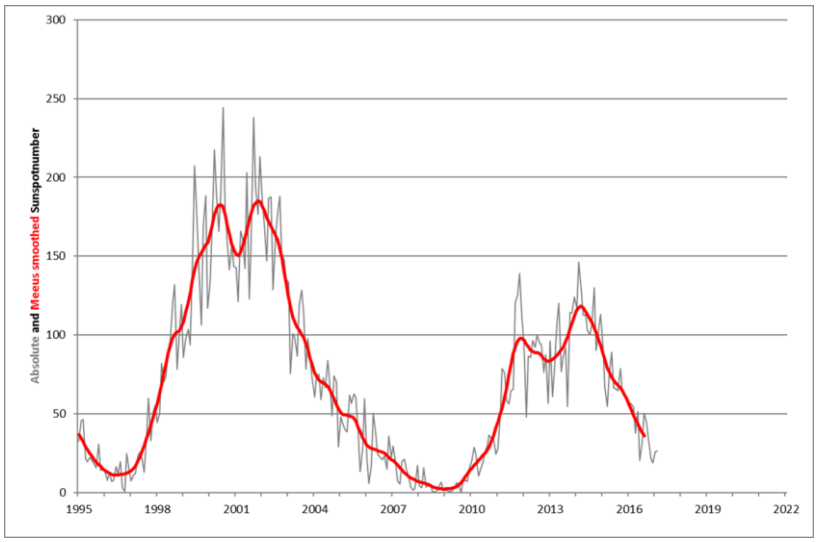

Figure 3: The evolution of the monthly and monthly smoothed SN (1995-2016). Pending the smoothing formula used, SC24 reached its maximum of 116.4 in April 2014 (SILSO formula), or 118.2 in March 2014 (Meeus formula).

In 2016, the highest daily sunspot number (111) was recorded on 4 March. There were 27 spotless days (see SILSO's Spotless Days page), with the week from 25 June till 1 July as the longest stretch with a blanc Sun. Throughout the year, sunspot activity was driven by the northern solar hemisphere. By far the largest sunspot group was NOAA 2529, which had a distinct heart shape and reached about 5 times the total surface area of the Earth. Several solar observers, using protective eclipse glasses, reported the sunspot group visible to the naked eye from 9 till 17 April. The region produced an M6 flare on 18 April and remained active well after it had started its farside transit.

The most flare-active region in 2016 was NOAA 2567, producing the highest number of M-class flares (7) as well as the strongest flare: an M7.6 event almost immediately followed by a spectacular M5.5 flare on 23 July. NOAA 2497 and NOAA 2615 were the only other sunspot regions that managed to produce more than one medium flare in 2016 (resp. 3 and 2). During the year, a total of (only) 16 M-class flares and no X-class flare were recorded. Only one (1) proton event was observed in 2016, a minor event on 2 January produced by NOAA 2473.

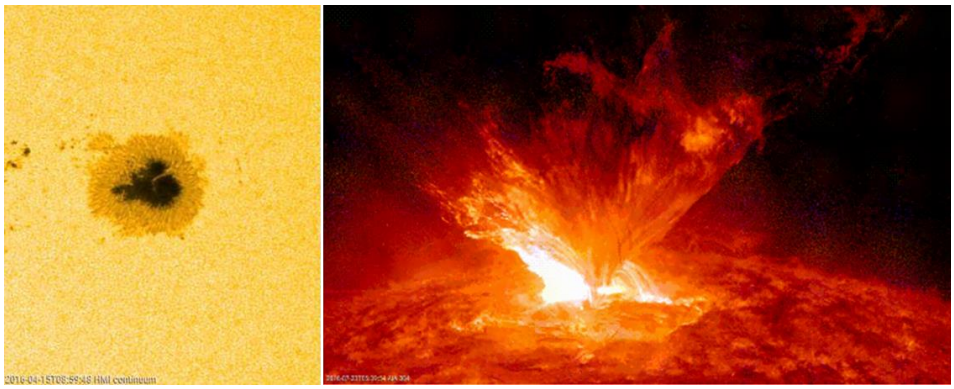

Figure 4: Left: NOAA 2529 was the largest sunspot region in 2016, displaying a distinct heart shape. Right: NOAA 2567 produced a strong and spectacular M5.5 flare on 23 July.

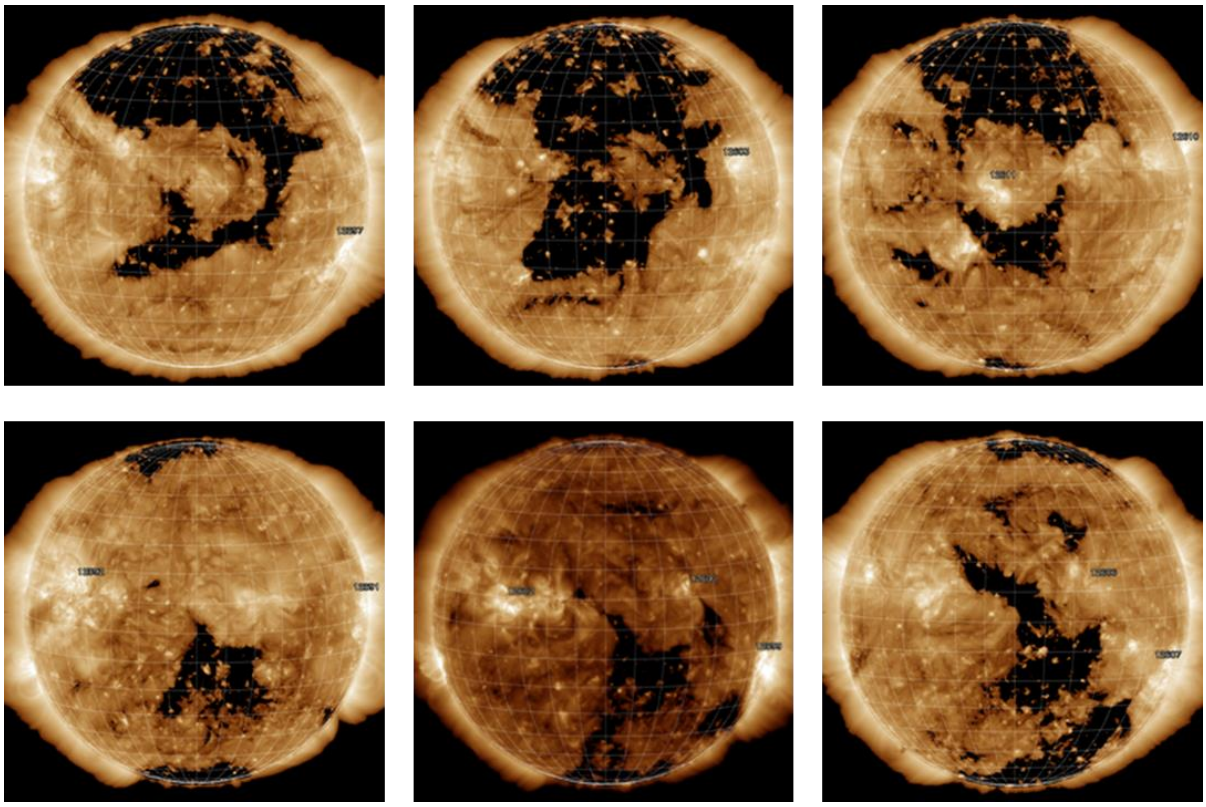

Figure 5: Particle streams from large coronal holes determined the earth environment in 2016. The top row displays extreme ultraviolet (EUV) images (SDO/AIA 193) of a coronal hole during its transit on 28 September, 25 October and 21 November. The bottom row shows another coronal on resp. 17 September, 14 October and 10 November. The associated particle streams drove an increase in energetic electron fluxes (energies ≥ 2 MeV) about every two weeks.

No severe geomagnetic storms were observed in 2016. In fact, the preliminary K_p index reached major storming levels (K_p = 7) on only 3 occasions: 6 March, 8-9 May, and 25-26 October. In all cases, the source of the disturbance was a high-speed stream (HSS) from a coronal hole (CH). Recurrent coronal holes determined the space weather throughout the year, which is typical at this stage of the solar cycle. The largest CH reached an area of 880 times that of the surface area of the Earth on 30 September. It had associated wind speeds near 800 km/s. Geostationary satellites recorded very high fluxes of energetic electrons (energies ≥ 2 MeV), which are an important source of electrostatic charging effects inside satellites.

The geomagnetic field was not very often disturbed by Coronal mass Ejections (CMEs). The most intense storms occurred on 1 January and 13-14 October, when the Dst index reached resp. -110 nT and -104 nT. These were the only two occasions that Dst dove beneath the -100 nT level in 2016. It forms a big contrast with 2015 when the largest geomagnetic storms of SC24 took place and Dst values below -200 nT were recorded. So far this solar cycle, no extremely severe geomagnetic storm has been observed (K_p = 9). There were also no important Forbush decreases, i.e. a > 3% decrease in the neutron flux, observed by neutron monitors (NM) on Earth (Oulu NM).

On 27 July, NOAA's Deep Space Climate Observatory (DSCOVR) became the prime operational real-time solar wind spacecraft. It replaced NASA's Advanced Composition Explorer (ACE) spacecraft, which has been in use since 1998 and serves now as a back-up. Figure 6 provides an example of the typical

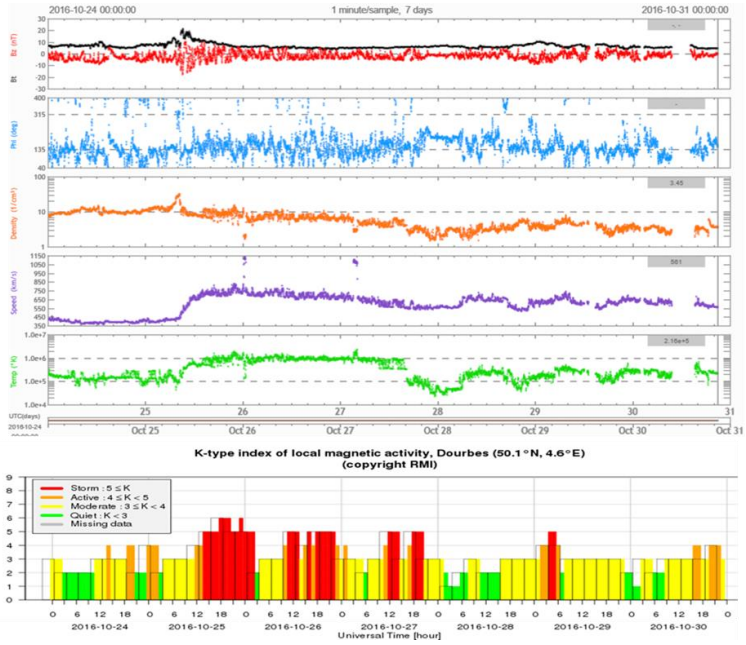

*Figure 6: The top graphs show DSCOVR solar wind data for the week from 24 till 30 October. See text for further explanations. The bar diagram at the bottom shows the resulting geomagnetic disturbance as recorded by magnetometers in **Dourbes**, Belgium. The K index regularly reached storming levels (K ≥ 5) for several days.*

DSCOVR graphs. It shows the strength (black and red) and orientation (blue) of the interplanetary magnetic field, as well as the density (orange), speed (purple) and temperature (green) of the solar wind. It covers the week from 24 till 30 October and shows the arrival of the high speed stream on 25 October from the aforementioned huge coronal hole.

The year 2016 can certainly be considered as a transition year towards the next solar cycle minimum. Decreasing sunspot numbers and flaring activity, continued influence of (trans-equatorial) coronal holes, polar faculae activity (in particular near the southern solar pole), gradually increasing numbers of spotless days,… : These are just a few of the signs that we are entering a period of reduced solar activity before starting a new solar cycle.

Another sign occurred on 20 December when what seems to be the first sunspot group of the new solar cycle (SC25) was observed at a latitude of -23°. This does not mean that the current SC24 has ended. Indeed, sunspot cycles usually overlap each other, occasionally up to 4 years. That's what's happening right now: Cycle 24 is heading down and simultaneously, cycle 25 gradually gains strength until it produces enough sunspots to take over from "old" cycle 24 and start a new solar cycle, expected around 2019.

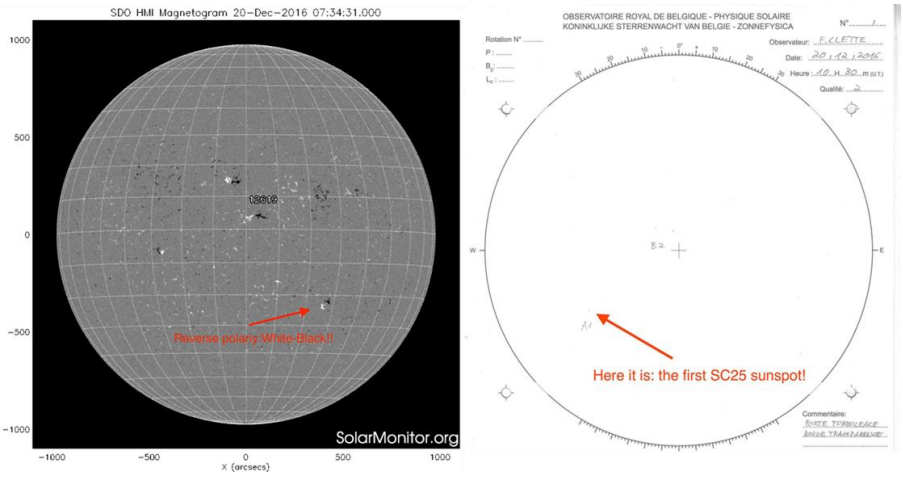

*Figure 7: On the left a magnetogram by SDO showing the new cycle region NOAA 2620. Note it has the same magnetic configuration as sunspot groups on the northern hemisphere (black first, then white), in contrast to regions on the southern hemisphere (white first, then black). The group was also recorded by observers using the **USET** solar telescopes (Uccle Solar Equatorial Table), as can be seen on the (mirror-reversed) drawing on the right.*

Public Outreach meets Science

The ESWW back in Oostende!

The 13th European Space Weather Week (ESWW13) took place in the Casino Kursaal of Oostende from 14 till 18 November. This international space weather conference was organised already for the 11th time by the Solar-Terrestrial Centre of Excellence (STCE). Participants were not confined to Europe, but really came from all sides of the world, representing countries such as Australia, New Zealand, South-Africa, Brazil, Japan, China and South-Korea. The nearly 400 scientists, engineers, satellite operators, power grid technicians, communication specialists,… gathered to discuss the latest on solar activity and how it influences the earth environment and our technologies.

Figure 8: The Tutorial's "sofa session" on 10 years STEREO was hosted by Andrei Zhukov and had Pierre Rochus (CSL) and Barbara Thompson (NASA/GSFC).

No less than 15 topics were programmed in daily series of 3 parallel sessions. They covered a wide variety of space weather aspects, such as solar energetic particle events, space climate, space weather tools and modelling. Daily keynote lectures introduced the attendees to each series of sessions. Quite some participants had to make tough choices which sessions and presentations they wanted to attend! The related poster sessions included also electronic posters ("e-posters"). The afternoon was reserved for the working meetings (20!), providing the participants the opportunity to discuss in-depth key issues in an interactive style, thus complementing the sessions.

There were also more relaxing activities such as the Tutorial on Monday, which focused, not surprisingly, on space weather forecasting. It started with a sofa session on 10 years STEREO. It was followed by 4 hands-on activities, where you could draw sunspots, build/recognize spacecraft, make your own space weather predictions, or visit the B.USOC. A panel discussion on the socio-economic impacts of space weather concluded

Figure 9: Drawing sunspots was one of the Tutorial's activities.

this fun activity. The dedicated space weather Fair on Wednesday afternoon had 21 stand holders! In the spacious "Hall of Honour", visitors could walk from stands on ESA Expert Service Centres, flare forecasting, or radiation doses, to more interactive stands where you could ring the sunspots, make your own CME, or create a solar movie with JHelioviewer.

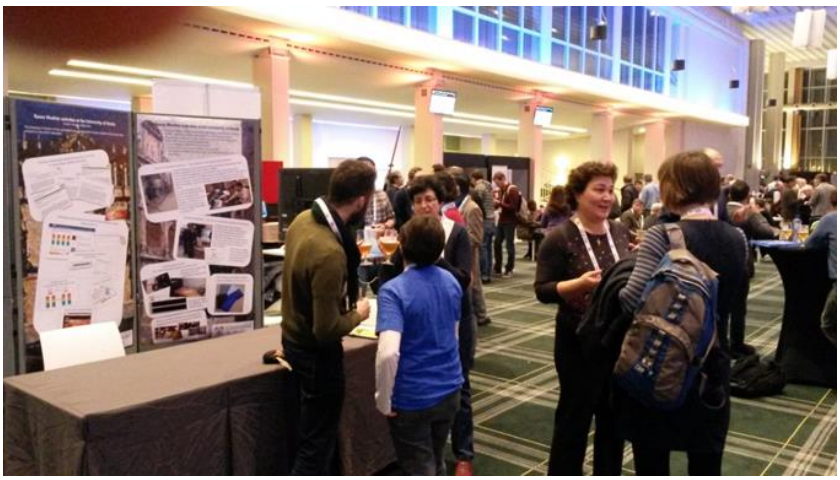

Figure 10: The ESWW's Fair in full swing!

Throughout the week, ESWW participants could also play the online space weather quiz (with certificates for outstanding performances!), and daily space weather forecasts were presented by 5 forecast centres (Spain, USA, UK (2) and Belgium).

Finally, the attendees could really socialize during the after-hours activities. On Monday, the welcome reception was preceded by an impressive medal award ceremony. On Tuesday, there was a wonderful music evening in the Casino Lounge, where some participants surprised the audience with their remarkable musical and vocal skills. On Wednesday, the Fair was followed by the traditional beer-tasting, where most participants tasted more beers than there were sunspot groups present on the solar disk. That was not so difficult, with a nearly spotless Sun! On Thursday, the conference dinner took place in the Hippodrome (buildings of the Wellington Racetrack). Most guests arrived with soaking wet clothes (courtesy of a good Belgian shower), but were able to warm themselves with good food and drawing some nice cartoons. Also, the 6 winners of last year's bet on the number of X-class flares got a sweet award.

Once again, the enthusiasm and drive of the participants and organisers assured another successful edition of the ESWW. Thank you all, and see you next year!

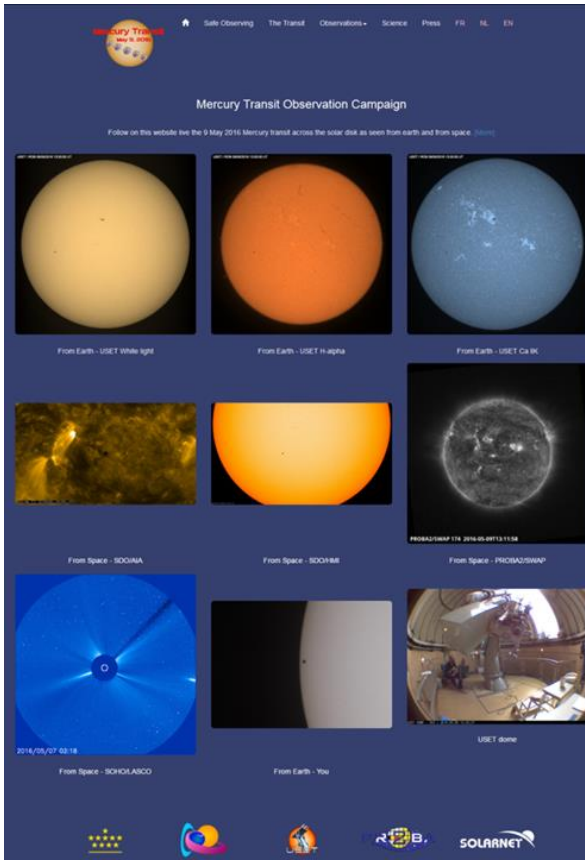

Figure 11: A view on the STCE webpage specifically created for the Mercury transit.

Mercury transits the Sun

The Mercury transit of 9 May generated quite some interest from the media and the general public. The STCE created a website with imagery from the USET solar telescopes and the satellites PROBA2 and SDO.

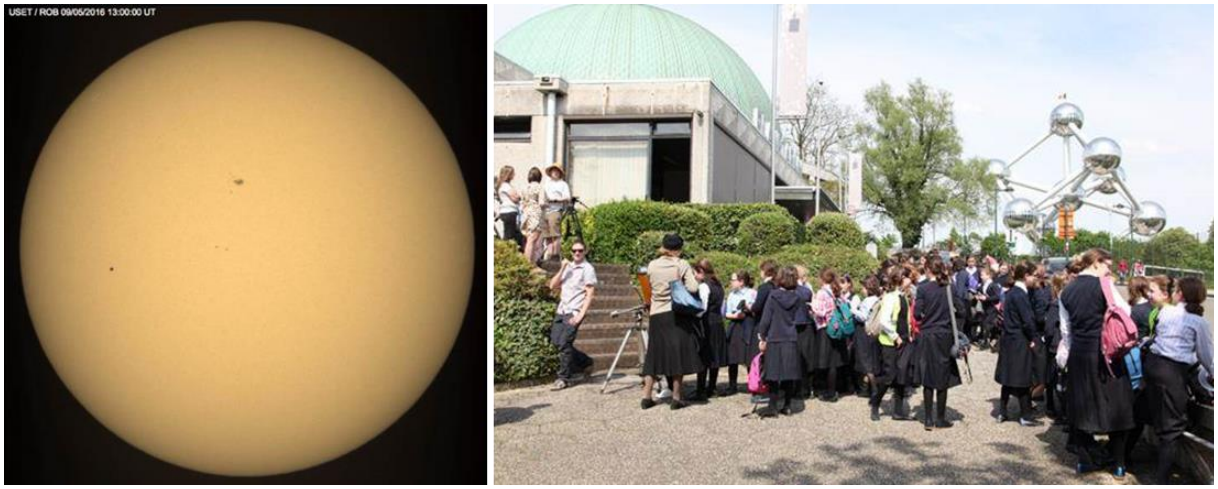

Figure 12: (left) A picture of the Mercury transit taken by the USET white light solar telescope. The planet's tiny silhouette can be seen as a tiny black dot on the left on the solar disk. The other "blemishes" near the disk's centre are genuine sunspots. (right) This picture by Anne-Lize Kochuyt shows a large group of children interested in watching the Mercury transit through one of the Planetarium's solar telescopes. It got also visits from several radio- and TV-stations, such as BRUZZ.

There was also a page with coronagraphic imagery from SOHO/LASCO (before/after transit day), as well as a page where solar observers could upload their own pictures of the event.

The solar telescopes in Uccle observed the Sun in white light, H-alpha (red part of the spectrum) and Calcium IIK (violet part of the spectrum). The images got a dedicated colour to distinguish one wavelength from the other. Clouds interfered regularly with the observations, but the first half of the transit was well covered. Far above the clouds, solar satellites were able to observe the entire event. Even the PROBA2/SWAP telescope, observing the Sun in extreme ultraviolet at a modest resolution, was able to image relatively well Mercury's puny silhouette. Plenty of clips and images can be found at PROBA2's special webpage for this phenomenon.

The Planetarium at the Heysel was open to the general public. A few hundred of interested visitors and school children took a look through the solar telescopes, and got plenty of explanations from the guides. Also the media were present and reported extensively in the news and on their webpages. The next Mercury transit will take place on 11 November 2019 (NASA/GSFC page), but will only be partially visible from Belgium.

A book for the large audience about space weather

A book concerning the effects of space weather has been published for the large public in 2016 by the Académie en Poche Editions. It is entitled

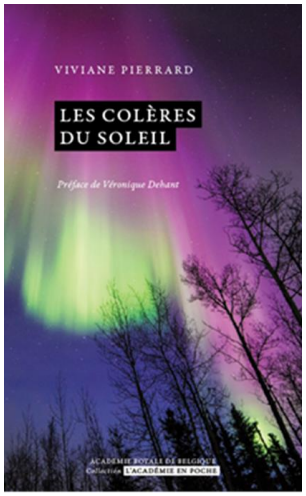

Figure 13: Cover of the book published by Academy Editions illustrating an aurora (©Pierrard, 2016).

« Les colères du Soleil » and was written by Viviane Pierrard. It shows the Belgian expertise in this scientific field in the framework of the Solar-Terrestrial Centre of Excellence created in 2006. This book follows a course for the large public that was presented at College Belgium. It is illustrated with nice, coloured figures from NASA and ESA.

The book presents the Sun, our star that provides light and heat necessary for life here on Earth. The Sun emits also a continuous flux of particles that fills the interplanetary space: the solar wind. Sometimes, sudden eruptions appear at the surface of the Sun. Such eruptions can generate nice auroras but they also modify the characteristics of the space environment of the Earth where artificial satellites circulate, causing disturbances for the communications or GPS positioning, for instance. The book describes the effects of the solar wind on the space environment of the Earth. Our planet is protected by its magnetic field so that most of the particles are deviated. But they generate perturbations, like geomagnetic storms, which are the focus of space weather research.

Figure 14: The "ringing sunspots" posed a formidable and noisy challenge to the brave participants at the ESWW!

Fundamental Research

Topical issue of Solar Physics "Sunspot Number Recalibration"

2016 was marked by a new milestone in the ongoing recalibration and redefinition of the International Sunspot Number series initiated in 2015 by the World Data Center (WDC) SILSO run by the OD Solar Physics at the ROB. In just a few months, the 2015 release of the first revised version of the reference sunspot number series triggered a revival of international research in the field of the long-term solar activity studies.

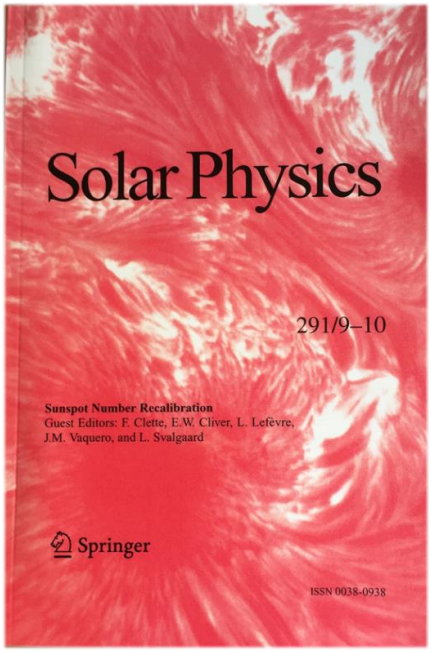

Figure 15: Front page of the Solar Physics Topical Issue on "Sunspot Number Recalibration".

In response to this global interest, two researchers from the ROB (Frédéric Clette, Laure Lefèvre) together with colleagues from the National Solar Observatory (USA), Stanford University (USA) and the University of Extremadura (Spain) proposed a special topical issue dedicated to the revised sunspot number to the editors of Solar Physics (Springer), the main journal on solar research. The proposed topic was approved and the proposers acted as guest editors for this special volume, which proved to be highly successful. Indeed, the final printed volume gathered 34 articles, to which a few more late articles were added in on-line form. (Vol. 291, N° 9-10, 659 pages, ISSN: 0038-0938 (Print) 1573-093X (Online))

Moreover, the SILSO researchers contributed three main articles as first authors, and were associated with three other articles written jointly with different foreign collaborators. Those articles described all main corrections introduced in the current official version of the sunspot number distributed by the WDC-SILSO, while one article led by T. Dudok de Wit investigated for the first time the statistical properties of the random errors present in the raw sunspot data forming the base of this reference sunspot index. This ground-breaking study reveals a dual nature, mixing two distinct contributions, one associated with the random solar variations themselves and one truly associated with errors in visual sunspot counts.

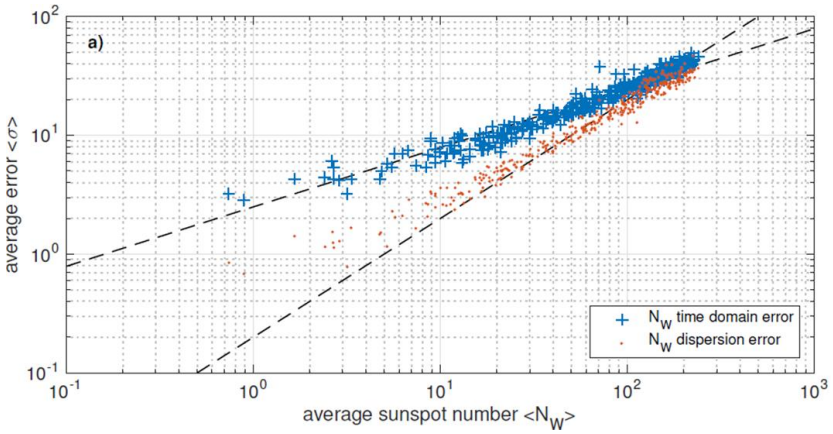

Figure 16: Variation of the time domain error (blue) and dispersion error (red) as a function of the average sunspot number. The clear double distribution shows the relative contribution of two distinct components of the random errors in sunspot counts: random component of solar variability (Poisson statistics) and counting errors made by the observers (Gaussian statistics).

This topical issue covered various implications of the ongoing SILSO revision work. Several papers presented newly recovered sunspot data and updated historical databases. Other papers presented new additional or alternate corrections to the sunspot number series, demonstrating that further improvements are needed and will benefit from the recovery of lost or neglected data combined with state-of-the-art statistical processing methods. As a validation of recent changes, several articles investigated the correlation between the updated sunspot number series and other direct or indirect solar activity indices, like total magnetic field measurements or cosmogenic isotopes from polar ice cores. Most results confirm that as a result of the revision, there is a better agreement between the new sunspot series and the parallel indices, and that past unexplained discrepancies are reduced or eliminated.

Finally, a few articles are considering implications of the revision by repeating some past analyses that rely on the sunspot number as a key input parameter. Indeed, a wide range of studies in various disciplines rely on the centuries-old sunspot number series. Overall, this volume thus concentrates a first wave of studies in a single broad panorama. Already abundantly cited after just a few months, it should provide over the coming years a key reference for all solar physicists contributing to the growing research on the long-term reconstruction and prediction of solar activity and its impact on the Earth.

MHD modeling of torsional waves in the solar corona

The solar corona, an outer layer of the solar atmosphere, is filled with rarified and magnetized plasmas (charged particles). Due to symmetry, coronal plasma is structured into cylindrical magnetic tubes. Thus, magnetic loops and open field lines are the basic bricks of the solar corona (Figure 17).

Magnetic tubes support various types of oscillations. Existence of these oscillations is important in particular for the fundamental problem of solar corona heating: oscillations are considered among two main candidates to transport energy from the lower layers of the solar atmosphere into the corona, where the energy is released. By means of numerical analysis we studied how torsional oscillations can dissipate, i.e. release their energy in the solar corona.

There are four basic types of oscillations in magnetic flux tubes: sausage, kink, tube, and torsional (Figure 18).

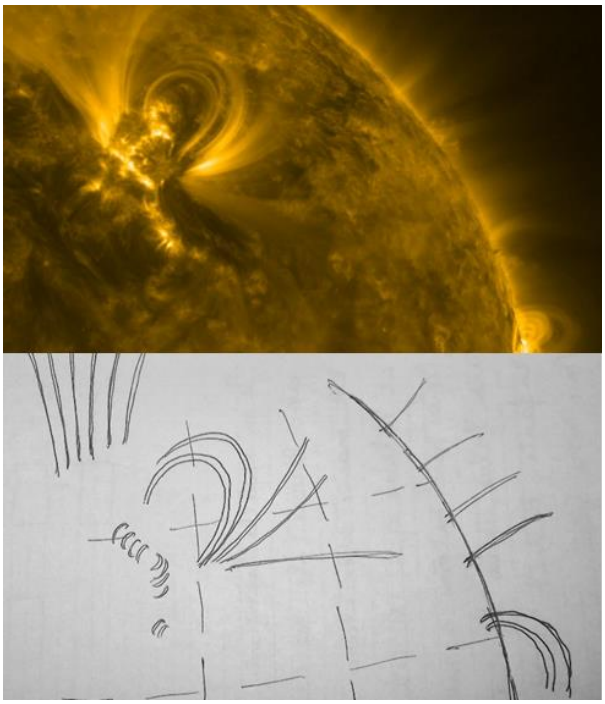

Figure 17: Solar corona observed in the extreme ultraviolet wavelength λ=17.1 nm by the SDO/AIA telescope (top) and a sketch with open and closed magnetic field lines (bottom).

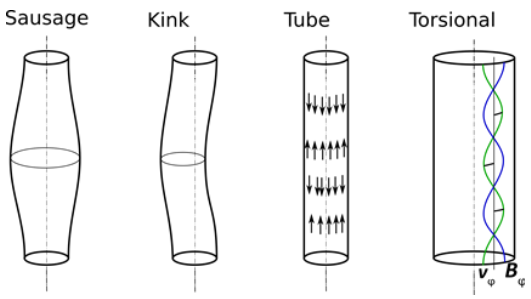

Figure 18: Types of oscillations in magnetic flux tubes.

The first three types of oscillations are called compressive, since during the oscillation period the plasma density is perturbed. These types of oscillations are extensively studied since pioneering work of Edwin & Roberts in 1983. Compressive oscillations are prone to decay and reflection in the transition region of the solar atmosphere (the region where plasma density drastically decreases by several orders of magnitude to 10^9 cm^{-3}, and plasma temperature increases from several thousands, to approximately one million degrees Kelvin), so the amount of energy they can release in the corona is not enough to solve the fundamental problem of coronal heating.

Torsional oscillations differ from the previous three types: they are incompressible and are less susceptible to dissipations in the transition region, so there is higher possibility they carry necessary amount of energy to the corona. But indeed, it is important to figure out the mechanisms how torsional oscillations dissipate their energy in the corona.

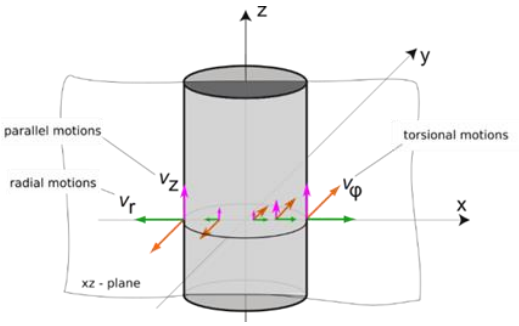

Figure 19: Magnetic flux tube with original torsional motions and induced radial motions and parallel motions.

We numerically analyzed the dynamics of propagating torsional waves and payed particular attention to nonlinear effects. These effects are usually not considered at all when one analyzes the oscillations analytically. Not surprisingly, because the effects are small and tend to disappear when the initial oscillation is weak. But they are always present in real solar plasma and make their small but constant contribution.

We found many effects that may result in energy dissipation. For example, torsional motions induce parallel and radial motions (Figure 19). Parallel motions are pulsating (periodically change from zero to

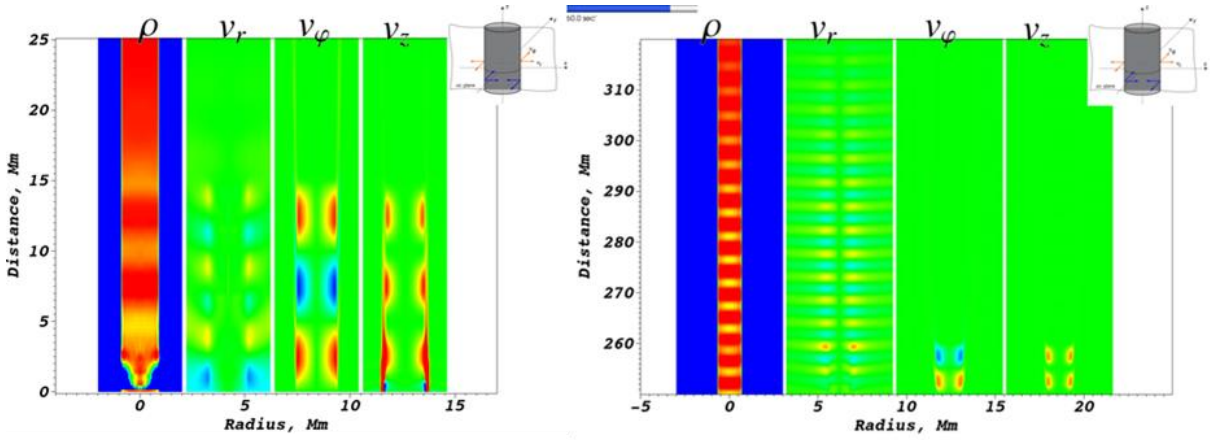

Figure 20: Central cross-section of a magnetic flux tube with plasma density ρ, radial velocity v_r, azimuthal velocity v_φ and parallel velocity v_z. Left panel: early phase of the wave propagation. Right panel: late phase of the wave propagation, induced sausage wave travels ahead of mother torsional wave.

particular value), but are always pointed in the same direction. Radial motions are oscillating inward and outward, i.e. they consist of one of the oscillations mentioned above – sausage oscillations (they are compressible and also prone to decay). The energy necessary for the development of induced parallel and radial motions is obtained from the energy of the initial wave! Torsional motions also result in other effects, such as wave steepening and nonlinear phase mixing. Snapshots with results of numerical simulations are presented in Figure 20.

We found another effect that has not been predicted by analytical theories: the observed nonlinear effects are more pronounced near the tube's boundary and are absent near the tube's axis. This fact proves that our understanding of the phenomena requires improvement.

All the observed nonlinear effects can serve as a mechanism for the dissipation of energy of torsional oscillations in the solar corona.

A new type of solar coronal radio bursts (Av-bursts)

Radio observations of the solar corona provide an important tool for the remote sensing of coronal processes. Narrow-band coronal radio bursts in the frequency range 23-35 MHz with frequency drift rates ~ 100 kHz/s have been discovered recently using large radio telescopes UTR-2 and URAN-2 (Ukraine). Radio waves at these frequencies are generated at heliocentric radial distances of 2-3 solar radii. Since the emission sources of these bursts propagate with near-Alfvén velocities, we call them Av-bursts. An example of Av-bursts is presented in Figure 21.

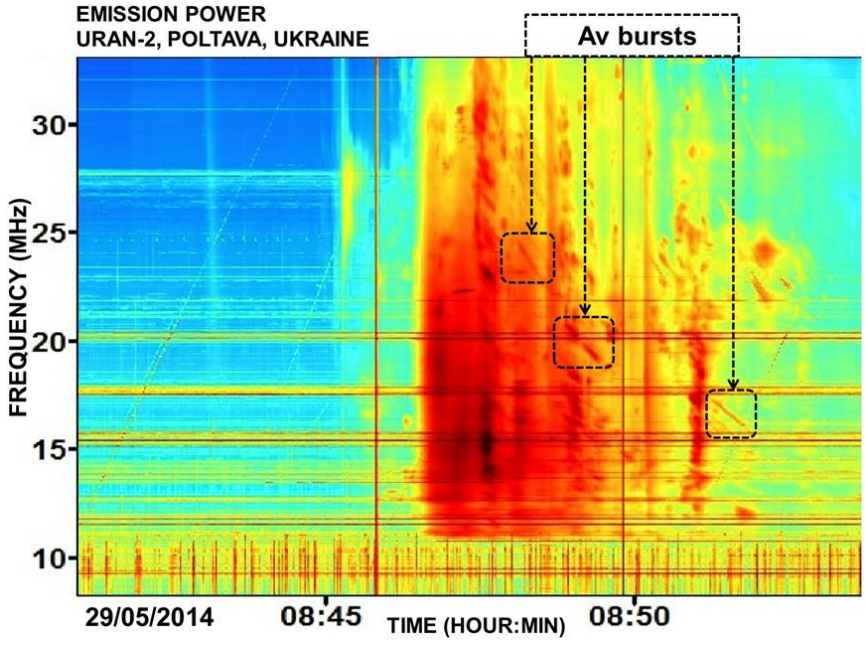

Figure 21: Radio spectrogram recorded on 29/05/2014 by URAN-2. The Av-bursts (strips with decreasing frequency tones) are encircled by the dashed lines. Inclinations of Av-bursts give their frequency drift rates that can be used to estimate propagation velocities of their sources.

In collaboration with Ukrainian colleagues, we have studied Av-bursts and their generation mechanisms. We propose the following scenario for Av-bursts (Figure 22).
First, kinetic Alfvén waves (KAWs), generated by magnetic reconnection in solar flares, propagate upward together with associated density cavities. Langmuir waves, excited locally by the electron beams, are then trapped and accumulated in the cavities. Finally, as the KAWs propagate toward decreasing plasma density, the high-amplitude Langmuir waves are gradually released and

generate fundamental radio emission by Langmuir-ion scatterings.

Observed properties of Av radio bursts provide valuable information for deducing parameters of coronal plasma (local density, temperature, and magnetic field) and kinetic-scale Alfvén waves (wavelengths and amplitudes).

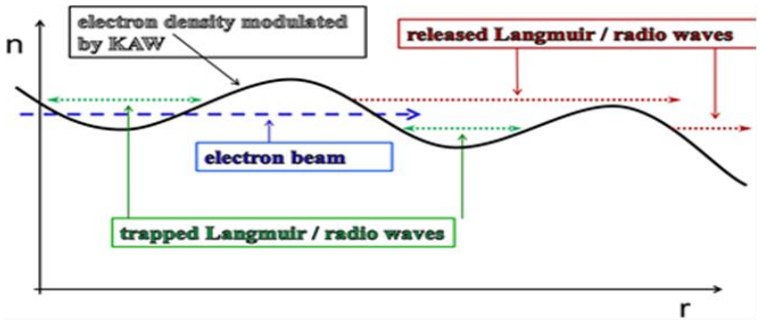

Figure 22: Proposed generation mechanism for Av-bursts (see explanation in text).

The detection of ultra-relativistic electrons by LYRA on board PROBA2

PROBA2 is a small European Space Agency's (ESA) satellite with a scientific mission to explore the solar "atmosphere" (also called corona) and the Sun's effect on the near-earth environment. LYRA (Large Yield RAdiometer, formerly LYman alpha RAdiometer) is one of the two main instruments on board the satellite, designed to observe ultraviolet to soft X-ray emission from the solar corona with extremely high cadence. It measures light from four different ranges of wavelength, chosen for their relevance to solar physics, aeronomy and space weather, in three redundant units (i.e. each unit contains all four bands).

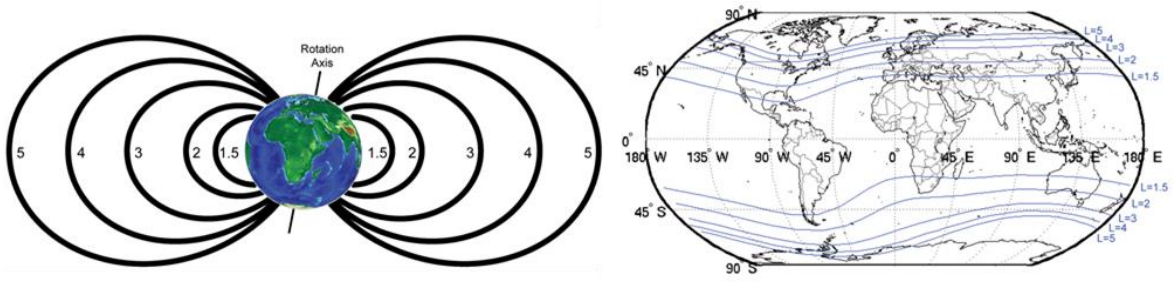

Figure 23: A conceptual drawing of Earth's magnetic field (left) and the map of the magnetic field lines on the surface of Earth (right). Both images depict the Earth's magnetic field when undisturbed by space weather. The left image is an approximate representation while the right image is calculated by a semi-observation model fitting. The magnetic field lines of the left image that close 1.5, 2, 3, 4, and 5 Earth radii away of Earth's centre are labelled as L=1.5, 2, 3, 4, and 5 on the right image.

Although LYRA is designed to detect light, it also succeeded to detect ultra-relativistic electrons (i.e. electrons with energies above 1 MeV) that penetrate into the Earth's ionosphere and reach the altitude of PROBA2 (about 700 km). Those electrons are known to originate from the solar wind and get trapped by Earth's magnetic field at an altitude of thousands of kilometers. LYRA's detections demonstrate that, under certain conditions, these particles can become "trapped" by Earth's magnetic field and fall to the altitude of PROBA2 and possibly below.

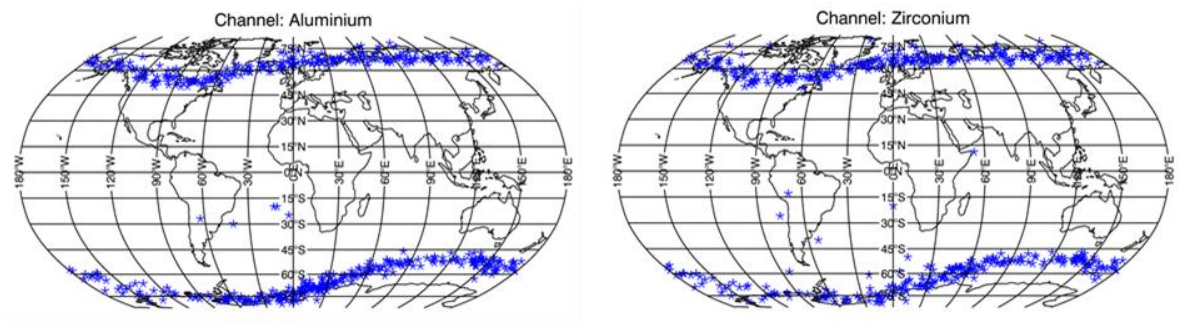

Figure 24: Maps of the location of the detections made by the LYRA's Aluminum (left) and Zirconium (right) channels. Also known as channels 3 and 4 respectively, those channels are named after the ions of the solar corona they are designed to observe best. The concurrence of the locations is strong evidence for the detection of highly relativistic electrons.

Perhaps the most intriguing characteristic of the electron detections is the effect that the local time has on the likelihood of detecting the phenomenon. To ensure continuous viewing of the Sun, PROBA2 flies from pole-to-pole and from dawn-to-dusk. It was therefore possible to split each orbit into two parts and study the effect that the sunlight has on the phenomenon. The compelling result is that there are eight times more events during the dawn than the dusk part of the orbit!

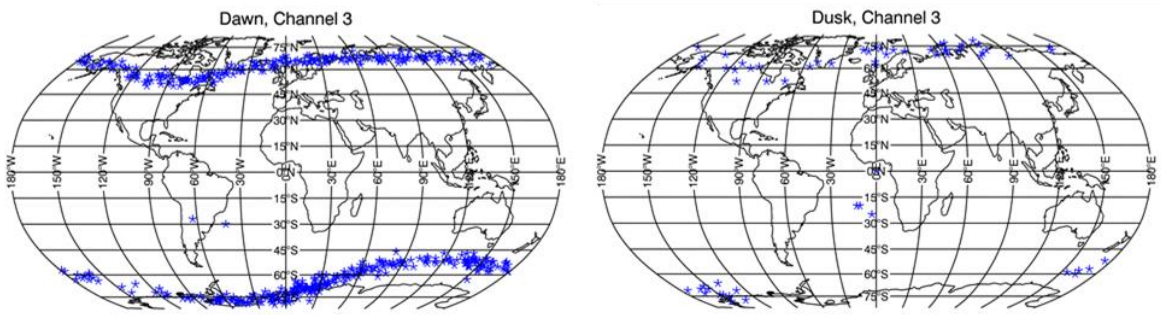

Figure 25: Maps of the detections made on channel 3 (Aluminum) when the satellite flies over the dawn (left) and dusk (right) sides of the Earth. Although the geographical distribution of the detections remains the same, it is eight times more likely for a detection to take place at the dawn part of the obit than at dusk.

Various mechanisms have been proposed by a team of scientists, led by the PROBA2 science team, for the explanation of the physical process that results in the LYRA detections. Nevertheless, those explanations are qualitative, while a full quantitative model has been elusive so far. Hence, it may take years until we have a more detailed view of this captivating phenomenon.

Numerical and observational study of stealth CMEs

The prediction of space weather is a core service provided by the Solar Influences Data analysis Center (SIDC) at the Royal Observatory of Belgium (ROB). Despite the availability of various datasets providing a continuous view of the Sun and its activity, occasionally space weather events occur that are stealthy enough to surprise even experienced forecasters. Examples are front-sided coronal mass ejections (CMEs) without a clear source region and their associated geomagnetic storms. For these events, there

are little warning signs to alert the forecaster of their occurrence and hence the resulting storm will likely not be predicted. In order to improve the forecasting of this type of geomagnetic storms, we need a better understanding of the initiation of such stealth events.

In this PhD project, which started at ROB on 16 October 2016, the focus is on stealth CMEs and how they differ from more typical solar eruptions. Stealth CMEs are unusual CMEs that are clearly observed in multi-viewpoint coronagraph observations as front-sided events, but lack signatures of eruption in the low corona and on the solar disk. These CMEs without low-coronal signatures (LCS) were studied observationally by D'Huys et al. (2014). From their sample of 40 stealth events, these authors concluded that CMEs without LCS are generally narrow and slow events with a kinematic evolution that is compatible with the breakout scenario or an ideal MHD instability as eruption mechanism.

The objective for this study is to combine observational and numerical studies of stealth eruptions in order to determine how these events are triggered and driven and in what sense they differ from more typical solar eruptions. We aim to improve the forecasting of the geomagnetic impact of stealth eruptions by searching for similarities between the observed events and by comparing the observations to the results of the numerical modelling.

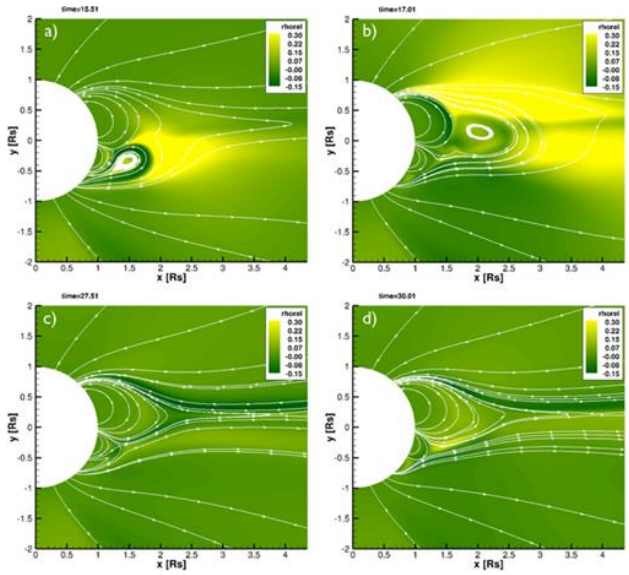

Figure 26: Snapshots of the time evolution of the relative density and of the selected field lines during the formation of the structure associated with the first CME (a), its movement towards the equator (b), the rise of the southern arcade (c), and the associated second CME (d) (Bemporad et al. 2012).

Dana Talpeanu, the PhD student, supervised by Elke D'Huys at ROB, started simulating stealth CMEs with the code AMRVAC developed at KU Leuven by trying at first to reproduce the previous work of Francesco Zuccarello and Alessandro Bemporad (Zuccarello et al. 2012, Bemporad et al. 2012). They numerically modelled a sympathetic event, very similar to a stealth CME (Figure 26), using an earlier version of the code. Figure 27 represents one of the current simulations of the θ component of the magnetic field (colour scale) and magnetic field lines (black lines). The θ component represents one of the two components that are perpendicular to the radial direction (pointing away from the Sun), and to each other. As it can be seen, the overall configuration resembles the one from Bemporad et al. (2012), but it is not perfectly matching. This is a work in progress and once the structures coincide, Dana Talpeanu will start applying the shearing motions in order to obtain CMEs in a similar way as Francesco Zuccarello and Alessandro Bemporad did.

Afterwards, this study will be extended by using events from the list of 40 events identified by Elke D'Huys during her PhD thesis and make a parameter study on them, which could reveal the range of global magnetic field strength that allows stealth events and may identify other crucial parameters as well. The main purpose is to develop a more specific numerical model for stealth CMEs. This could provide a clearer view on the eruption mechanisms at work in the case of stealth events and improve the forecast of their associated geomagnetic perturbations.

In a second phase of the project, the plan is to study the geo-effective stealth CMEs. The starting point will be a list of CMEs that produced geomagnetic storms and that are suspected to be stealth events.

The ultimate goal of this project is to gain insights into the processes that cause and drive stealth eruptions, their geomagnetic effects and how they differ from more typical solar eruptions. We aim to do this by combining observations and model predictions. By examining specific physical properties of these unusual eruptions in observations and comparing them to the output of numerical models, we can refine the models and decide which of the proposed eruption initiation processes is actually at work. Because these stealth eruptions may cause hazardous space weather conditions without being detected, improvements in our understanding of their origins will advance our ability to predict the onset of such space weather events.

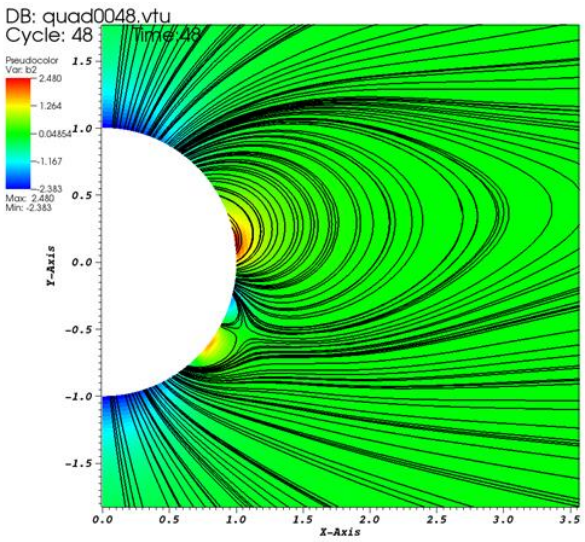

Figure 27: The simulated background magnetic configuration using MPI-AMRVAC; θ component of the magnetic field (colour scale) and magnetic field lines (black lines).

HELmet streamers In the solar corona and their OScillations (HELIOS)

Figure 28: White-light solar corona observed during the total solar eclipse on 13 November 2012 in Australia (courtesy D. Finlay, C. Emmanoulidis, M. Druckmüller). The coronal structure is dominated by quasi-radial streamers.

The corona is the outermost layer of the solar atmosphere, extending far above the solar surface. Since it is very hot, the material is in a plasma state: an ionised gas that is influenced by the magnetic field. It is rather well described by the magnetohydrodynamic (MHD) equations, which include the magnetic/electric forces in the fluid equations.

The structure and dynamics of the solar corona is an important and overarching open issue in astrophysics. The magnetized corona is the source of the solar wind that affects the Earth (space weather), as well as the source region of powerful eruptions – observed in the form of solar flares and coronal mass ejections (CMEs). It is not well understood when and why some structures erupt to become a CME. This is important, because space weather has a direct influence on our highly technological society: it may disturb, among others, satellite communication (GPS signals), electric power transmission, oil and gas pipelines.

Our current understanding of the corona assumes that its dynamics is dominated by the magnetic field: one can often say that magnetic loops are the building blocks of the solar corona. This is true if one looks at the low corona typically observed by extreme-ultraviolet (EUV) imagers. However, if one also looks higher to get a more complete picture, it becomes evident that a loop system is generally surmounted by a quasi-radial bright structure that, together with the underlying loops, forms a coronal helmet streamer (see Figure 28). The transition of observed morphologies from loop-like to quasi-radial structures marks the fundamental physical transition from the magnetic field-dominated regime (low corona) to the solar wind outflow-dominated regime (high corona). It is therefore coronal streamers that are the true building blocks of the solar corona, especially near the maximum of the solar activity when the contribution of the other major coronal constituent (coronal holes) is small.

Recently, transverse waves were observed in helmet streamers, typically after the passage of a CME. The CME-driven shock wave moved the streamer sideways, and a decaying oscillation of the streamer was observed after the CME passage, as can be seen in Figure 29. All the previous works reported observations of streamer oscillations taken from a single vantage point (typically the SOHO spacecraft).

The general aim of this PhD project, which Bieke Decraemer started on 1 October 2016, is to characterize coronal streamers using observations of their oscillations in three dimensions, and to develop analytical and numerical models that allow for coronal seismology of the transverse oscillations of helmet streamers.

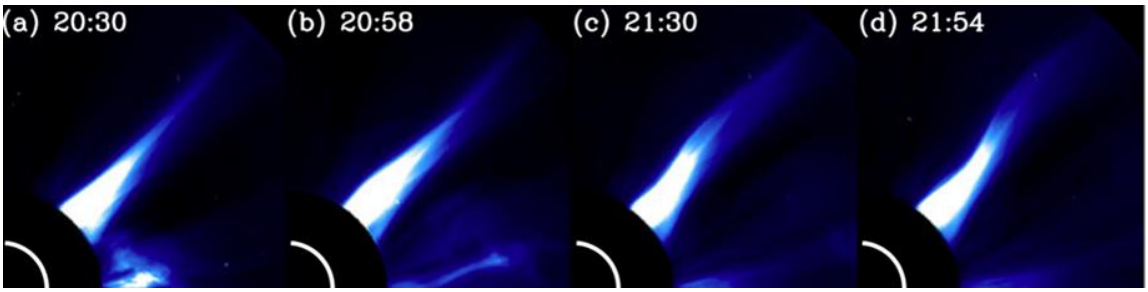

Figure 29: Wavelike motion of a streamer stalk observed by SOHO/LASCO C2 on 5 June 2003, as an aftermath of the CME impact. Figure taken from Feng et al. (2011).

Coronal seismology is the technique where observed coronal wave parameters are used to estimate physical properties of the corona, by the comparison with theoretical models for the coronal structures and their waves. In the last 15 years, the technique of coronal seismology has been very successful in measuring various parameters in the solar corona. This project will contribute to the field of coronal physics by seismologically measuring physical parameters in helmet streamers. These regions are important for understanding the initiation and propagation of CMEs, and thus the envisaged seismology can gain additional insight in these key questions.

Scientific literature makes it abundantly clear that the mathematics becomes rather complicated for the description of waves in current sheets, prohibiting easily accessible seismological estimates of the streamer's properties or even a mode identification. This sets the scene for the modeling part of this proposal: we aim to develop robust models for streamers and their transverse waves, which allow for mode identification and an inversion of the observed wave properties, to make useful estimates of the streamer structure. To complement this part, the characteristics of coronal streamers must be first

investigated with observations from multiple vantage points. To test the models developed in this project, we also must obtain observations of the oscillations from these multiple vantage points. The goal is to achieve a good correspondence between reality, i.e. the observations, and simulations, i.e. the results predicted by the models. Only in this way the technique of seismology will give us reliable results on the physical parameters of the solar corona.

*Figure 30: The primary school **Ingenium** for advanced and gifted children visited the Royal Observatory and BISA on 27 April. Their enthusiasm and creative questions were an inspiration for all scientists and guides.*

Instrumentation and experiments

Space Technology & Calibration Laboratories

Radiation from space and the Sun, as well as atmospheric effects, play a key role in the sun-space-earth research and the technology that has to deal with them, such as communication and high-tech navigation systems. This explains the large interest in ground- and space-based instruments that measure the electromagnetic radiation. However, a production line for scientific and technical instruments doesn't exist. Science and technological projects that are set up to develop a tailored instrument, usually span several years. Moreover, inventing an instrument from scratch is not so obvious. It is also not very efficient that each instrument has to go through the same growing pains and ageing illnesses dealing with stubborn hard- and software problems. But, the "Space Technology & Calibration Laboratories" (STCL) comes to the rescue!

Figure 31: Two complementary groups i.e., the Advanced Technology for Solar Observations (ROB) and the Optics Laboratory facilities (BISA) joined their efforts to support the needs concerning high-quality characterization and calibration of space- and ground-based instruments and their components. The instrument calibration activities include the pre-flight calibration, the onboard calibration procedures and degradation assessment that are required to understand the instrument, and prepare the scientific exploitation of its data.

STCL utilizes all the expertise and laboratory facilities available in the Solar-Terrestrial Centre of Excellence in order to provide adequate support to any team developing an instrument. The STCL knows how to fully characterize an instrument and has an idea on how its performance and ageing is influenced while flying through hostile environments such as space. The STCL is also familiar with famous laboratories such as the synchrotron facilities in Berlin and the cyclotron in Louvain-la-Neuve. There, it is verified if an instrument is launch-and-space proof, resistant to harmful particle impacts, and much more. These labs help to understand how an instrument compares with other instruments such that the data can be completely understood and fully exploited.

The long term goal of the STCL is to enhance the build-up expertise in scientific fields related to the design, development, calibration and degradation assessment of instruments. More specifically:

- Build a research and experimental laboratory facility for high-quality instrument calibration, flight/instrument operations, and preparation to science;

- Define calibration standards for space-based instruments and their subsystems at Belgian level and assure their traceability. Co-operate with European and international organisations responsible for quality infrastructure dedicated to calibration measurements and metrology standards;
- Design future space-based instruments and on-board calibration systems by developing and characterizing prototype systems (R&D), data compression, processing and exploitation;
- Understand instrument ageing: degradation, contamination/cleanliness issues, modeling & simulation.

Figure 32: A view inside one of the STCL labs during the STCE Annual Meeting 2015.

The STCL will also provide multidisciplinary R&D support for the development of advanced space technologies, i.e. the next generation of scientific instruments.

Highlights in solar radio astronomy at ROB

Solar radio emissions accompanying eruptive events (flares, filament eruptions, Coronal Mass Ejections) can occur at any wavelength of the radio spectrum. This is a major difference with other domains in radio astronomy that are primarily "confined" to well identified frequencies corresponding to emission lines of atoms or molecules. The VHF and UHF band (30 – 3000 MHz) is of the utmost importance as it corresponds to heights covering the whole corona, from the transition region with the chromosphere to the boundaries of the interplanetary space. Particles accelerated during flares or by shock waves produce radio signatures observable over this whole frequency range, providing insights in the eruptive processes taking place.

Since 2008, the Royal Observatory of Belgium operates in Humain, near Marche-en-Famenne, a small solar spectrograph called Callisto, covering the frequency band 45-447 MHz. Callisto is an analogic receiver based on a commercial TV tuner driven by dedicated electronics and designed by C. Monstein from ETH Zürich. It is connected to a broad band antenna mounted on the side of a 6-m Sun-tracking parabola. The Callisto receiver in Humain is part of a worldwide network of identical instruments that provide near real-time radio observations of the Sun.

	Callisto	*ARCAS*	*HSRS*
Frequency band	45 – 447 MHz	45 – 450 MHz	275 – 1495 MHz
Frequency resolution	63 kHz	98 kHz	98 KHz
Time resolution	250 ms	~ 84 ms	~ 250 ms
Number of freq.	200	~ 4200	~ 12500

Figure 33: Table with the technical performances of the solar radio spectrographs in Humain. The frequency resolution of Callisto varies in practice and is bigger than the one mentioned here.

In 2015 and 2016, the radio group of the solar physics department

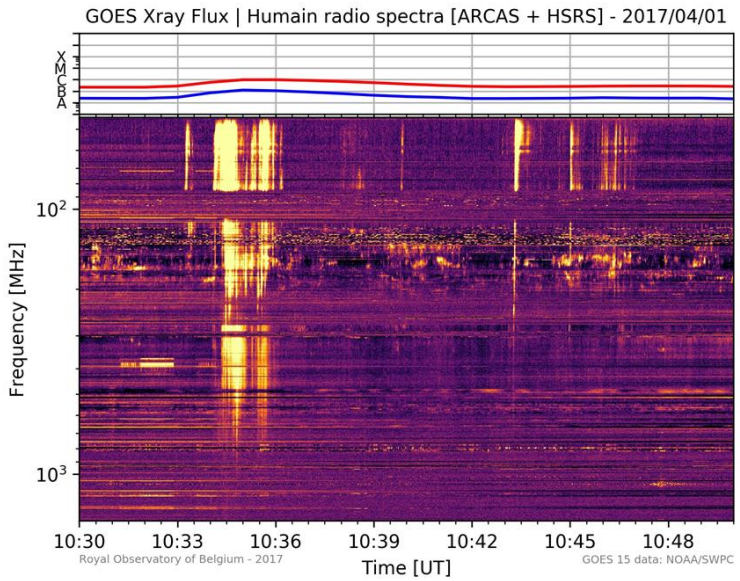

Figure 34: A group of type III bursts linked to a B9.8 flare. The "interruption" around 100 MHz is due to a filter that attenuates the FM band. Between 100 and 200 MHz, a noise storm can be seen as narrow band intermittent emissions.

set up two new receivers that are aimed at expanding the frequency range and at improving the frequency resolution of Callisto (200 frequencies spread over the whole band). One of the receivers, HSRS, is connected to a broad band antenna (300 – 5000 MHz) located at the focus of the 6-m dish. It was set up in August 2015 and has since observed more than 60 noticeable radio events, despite the low level of solar activity. The second receiver, ARCAS, installed in October 2016, shares the same antenna as Callisto.

HSRS and ARCAS are identical digital receivers based on Software Defined Radio devices. They differ only by a single removable electronic card that defines the frequency band. These devices can be programmed using an open source library to build up many different applications (most of them being not radio astronomy related). In our case, both receivers were programmed to implement a wide band spectrometer. The instantaneous bandwidth is about 20 MHz, a limitation that results from the amount of data that can transit through the Ethernet port connecting each receiver to its PC. To scan a certain band, one has to tune the receiver at a certain frequency, *calculate* the spectrum over 20 MHz (through a Fast Fourrier Transform over the various frequencies within the 20 MHz band), and tune again the receiver to the next frequency, about 20 MHz apart. The overall performances of the instrument now operational in Humain are summarized in the accompanying table (Figure 33).

The finer frequency resolution of the new receivers allows us to observe in bands that were mostly inaccessible with Callisto (like the band 110 – 150 MHz). For example, relatively narrow band emissions such as noise storms associated with strong sunspots can now fully be observed with ARCAS. The combination of ARCAS and HSRS gives to the scientists of the Solar Physics & Space Weather department of the ROB an unprecedented view on radio emissions linked to eruptive processes. An example is given in

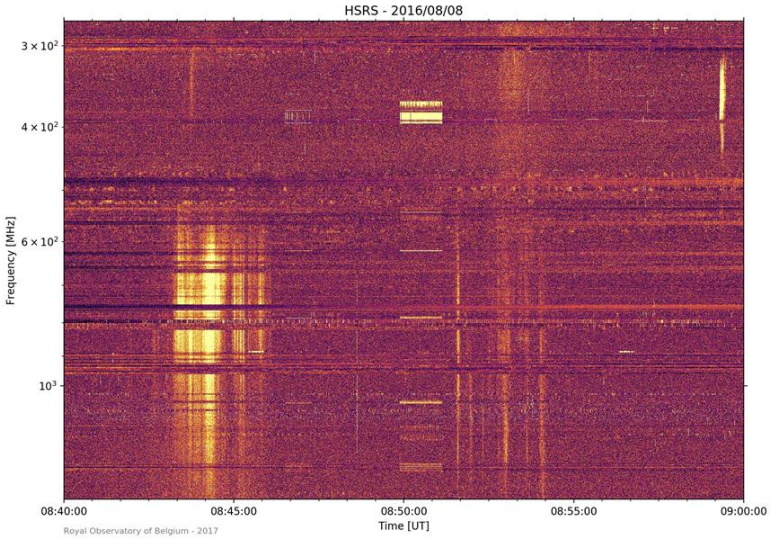

Figure 35: Pulsations observed above 600 MHz with HSRS on 8 August 2016.

Figure 34, where a group of intense type III bursts, superposed on a noise storm, is observed in association with a B9.8 flare on 1 April 2017. Indeed, the low level of solar activity since the setup of ARCAS in Oct. 2016 forced us to illustrate this instrument with an event that took place in the spring of 2017.

The HSRS spectrograph covers a frequency range that is monitored by only a few instruments in western Europe. Above about 500 MHz, in the decimetric frequency range, radio bursts closely related to particle acceleration taking place near flare sites can be observed, such as decimetric pulsations which are similar to Type III, but with "infinite" frequency drift (Figure 35).

On instrumental errors and related correction strategies of ozonesondes

More than 50 years already, light-weight instruments ("ozonesondes") attached to weather balloons are launched worldwide to measure the ozone concentrations in the Earth's atmosphere as a function of altitude. Although a minor constituent in the atmosphere, the ozone layer (reaching its maximum concentrations around 20-25 km) protects us from the harmful solar UV radiation, but at lower altitudes (around 10 km) ozone acts as a greenhouse gas. In the lowermost atmospheric layers (up to 3 km), ozone on the other hand is harmful for human health and can cause respiratory problems. As ozone affects life on Earth in different ways depending on its location in the atmosphere, the knowledge and time variability of the vertical distribution of ozone is very important.

Figure 36: Ozonesonde calibration in the RMI lab.

Ozonesondes provide the vertical distribution of ozone at very high vertical resolution (typically a few 100 m), up to altitudes in the range of 30–35 km and constitute the most important data source to derive long-term vertical ozone trends. Ozonesondes consist of a miniature piston pump that brings the air into 2 cells, filled with electrochemical solutions that react only with ozone molecules. As a consequence, a major concern for any research with ozonesonde measurements is the data homogeneity and consistency because every profile is obtained with a unique instrument and different types of ozonesondes exist. Consequently, every ozonesonde needs to be prepared and checked thoroughly prior to launch. To have consistency between different ozonesonde stations, it is essential to have agreement on procedures for preparation as well as agreement on procedures for data processing and analysis. Therefore, an Ozonesonde Data Quality Assessment (O3S-DQA) has been initiated with the aim to provide a revised, homogeneous dataset with corrections applied for biases related to instrumental changes (such as sonde type or electrolyte

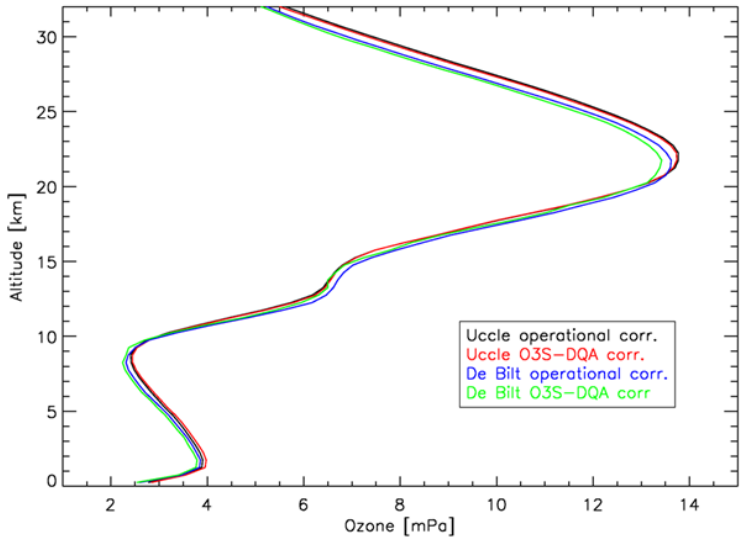

Figure 37: Vertical average ozone profiles for the ozonesonde stations Uccle and De Bilt and for different correction algorithms applied to the measurements (operational corrections vs. the O3S-DQA homogenized corrections, see text).

solution) in those cases where comparisons or laboratory experiments provide strong evidence for such corrections.

The ozonesonde stations at Uccle (Belgium) and De Bilt (the Netherlands) are separated by only 175 km and therefore have a similar vertical distribution of ozone, but use different ozonesonde types (or different manufacturers for the same electrochemical concentration cell (ECC) type), operating procedures, and correction strategies. As such, these stations form a unique test bed for the O3S-DQA activity. To study the impact of the corrections on the ozone profiles and trends, we compared the Uccle and De Bilt average ozone profiles (Figure 37) and vertical ozone trends (Figure 38), calculated from the operational corrections at both stations and the O3S-DQA corrected profiles. In the common ECC-type 1997–2014 period, the O3S-DQA corrections effectively reduce the differences between the Uccle and De Bilt ozone partial pressure values with respect to the operational corrections only for the stratospheric layers below the ozone maximum (see Figure 37). The upper-stratospheric ozone measurements at both sites are substantially different, regardless of the correction methodology used. The origin of this difference is not clear. The discrepancies in the tropospheric ozone concentrations between both sites can be ascribed to the problematic background measurement and correction at De Bilt, especially in the period before November 1998.

Despite their large impact on the average ozone profiles, the different (sensible) correction strategies do not change the ozone trends significantly, usually only within their statistical uncertainty due to atmospheric noise (see Figure 38). The O3S-DQA corrections bring the Uccle and De Bilt ozone trend estimates for 1997–2014 closer to each other in the lower stratosphere and lower troposphere. Throughout the whole vertical profile, these trend estimates are, however, not

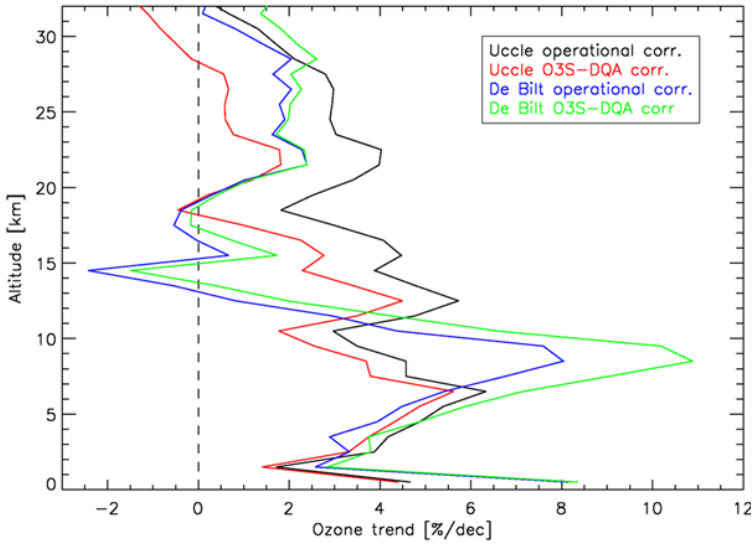

Figure 38: Vertical distribution of the linear relative trends for different correction strategies applied to the Uccle and De Bilt ozonesonde data for the 1997–2014 time period. The trends are estimated for layers of 1 km height.

significantly different from each other, and only in the troposphere significantly positive. The finding that the applied correction method determines whether the ozone trend is significantly positive or not, is important in present-day ozone research. Indeed, the beginning of the period 1997–2014 coincides with the mid-latitude stratospheric peak values of the equivalent effective stratospheric chlorine (EESC) abundance. The EESC is a sum of chlorine and bromine derived from Ozone Depleting Substances (ODS) tropospheric abundances weighted to reflect their potential influence on ozone. Because the EESC had already returned 38–41% from its peak value by the end of 2012, a major issue in current ozone research is whether the onset of ozone recovery can be detected. Our study (Van Malderen et al., 2016) demonstrates that, at least for measurements with ozonesondes, caution is needed before qualifying a (statistically) significant ozone increase as the onset of ozone recovery.

*Figure 39: The Sun shines brightly for **ASGARD**. Teams from secondary schools can propose their own scientific experiment and instruments to send to the stratosphere (near-space) with a stratospheric balloon from the Royal Meteorological Institute (RMI).*

Applications, Modeling and Services

Setting up the expert service centre for space radiation

Space weather affects end-users in a wide range of sectors applicable to Earth and the heliosphere. In the frame of its Space Situational Awareness (SSA) programme, the European Space Agency (ESA) is establishing a Space Weather (SWE) Service Network to support end-users by focusing on providing space weather services. This is done by considering three factors: mitigate the effects of space weather on their systems, reduce costs and improve reliability. The network is organised around five Expert Service Centres (ESCs) covering Solar Weather, Heliospheric Weather, Space Radiation Environment, Ionospheric Weather, and Geomagnetic Conditions. Furthermore, the ESCs are supported by the SSA Space Weather Coordination Centre (SSCC) that offers first line support to the end users.

Figure 40: The SSA SWE Space Radiation ESC webpage © ESA

Due to its expertise in space particle radiation, the Royal Belgian Institute for Space Aeronomy (BISA) has been the coordinator of the SSA Space Radiation ESC (R-ESC) since it was set up during the Preparatory Phase of the SSA SWE programme and has continued in this role during Period 2. On 24 September 2015, the P2-SWE-I ESC Kickoff Meeting was held at ESOC in Darmstadt, Germany where the ESA SSA SWE programme is located. This was followed by the P2-SWE-I ESC Definition Workshop on 18 January 2016 that allowed the five ESCs to meet and define the issues that would be applied in the rest of the project. In order to fulfil SSA SWE customer requirements as the SSA SWE Service Network continues to develop, the range of products currently provided and in development within the SWE network were reviewed and priority development needs were identified during the successful three-day P2-SWE-I ESC Thematic Workshop in May 2016.

The R-ESC currently consists of an interdisciplinary network of eleven Expert Groups that are supplying products related to particle radiation (ambient plasma, solar energetic particles, radiation belts, galactic

cosmic rays) as well as micron-size particulates (from meteoroids and space debris). R-ESC products provide users a large spectrum of applications covering different satellite orbits as well as airline altitudes. Unique observations that characterize these natural phenomena, as well as a greater understanding of their effects on technologies and biological systems, fall all under the umbrella of the R-ESC. To this effort, BISA provides four products: The COronal Mass Ejections and Solar Energetic Particles (COMESEP) Alert System, the Solar Energetic Particle Environment Modelling (SEPEM) Application Server, the SPace ENVironment Information System (SPENVIS), and the SWIFF Plasmasphere Model (SPM).

In addition to the coordination of the network, which includes project management, BISA is also providing asset/roadmap reviews related to services for Spacecraft Design, Spacecraft Operation, Spacecraft Launch Operation, Human Spaceflight, and to Airline, as well as organising a targeted test user campaign for the aforementioned user domains. Furthermore, to engage space weather end-users in discussions with product and service providers, the "Space Weather and Operational Post Event Analysis" End User Lunch was held at the Thirteenth European Space Weather Week (ESWW13). Results from the above mentioned activities were fed into the R-ESC Definition and Development Plan, a living document that continuously is being updated throughout the project duration.

Looking ahead, the R-ESC is paving the way forward for the future expansion of the network while making sure that its mission to provide and develop functionalities, capabilities and expertise needed in the Space Radiation domain is maintained.

Constraining CMEs and Shocks by Observations and Modelling

As a response to the BRAIN networking call the project proposal with the acronym CCSOM (Constraining CMEs and Shocks by Observations and Modelling throughout the inner heliosphere) was submitted and successfully accepted in the second half of 2016. CCSOM is led by Royal observatory of Belgium (ROB) with J. Magdalenic as a project coordinator. The project is based on the close collaboration of ROB, Katholieke Universiteit Leuven (KU Leuven), University of Helsinki and Graz University.

In the framework of CCSOM, the physics of coronal mass ejections (CMEs) and associated shock waves will be addressed. The observations will be compared with modeling results from EUHFORIA (EUropean Heliospheric FORecasting Information Asset), a recently developed model at the KU Leuven and University of

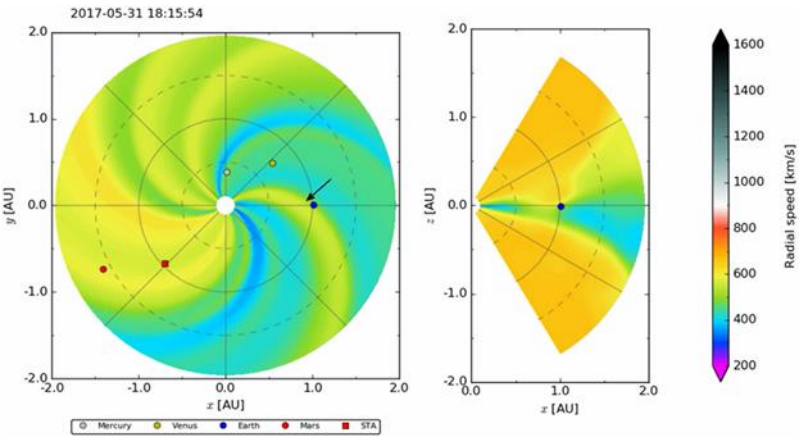

Figure 41: The solar wind modeling with EUHFORIA predicting the arrival of the fast flow associated with the coronal hole that transited the central solar meridian late on 27 May 2017. The colour indicates the solar wind radial speed in the ecliptic plane (view from above; left) as well as a meridional plane containing Earth (side view; right). The fast solar wind of about 650 km/s was expected to arrive at the Earth on 31 May at about 18:00 UT. The black arrow points at the fast solar wind flow which has reached the Earth.

Helsinki (led by resp. S. Poedts and J. Pomoell). EUHFORIA is a physics-based prediction model of the solar wind and CMEs in the inner heliosphere (presently similar to the state-of-the-art model ENLIL) which will be improved, tested and verified in the framework of this project. The major breakthrough with EUHFORIA will be its ability to model the CME and the CME-driven shock wave in realistic background solar wind conditions.

In summary, the project aims at making a breakthrough in studies of CME and CME-driven shock wave propagation in the inner heliosphere by combining observations with numerical simulations that will be well beyond what these models can currently do. This project will ultimately deliver, together with a number of scientific publications, a fully operational and scientifically validated heliospheric code for modeling the solar wind and CME propagation. It will give Europe an asset in predicting heliospheric space weather conditions with a novel simulation that will be the new state-of-the-art in heliophysics. During and at the end of the project the model will be set up and running principally at ROB for the use in space weather operations of the Regional Warning Center Belgium (RWC Belgium).

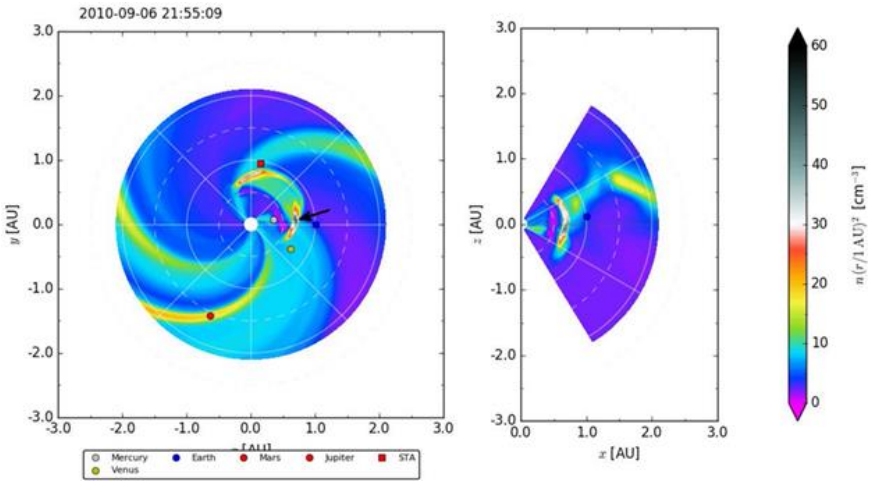

Figure 42: First results of EUHFORIA modeling the propagation of the CME (at present, the starting height of modeling is 0.1 AU, similar to ENLIL) observed on the Sun on 4 September 2010. The colour indicates the plasma density in the ecliptic plane (view from above; left) as well as a meridional plane containing Earth (side view; right). The black arrow points to the CME front approaching the Earth (blue circle).

EUHFORIA will reinforce the place of Belgium in the space weather community. We expect therefore a strong positive impact on the expertise in solar physics and space weather accumulated over the years in Belgium as well as a significant leap for the whole scientific community in Europe and beyond.

The first tests of EUHFORIA were performed during the last few months. Presently, EUHFORIA is modeling the solar wind propagation (see Figure 41), and the first statistical studies of solar wind modeling with EUHFORIA, in the framework of CCSOM, are in progress (Graz University).

Furthermore, initial tests of EUHFORIA modeling the CME propagation are being performed by M. Mierla from ROB and C. Scolini, PhD student under supervision of L. Rodriguez (ROB) and S. Poedts (KUL).

Figure 42 shows the results of modeling CME propagation (event was first observed on the Sun on 4 September 2010) using EUHFORIA.

High-resolution K index nowcast of the local magnetic activity

The main purpose of the geomagnetic activity indices is to quantify the degree of the geomagnetic field disturbance (local or global) and to characterize the origin and time scale of the field variations. The K index accounts for the morphological characteristics of the transient irregular variations of the field and it is designed to characterize the geomagnetic activity during a 3-hour interval at a certain location. The K index is derived from the amplitude of the variations of the field's horizontal components after subtracting the daily solar regular (S_R) variation for the particular component. The K index is an integer between 0 (indicating 'very quiet' geomagnetic field) and 9 ('very disturbed' geomagnetic field), corresponding to the larger of the two ranges measured in the field's horizontal components over the specified 3-hour period. In fact, the K index is a code, and although expressed in integers, it refers to a level ("class") on a quasi-logarithmic scale consisting of 10 gradually increasing ranges. The same 3-hour (UT) intervals (00–03, 03–06, … , 21–24) are used at any station where K indices are produced.

The K index is a popular choice among ionosphere/space weather researchers. For example, one of the main space weather references, the NOAA Space Weather scales, uses the planetary K index (K_p) as a physical measure for estimating the geomagnetic storm effects on spacecraft, power and other systems. Another example is the most advanced global empirical model of the ionosphere, the COSPAR International Reference Ionosphere (IRI) model which requires the K_p value as a key input parameter. The local K index is also used in RMI services, e.g. for alerting users of ongoing magnetic storms and for operational monitoring of the ionospheric activity.

Currently, several centres offer real-time estimates of the geomagnetic activity based on ground-based measurements. For example, the German Research Centre for Geosciences (GFZ) offers Quicklook K_p index estimates updated once every 3 hours. The US Space Weather Prediction Center (SWPC) provides a K_p index nowcast but, again, once every 3 hours. Space-based measurements (of the solar wind parameters) are also being used for nowcast and short-term prediction of the planetary K index. Although the cadence is higher (15 minutes), the nowcast is based on an assimilative model and availability of the ACE (Advanced Composition Explorer) satellite data is often unreliable.

It has already been established that the standard, fixed 3-hour time scale for producing the K index is much larger than the characteristic time of various phenomena associated with an elevated geomagnetic activity. These include disturbances in the ionosphere that are of particular interest because of their (adverse) effects on present-day radio communications and navigation practices. Such disturbances are known to propagate fast (up to about 600 m/s) and are thus capable of covering large regions (e.g. Europe) in a couple of hours during major geomagnetic storms. It is clear that, should a (sudden) storm onset occur at the beginning of a 3-hour period for which the standard K index is based on, the generation and propagation of the ionospheric disturbance would be missed by the time the K index for this period is produced. From this aspect, there is currently a demand for services providing real-time assessment of the (local and global) magnetic activity on a shorter time scale and alerting the users for the purpose of taking mitigating actions.

In response to this demand, the RMI Ionosphere and Space Weather research group developed a novel operational system for estimating, in real time, the local magnetic activity via a K-type index (K*) which closely resembles the standard K index. The main difference from the standard (post-processing) methods is in the way of determining the solar regular variation of the geomagnetic field: The new, real-time approach uses data from past measurements only. Another difference is that the concept of fixed

3-hour time periods (0-3, 3-6, ..., 21-24), each characterized with a single K value, is abolished. Instead, in the new approach, a K* value is derived at any time using data from the most recent 3 hours. Following this approach, the nowcast system is based on a fully automated computer procedure for real-time digital magnetogram data acquisition, data screening, establishing the field's regular variation, calculating the K* index, and issuing an alert whenever storm-level activity is indicated. Initially, the nowcast cadence was 1 hour, which was much better than the K index estimates available elsewhere. Another important feature of this nowcast system is the strict control on the data input and processing, allowing for an immediate assessment of the quality of output. The quality control employs the fact that a complete and sound dataset provides the ideal platform for reliable, closest-to-definite index production. The service was well accepted and used in several national and international projects, e.g. the European Union's 7-th Framework Programme (FP7) project AFFECTS (Advanced Forecast For Ensuring Communications Through Space).

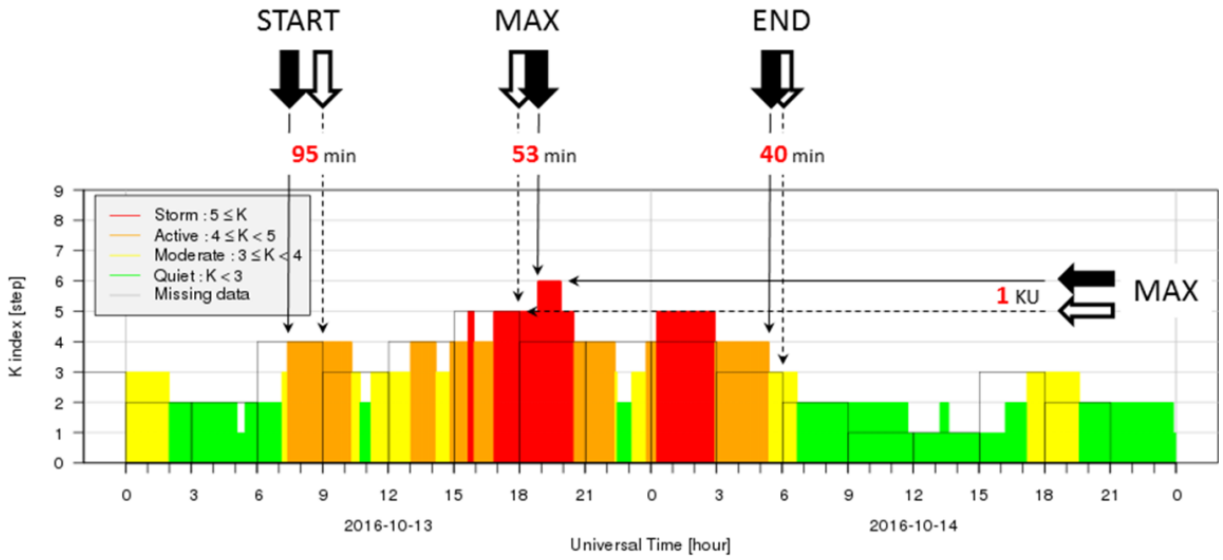

Figure 43: K index nowcast at 1 minute resolution based on digital magnetogram measurements at Dourbes during the storm event of 13-14 October 2016. The black boxes indicate the standard 3-hourly values of the index, while the colour bars indicate the 1-minute values. The improvement of the nowcast from 3-hour (white arrows) to 1-min (black arrows) resolution is 95 min for the start of the storm, 53 min for the maximum, and 40 min for the end. The strength of the storm is corrected by 1 K unit.*

Thanks to the improvements in data acquisition, computer power, and network infrastructure, we were able to improve the algorithm for the K* index estimation and the associated nowcast and alert system. The digital magnetogram measurements come at 1-minute resolution and are immediately transferred through the network to the processing software. After data cleaning, the daily solar regular variation curve is determined based on the 27-day running median. The regular variations are removed by subtracting the median values from the instantaneous measurements and thus the residual time series are produced. This is followed by calculating the range, i.e. the difference between the maximum and minimum values in the last 3 hours, from which range the K* index is determined. Although the K* index is still based on the previous 3 hours of data, it can now be calculated at a cadence of 1 minute. *Such a high cadence for the K index has never been achieved before and the service is the first of its kind in the world.*

The improvement is demonstrated in Figure 43 showing the K* index nowcast performance during a recent geomagnetic storm. Four parameters of the storm are of particular interest for the users: the strength of the storm (i.e. the maximum value of K) and the times of start, maximum, and end of storm. Apparently, if a K value is produced once every 3 hours, the nowcast will offer this value at the end of the 3-hour period (see the white arrows). This means that the uncertainty, with reference to the exact moment of the event, will be as large as 3 hours. If the cadence is 1 hour, the K value will be available at the end of the 1-hour period (see the grey arrow), i.e. the uncertainty is narrowed to 1 hour. With a 1-minute cadence however, the uncertainty becomes less than a minute, which means that, in practice, the exact moment of the event can be pinned down. Overall, the improvement in the K nowcast, by increasing the cadence from 3 hours to 1 minute, is substantial. In this particular storm case, the start of the storm was "moved ahead" by more than 1.5 hours. It should be noted that such significant improvements in the nowcast are to be expected during almost every storm event.

The new 1-minute resolution K* index nowcast and alert service is available online for all interested users.

The EUREF GNSS Infrastructure

The EUREF Permanent GNSS Network (EPN) is a network of continuously operating GNSS stations (Global Navigation Satellite Systems, such as GPS, GLONASS, Galileo, Beidou...) installed at stable locations all over Europe (Figure 44). All contributions to the EPN are provided on a voluntary basis, with more than 100 European agencies and universities involved. The EPN operates under the umbrella of the IAG (International Association of Geodesy) Regional Reference Frame sub-commission for Europe, EUREF. The primary purpose of the EPN is to provide access to the European Terrestrial Reference System (known as ETRS89). Supported by EuroGeographics and endorsed by the INSPIRE Directive 2007/2/EC, the ETRS89 forms the backbone for all geolocation data on the European territory.

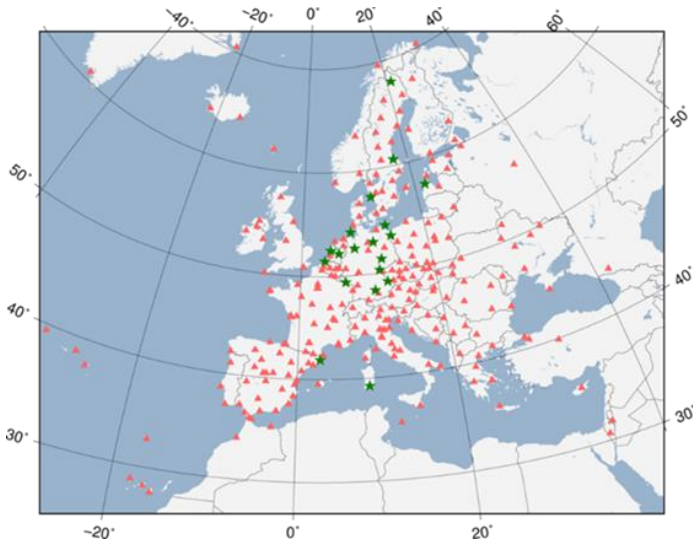

Figure 44: EPN GNSS tracking stations (Status December 2016 - 294 stations in total). Green stars (*) indicate stations included in the EPN in 2016.

The EPN Central Bureau is responsible for the daily monitoring and management of the EPN GNSS network. It is located at the ROB, and supported by the STCE. ROB also maintains the historical GNSS data centre of the EPN, providing European GNSS data and associated metadata going back to 1996 in open access. Since 2009, ROB also operates, with STCE support, one of the three EPN broadcasters, providing access to EPN data in real time.

As EPN Central Bureau, ROB commits significant resources to monitor EPN data availability and quality, and ensures that station owners keep their station metadata promptly up to date. These

metadata are mandatory for a correct analysis of the GNSS data and a proper interpretation of the results. In addition, also operators of national GNSS networks submit today their GNSS metadata to the EPN CB for validation and distribution. As a result, today, ROB is providing access to a unique collection of GNSS meta-data for about 1400 European GNSS stations.

Next to maintaining the ETRS89, the GNSS data from the EPN are used for scientific applications such as the monitoring of tectonic deformations and the conversion of relative tide gauge measurements of sea-level in the same height reference. Within the STCE, the EPN data are core input data for the remote sensing of the Earth's atmosphere (troposphere and ionosphere). Indeed, when travelling from GNSS satellites to receiving EPN antennas located on the Earth, the GNSS radio-frequency signals probe the various atmospheric layers and provide important information on the amount of atmospheric water vapour and the Total Electron Content (TEC).

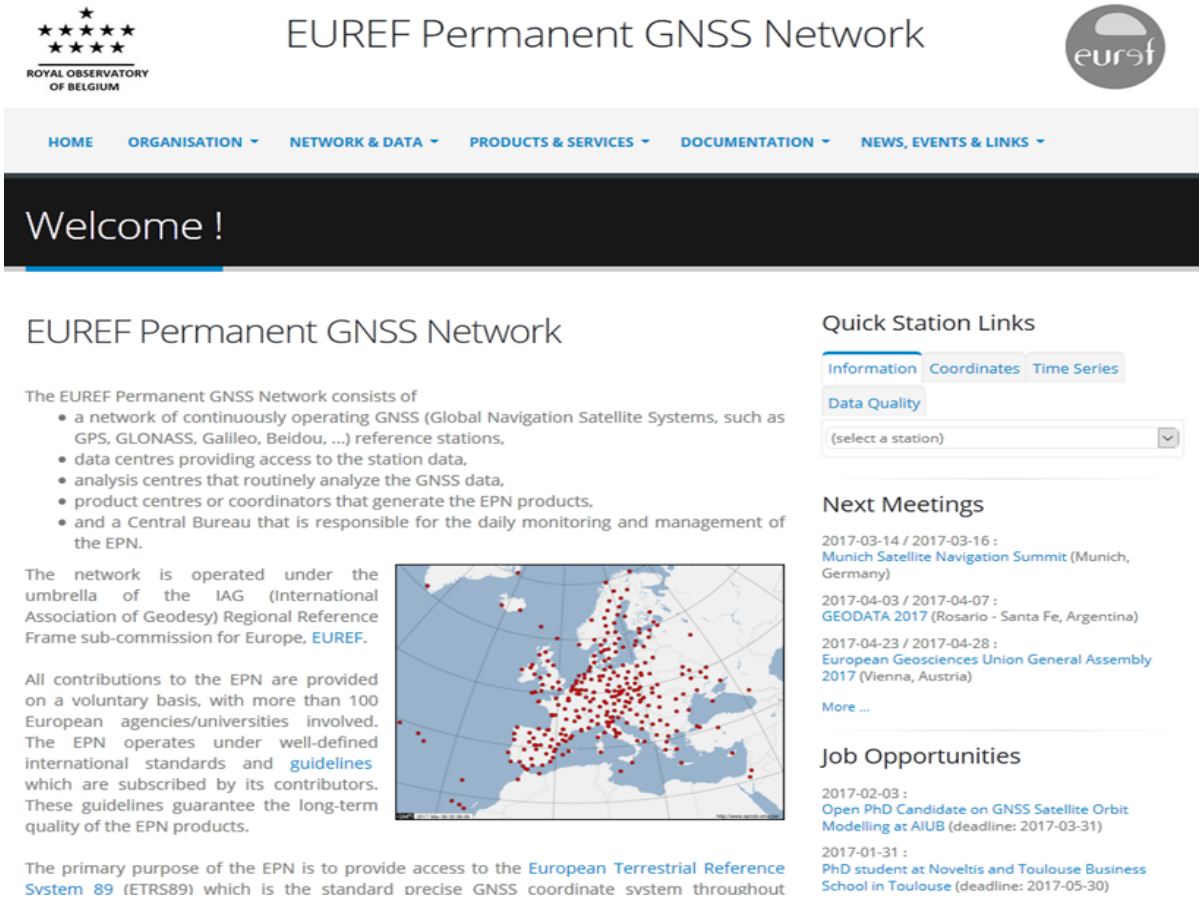

*Figure 45: Home page of the upgraded website of the **EPN Central Bureau**.*

Concerning the tropospheric research and services, all EPN data serve at monitoring the short-term variations of the atmospheric water vapour for meteorological applications (e.g. data assimilation in Numerical Weather Prediction models to improve forecasts). In that context, ROB/STCE contributes to the E-GVAP programme (EIG EUMETNET GNSS Water Vapour Programme) of EUMETNET by running a 24/7 day-in-day-out analysis centre providing several tailored products to European and worldwide meteorologists.

ROB/STCE also analyses the EPN data to validate climate model runs (past climate) and to study the long-term evolution and cycle of the water vapour in the atmosphere (climate research). For that, it performs a homogenous reprocessing of all historical GNSS data with reliable metadata to ensure the stability, precision and accuracy targeted in climate studies (e.g. the BRAIN.be CORDEX.be project). The EPN CB (Central Bureau) offers the major source of GNSS data and reliable metadata in Europe.

From the measured delays in the GNSS signals gathered within the EPN, the STCE computes ionospheric vertical Total Electron Content (TEC) maps over Europe and their variability. They are estimated in near real time every 15 minutes on a 0.5°x0.5° grid. The maps are displayed online at ROB/GNSS and data are available at ftp://gnss.oma.be Next to that, the long-term availability of EPN data were also exploited to develop an empirical model to predict the ionospheric TEC at a given latitude from only one solar parameter in entrance. Finally, the EPN data are used to detect solar radio bursts affecting the GNSS signal reception.

GNSS and the EPN network are in continuous expansion, and therefore increase the number of GNSS signals probing the Earth's atmosphere. In 2016, ROB integrated 19 new stations in the EPN network (Figure 44). The total number of EPN stations is now 294, distributed over 40 countries.

To respond to the changing GNSS landscape (more stations, real-time data, new satellite systems), a brand new EPN CB website (or alternative site ; Figure 45) went online in November 2016. The EPN CB website includes now

- Improved GNSS data quality checks,
- Improved station position time series,
- Improved GNSS data availability and data latency checks,
- Extended monitoring of real-time data streams,
- More intuitive menu structure to navigate through the web site.

In 2016, the number of users of our EPN CB web site increased with 20% compared to the previous year. In total, in 2016, the website had more than 7 million page views.

Monitoring of humidity field from a dense network

In mid-August 2010, torrential rains over Belgium occurred. The origin of this heavy rain was a depression, so called "Yvette" by German meteorologists. A cold temperature anomaly in altitude created this low-pressure situation. At first, a high altitude barometric hollow with a strong north-south component

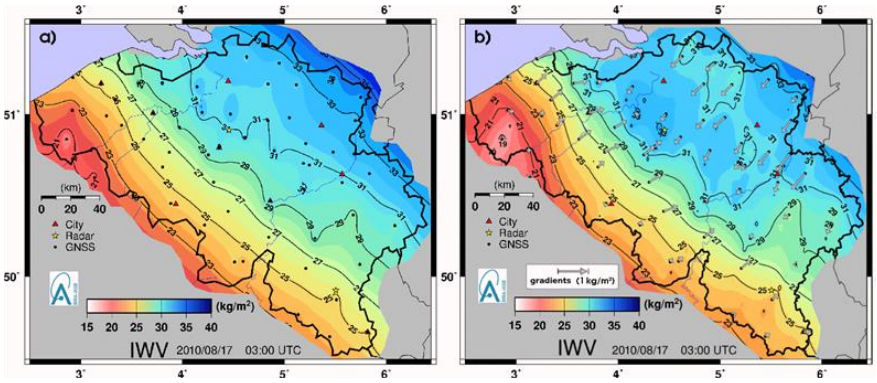

Figure 46: IWV imaging during the torrential rainfall of 15-17 August 2010 over Belgium: a) classical interpolation, b) integrating gradients.

had formed. Then the cold air moved towards the Southern regions, giving birth to this low-pressure area, topped with a dome of cold air. Yvette was surrounded by high pressure almost everywhere (including the famous Russian anticyclone which was a concern to many Muscovites, who were crushed at the same time by an unprecedented heat wave). Considering the slightly static behaviour of the neighboring anticyclones, this depression became mature (with occluded front) and literally emptied itself over Belgium. The location of Yvette had surprising consequences for Europe: at the end of the afternoon of 15 August, the temperature was warmer in Finland (65°N) than in the Northwest of Spain (43°N). This weather situation can be considered as a large-scale convective system, with a passage of a weather front in slow motion, over Belgium. In 72 hours, several Belgian rain gauge stations within a few hundred kilometers distance, measured about 100 mm (or l/m^2) of accumulated rainfall, representing 150% of the mean monthly ratio. This rather rare phenomenon usually occurs in Belgium only once every 20 years during the month of August.

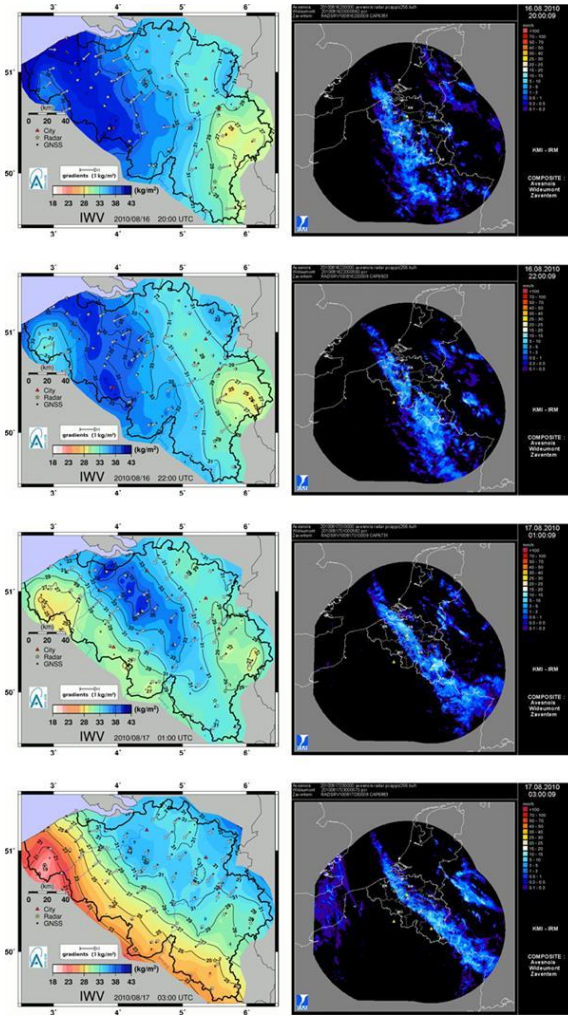

Figure 47: Imaging of IWV integrating horizontal gradients and composite radar precipitation in mm/h.

Belgium is covered by a dense network of about 70 GNSS stations (baselines from 5 to 30 km; see Figure 46). This network is under the responsibility of the Flemish and Walloon Government, the National Geographic Institute, and the Royal Observatory of Belgium (ROB; Eric Pottiaux). Zenith Total Delay of the neutral atmosphere (ZTD) and horizontal gradients of delays, running at the Royal Belgian Institute for Space Aeronomy (BISA; Hugues Brenot) using GAMIT software, have been retrieved with a time-resolution of 15 minutes. Using ZTD combined with synoptic measurements of surface pressure and temperature, provided by the Royal Meteorological Institute of Belgium (RMI; Roeland Van Malderen), images of the 2D field of Integrated Water Vapour content (IWV) have been generated for the whole period of this rainfall event. Figure 46 shows the improvement of the monitoring of the humidity field following the strategy presented by Brenot et al. (2013).

The motivation is to improve the horizontal distribution of the sites used to proceed to interpolated IWV imaging. Considering the axis indicated by a gradient, two additional IWV pseudo-observations have been considered (one wetter in the direction of the vector and the other one drier in the site direction). Tests with the Belgian network have shown that 10 km on either side of the GNSS site is the most relevant distance for detecting small scale structures of the troposphere (of a few kilometers). For each station, wet gradients (differential values in the zenith direction) have been converted into water vapour content gradients. To obtain pseudo-IWV, this kind of gradient can be

propagated horizontally by multiplying its amplitude by the distance in kilometers (Brenot et al., 2014). Figure 47 presents a precise characterization of the water vapour field during this event.

From the 16th to the 17th of August 2010, precipitation occurred over the whole Belgian country, as shown by radar imaging (Figure 47; courtesy of Laurent Delobbe, RMI). Occasionally, it may happen that after a storm, few isolated rain gauge stations record impressive accumulations. In the present case study, the entire country was affected. As well as this sudden heavy rainfall event, moderate rain took place continuously during more than 24 hours in some areas. Such situation is very unusual in summer for Belgium. IWV imaging of Figure 47 shows a contrast of dry and wet areas, basically in the northwest-southeast axis which describes precisely the convergence line between the warm and cold fronts (see at 01:00 UTC on 2010/08/17). The wet region corresponds exactly to the location of radar precipitation. The warm and dry area on the west side of Belgium is clearly identified. This weather front over Belgium was rigorously monitored by GNSS IWV imaging.

The Automatic LIDAR-ceilometer

Radiation fog is the most frequent cause of surface visibility below 1 km, and is one of the most common and persistent weather hazards encountered in aviation and to nearly all forms of surface transport. Forecasting radiation fog can be difficult, a number of approaches have been used to integrate the satellite data, numerical modeling and standard surface observations. These approaches lack generally the vertical and temporal resolution, representation of boundary layer and microphysical processes. They typically do not represent accurately the activation processes of fog droplets that depend on the chemical and physical properties of the aerosols.

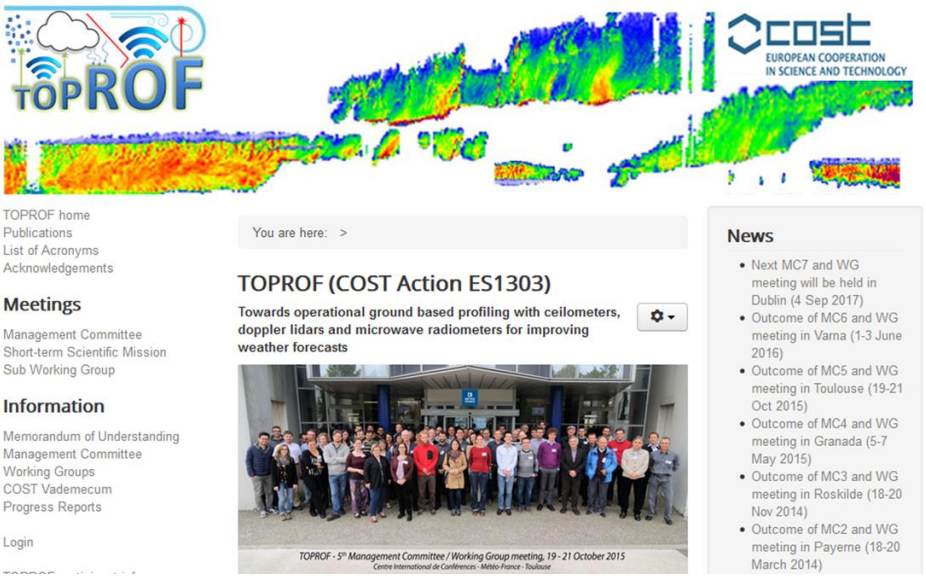

Figure 48: A view on the TOPROF website.

The attenuated backscatter profile measured by automatic LIDAR-ceilometer (ALC), primarily used to detect the cloud base height, may be influenced by atmospheric humidity especially during the preliminary stage of radiation fog formation. The hydroscopic aerosols in the boundary layer see their size increase

with their moisture content inducing an increase of the attenuated backscatter.

The monitoring of the hydroscopic growth process through the attenuated backscatter signal measured by ALC could provide useful warning to forecasters, in support of their fog forecast, minutes to hours prior to formation of radiation fog. In this context, a forward stepwise screening algorithm (PARAFOG) was developed (Haeffelin et al., 2016) and intends for use as a new decision support system for radiation fog forecasting based on analysis of the attenuated backscatter. This development was initiated in the framework of TOPROF (COST-ACTION) activities between the Royal Meteorological Institute of Belgium (RMI) and the Site Instrumental de Recherche par Télédétection Atmosphérique (IPSL, Institut Pierre-Simon Laplace).

RMI with the development of its ALC network in Belgium has now the possibility with PARAFOG to monitor in real-time the first stages of radiation fog in addition to monitor in real-time aerosol plumes such as volcanic ash clouds which might be also a hazard for air traffic.

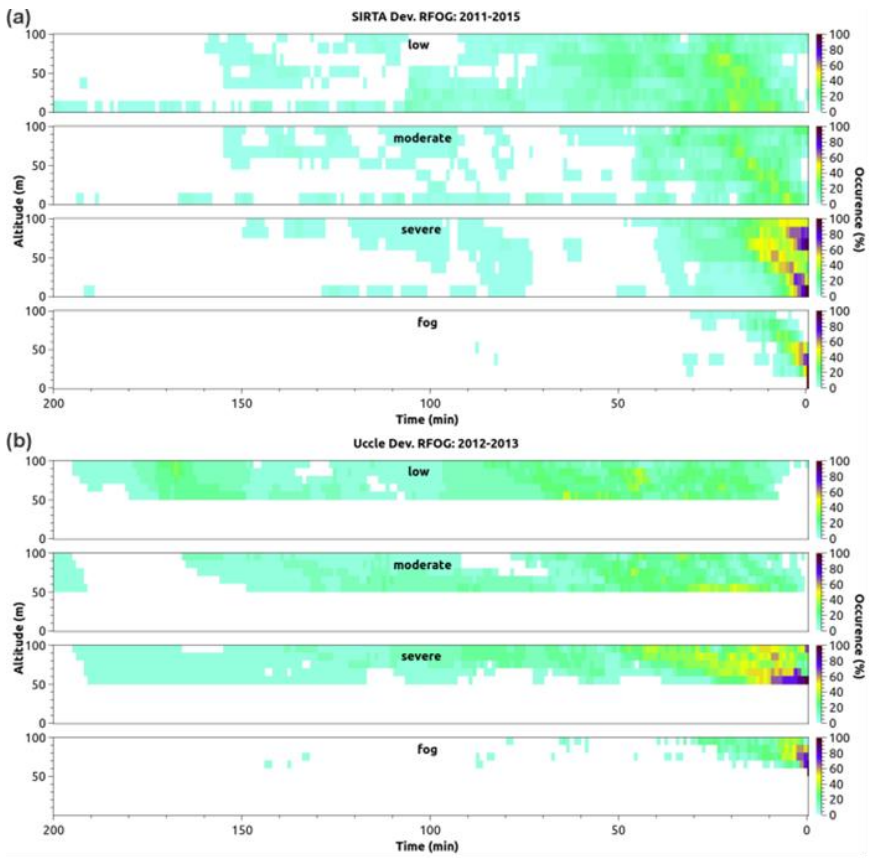

Figure 49: Frequency of occurrence of each alert level (no-alert or low, moderate, severe, fog alerts) for each altitude at ground level and each time before fog occurrence starts at SIRTA (a) and UCCLE (b). For each height / time interval, the sum of occurrence of all alert levels = 100% (incl. no alert).

Based on hydroscopic growth laws and on ALC measurements, PARAFOG derives pre-fog alerts of different levels that are used to provide warning minutes to hours prior to the formation of radiation fog. The study of several fog events observed with ALC on two different sites (one urban and one suburban site) by PARAFOG showed that the pre-fog alert levels don't occur at the same time prior to fog formation and don't occur at the same altitude. In this case, PARAFOG permits to highlight the effect of urban environmental conditions on the first stage of fog formation. Figure 49 shows for each altitude and each time before fog occurrence starts at ground level (at t = 0s), the frequency of occurrence of each alert level including no-alert or low-, moderate-, severe-, and fog-level alerts for the urban site (Uccle) and for the suburban site (SIRTA).

An explanation for the difference observed between the two sites may be that the 3D structure of the city canopy generates small-scale turbulence that tends to mix the air in the shallow surface layer. It slows down the cooling of this layer and makes it more difficult to reach a relative humidity higher than 100% at the surface more favorable for fog formation. Upward vertical motions can lead to cooling of rising moist plumes, enabling to reach a relative humidity higher than 100% a few tens or hundreds of meters above the ground at the urban site.

Figure 50: Getting ready for service! The LOC has its "Last Supper" before the ESWW13 is unleashed.

Publications

This overview of publications consists of three lists: the peer-reviewed articles, the presentations and posters at conferences, and the public outreach talks and publications for the general public. It does not include non-refereed articles, press releases, the daily, weekly and monthly bulletins that are part of our public services, … These data are available at the STCE-website or upon request.

Authors belonging to the STCE have been highlighted in the list of peer reviewed articles.

Peer reviewed articles

1. Bandic, M.; Verbanac, G.; Moldwin, M.; **Pierrard, V.**; Piredda, G.
MLT dependence in the relationship between plasmapause, solar wind and geomagnetic activity based on CRRES: 1990-1991
Journal of Geophysical Research, 121, 4397-4408, 2016, DOI: 10.1002/2015JA022278

2. Besliu-Ionescu, D. ; **Mierla, M.**; Maris-Muntean, G.
Analysis of the Energy Transferred from the Solar Wind into the Magnetosphere during the April 11, 2001 Geomagnetic Storm
Sun and Geosphere, 11, 97-104, 2016

3. **Clette, F.;** Cliver, E.W.; **Lefèvre, L.;** Svalgaard, L.; Vaquero, J.M.; Leibacher, J.W.
Preface to Topical Issue: Recalibration of the Sunspot Number
Solar Physics, 291, 2479-2486, 2016, DOI: 10.1007/s11207-016-1017-8

4. **Clette, F.; Lefèvre, L.**
The New Sunspot Number: Assembling All Corrections
Solar Physics, 291, 2629-2651, 2016, DOI: 10.1007/s11207-016-1014-y

5. **Clette, F.; Lefèvre, L.**; Cagnotti, M.; Cortesi, S.; Bulling, A.
The Revised Brussels-Locarno Sunspot Number (1981 - 2015)
Solar Physics, 291, 2733-2761, 2016, DOI: 10.1007/s11207-016-0875-4

6. Consolini, G.; Giannattasio, F.; Yordanova, E.; Vörös, Z.; Marcucci, M.F.; **Echim, M.;** Chang, T.
On the scaling features of magnetic field fluctuations at non-MHD scales in turbulent space plasmas
Journal of Physics: Conference Series, 767, 1, 012003, 2016, DOI: 10.1088/1742-6596/767/1/012003

7. **D'Huys, E.; Berghmans, D.; Seaton, D.B.**; Poedts, S.
The effect of limited sample sizes on the accuracy of the estimated scaling parameter for power-law-distributed solar data
Solar Physics, 291, 5, 1561-1576, 2016, DOI: 10.1007/s11207-016-0910-5

8. Dissauer, K.; Temmer, M.; Veronig, A.M.; Vanninathan, K.; **Magdalenic, J.**
Projection Effects in Coronal Dimmings and Associated EUV Wave Event
The Astrophysical Journal, 830, 2, 92, 2016, DOI: 10.3847/0004-637X/830/2/92

9. Douša, J.; Dick, G.; Kačmařík, M.; Brožková, R.; Zus, F.; **Brenot, H.;** Stoycheva, A.; Möller, G.; Kaplon, J. *Benchmark campaign and case study episode in central Europe for development and assessment of advanced GNSS tropospheric models and products*
Atmospheric Measurement Techniques, 9, 2989-3008, 2016, DOI: 10.5194/amt-9-2989-2016

10. Dudok de Wit, T.; **Lefèvre, L.; Clette, F.**
Uncertainties in the Sunspot Numbers: Estimation and Implications
Solar Physics, 291, 2709-2731, 2016, DOI: 10.1007/s11207-016-0970-6

11. Gogoberidze, G.; **Voitenko, Y.**
Imbalanced magnetohydrodynamic turbulence modified by velocity shear in the solar wind
Astrophysics and Space Science, 361, 364, 2016, DOI: 10.1007/s10509-016-2950-6

12. Gonzalez, A.; **Delouille, V.;** Jacques, L.
Non-parametric PSF estimation from celestial transit solar images using blind deconvolution
Journal of Space Weather and Space Climate, 6, A1, 2016, DOI: 10.1051/swsc/2015040

13. Grappin, R.; Müller, W.-C.; **Verdini, A.**

Alfvén-dynamo balance and magnetic excess in MHD turbulence
Astronomy & Astrophysics, 589, A131, 2016, DOI: 10.1051/0004-6361/201628097

14. Grison, B.; **Darrouzet, F.**; Santolík, O.; Cornilleau-Wehrlin, N.; Masson, A.
Cluster observations of reflected EMIC-triggered emission
Geophysical Research Letters, 43, 4164–4171, 2016, DOI: 10.1002/2016GL069096

15. Guerova G.; Jones J.; Douša J.; Dick G.; de Haan S.; **Pottiaux E.;** Bock O.; Pacione R.; Elgered G.; Vedel H.; Bender M.
Review of the state of the art and future prospects of the ground-based GNSS meteorology in Europe
Atmospheric Measurement Techniques, 9, 5385-5406, 2016, DOI: 10.5194/amt-9-5385-2016

16. **Gunell, H.**; Andersson, L.; **De Keyser, J.**; Mann, I.
Can the downward current region of the aurora be simulated in the laboratory?
Plasma Physics and Controlled Fusion, 58, 5, 054003, 2016, DOI: 10.1088/0741-3335/58/5/054003

17. Haaland, S.; Andre, M.; Eriksson, A.; Li, K.; Nilsson, H.; Baddeley, L.; Johnsen, C.; **Maes, L.**; Lybekk, B.; Pedersen, A.
Low-energy Ion Outflow Observed by Cluster
Magnetosphere-Ionosphere Coupling in the Solar System (Eds. C.R. Chappell, R.W. Schunk, P.M. Banks, J.L. Burch and R.M. Thorne), American Geophysical Union, 2016, DOI: 10.1002/9781119066880.ch3

18. Haeffelin, M.; **Laffineur, Q.;** Bravo-Aranda, J.-A.; Drouin, M.-A.; Casquero-Vera, J.-A.; Dupont, J.-D.; **De Backer, H.**
Radiation fog formation alerts using attenuated backscatter power from automatic Lidars and ceilometers
Atmospheric Measurement Techniques, 9, 5347-5365, 2016, DOI: 10.5194/amt-9-5347-2016

19. Hayes, L.A.; Gallagher, P.T.; Dennis, B.R.; Ireland, J.; Inglis, A.R.; **Ryan, D.F.**
Quasi-periodic Pulsations during the Impulsive and Decay phases of an X-class Flare
The Astrophysical Journal Letters, 827, L30, 2016, DOI: 10.3847/2041-8205/827/2/L30

20. **Hubert, D.; Lambert, J.-C.; Verhoelst, T.; Granville, J.; Keppens, A.;** … ; **Van Malderen, R.;** … ; and 35 co-authors
Ground-based assessment of the bias and long-term stability of 14 limb and occultation ozone profile data records
Atmospheric Measurement Techniques, 9, 2497-2534, 2016, DOI: 10.5194/amt-9-2497-2016

21. Kronberg, E.A.; Rashev, M.V.; Daly, P.W.; Shprits, Y.Y.; Turner, D.L.; Drozdov, A.; Dobynde, M.; Kellerman, A.C.; Fritz, T.A.; **Pierrard, V.; Borremans**, K; Klecker, B.; Friedel R.
Contamination in electron observations of the silicon detector on board Cluster/RAPID/IES instrument in Earth's radiation belts and ring current
Space Weather, 14, 449-462, 2016, DOI: 10.1002/2016SW001369

22. Krupar, V.; Eastwood, J.; Kruparova, O.; Santolik, O. ; Soucek, J. ; **Magdalenic, J.**; Vourlidas, A.; and 9 co-authors
An Analysis of Interplanetary Solar Radio Emissions Associated with a Coronal Mass Ejection
The Astrophysical Journal Letters, 823, L5, 2016, DOI: 10.3847/2041-8205/823/1/L5

23. **Lefèvre, L.**; Aparicio, A.J.P.; Gallego, M.C.; Vaquero, J.M.
An Early Sunspot Catalog by Miguel Aguilar for the Period 1914 - 1920
Solar Physics, 291, 2609-2628, 2016, DOI: 10.1007/s11207-016-0905-2

24. **Lefèvre, L.**; Vennerstrøm, S.; Dumbović, M.; Vršnak, B.; Sudar, D.; Arlt, R.; **Clette, F.; Crosby, N.B.**
Detailed Analysis of Solar Data Related to Historical Extreme Geomagnetic Storms: 1868 - 2010
Solar Physics, 291, 1483-1531, 2016, DOI: 10.1007/s11207-016-0892-3

25. Lemaire, J.; **Stegen, K.**
Improved Determination of the Location of the Temperature Maximum in the Corona
Solar Physics, 291, 3659-3683, 2016, DOI: 10.1007/s11207-016-1001-3

26. Maes, L.; Maggiolo, R.; De Keyser, J.
Seasonal variations and north-south asymmetries in the polar wind outflow due to solar illumination
Annales Geophysicae, 34, 961–974, 2016, DOI: 10.5194/angeo-34-961-2016

27. Masias-Meza, J.; Dasso, S.; Demoulin, P.; **Rodriguez, L.**; Janvier, M.
Superposed epoch study of ICME sub-structures near Earth and their effects on Galactic cosmic rays
Astronomy & Astrophysics, 592, A118, 2016, DOI: 10.1051/0004-6361/201628571

28. Moon, K.; Li, J.; **Delouille, V.; De Visscher, R.**; Watson, F.; Hero III, A.O.
Image patch analysis of sunspots and active regions. I. Intrinsic dimension and correlation analysis
Journal of Space Weather and Space Climate, 6, A2, 2016, DOI: 10.1051/swsc/2015044

29. Moon, K.; **Delouille, V.;** Li, J.; **De Visscher, R.**; Watson, F.; Hero III, A.O.
Image patch analysis of sunspots and active regions. II. Clustering via dictionary learning
Journal of Space Weather and Space Climate, 6, A3, 2016, DOI: 10.1051/swsc/2015043

30. Nilsson, H.; Hamrin, M.; Pitkänen, T.; Karlsson, T.; Slapak, R.; Andersson, L.; **Gunell, H.**; Schillings, A.; Vaivads, A.
Oxygen ion response to proton bursty bulk flows
Journal of Geophysical Research: Space Physics, 121, 8, 7535-7546, 2016, DOI: 10.1002/2016JA022498

31. Pant, V.; **Willems, S.; Rodriguez, L.; Mierla, M.;** Banerjee, D.; Davies, J.
Automated Detection Of Coronal Mass Ejections In STEREO Heliospheric Imager Data
The Astrophysical Journal, 833, 80, 2016, DOI: 10.3847/1538-4357/833/1/80

32. Patsourakos, S.; Georgoulis, M.K.; Vourlidas, A.; … ; **Podladchikova, O.;** and 32 co-authors
The Major Geoeffective Solar Eruptions of 7 March 2012: Comprehensive Sun-to-Earth Analysis
The Astrophysical Journal, 817, 1-22, 2016, DOI: 10.3847/0004-637X/817/1/14

33. Pavluk, Yu.; **Podladchikova, O.**; Podladchikov, V.N.
Stereoscopic Analysis of A Coronal Wave
System Research Information Technologies, 97, 73-77, 2016, DOI: 10.20535/SRIT.2308-8893.2016.2.09

34. **Pierrard V.;** Lazar M.; Poedts, S.; Stverak, S.; Maksimovic, M.; Tranicek, P.M.
The Electron Temperature and Anisotropy in the Solar Wind. 1. Comparison of the core and halo populations
Solar Physics, 291, 2165-2179, 2016, DOI: 10.1007/s11207-016-0961-7

35. Pierrard, V.; Lopez Rosson, G.
The effects of the big storm events in the first half of 2015 on the radiation belts observed by EPT/PROBA-V
Annales Geophysicae, 34, 75-84, 2016, DOI: 10.5194/angeo-34-75-2016

36. **Pierrard V.; Moschou S.;** Lazar, M.; **Lopez Rosson G.; Borremans, K.**
Kinetic models for solar wind and inner magnetosphere
30th International Symposium on Rarefied Gas Dynamics, AIP Conference Proceedings, 1786, 160001, AIP Publishing, Henning Struchtrup Ed., 2016, DOI: 10.1063/ 1.4967658

37. Plotnikov, I.; Rouillard, A.P.; Davies, J.; Bothmer, V.; Eastwood, J. P.; Gallagher, P.T.; Harrison, R.A.; Kilpua, E.; Möstl, C.; **Rodriguez, L.**
Long-Term Tracking of Corotating Density Structures using Heliospheric Imaging
Solar Physics, 291, 6, 1853-1875, 2016, DOI: 10.1007/s11207-016-0935-9

38. **Rodriguez, L.**; Masías-Meza, J.J.; Dasso, S.; Demoulin, P.; **Zhukov, A.N.**; Gulisano, A.M.; **Mierla, M.**; Kilpua, E.; **West, M.**; Lacatus, D.; Paraschiv, A.R.; Janvier, M.
Typical Profiles and Distributions of Plasma and Magnetic Field Parameters in Magnetic Clouds at 1 AU
Solar Physics, 291, 7, 2145-2163, 2016, DOI: 10.1007/s11207-016-0955-5

39. **Ryan, D.F.; Dominique, M.; Seaton, D.B.; Stegen, K.**; White, A.
Effects of flare definitions on the statistics of derived flare distributions
Astronomy & Astrophysics, 592, A133, 2016, DOI: 10.1051/0004-6361/201628130

40. Sapundjiev, D.; Stankov, S.M.
Statistical analysis and modeling of the local ionospheric critical frequency: a mid-latitude single-station model for use in forecasting
Acta Geophysica, 64, 3, 810-824, DOI: 10.1515/acgeo-2016-0029

41. Shevchuk, N.V.; Melnik, V.N.; Poedts, S.; Dorovskyy, V.V.; **Magdalenic, J.**; Konovalenko, A.A.; Brazhenko, A.I.; Briand, C.; Frantsuzenko, A.V.; Rucker, H.O.; Zarka, P.
The Storm of Decameter Spikes During the Event of 14 June 2012
Solar Physics, 291, 1, 211-228, 2016, DOI: 10.1007/s11207-015-0799-4

42. Slemzin, V.A.; Ulyanov, A.; Gaikovich, K.; Kuzin, S.V.; Perstov, A.; **Berghmans, D.; Dominique, M.**
Validation of the Earth atmosphere models using the solar EUV solar occultation data from the CORONAS and PROBA 2 instruments
Journal of Space Weather and Space Climate, 6, A7, 2016, DOI: 10.1051/swsc/2015045

43. Stolovitch, L.; **Verstringe, F.**
Holomorphic Normal Form of Nonlinear Perturbations of Nilpotent Vector Fields
Regular and chaotic dynamics, 21, 410-436, 2016, DOI: 10.1134/S1560354716040031

44. Usanova, M.E.; Mann, I.R.; **Darrouzet, F.**
EMIC Waves in the Inner Magnetosphere
Low-Frequency Waves in Space Plasmas (Eds. A. Keiling, D.-H. Lee, V. Nakariakov),. American Geophysical Union,

Geophysical Monograph Series, 2016, DOI: 10.1002/9781119055006.ch5

45. Valentini, F.; Perrone, D.; Stabile, S.; Pezzi, O.; Servidio, S.; De Marco, R.; Marcucci, F.; Bruno, R.; Lavraud, B.; **De Keyser, J.**; Consolini, G.; Brienza, D.; Sorriso-Valvo, L.; Retino, A.; Vaivads, A.; Salatti, M.; Veltri, P.
Differential kinetic dynamics and heating of ions in the turbulent solar wind
New Journal of Physics, 18, 125001, 2016, DOI: 10.1088/1367-2630/18/12/125001

46. **Van Malderen, R.;** Allaart, M.A.F.; **De Backer, H.;** Smit, H.G.J.; **De Muer, D.**
On instrumental errors and related correction strategies of ozonesondes: possible effect on calculated ozone trends for the nearby sites Uccle and De Bilt
Atmospheric Measurement Techniques, 9, 3793-3816, 2016, DOI: 10.5194/amt-9-3793-2016

47. Vaquero, J.M. ; Svalgaard, L.; Carrasco, V.M.S.; **Clette, F.; Lefèvre, L.**; Gallego, M.C.; Arlt, R.; Aparicio, A. J.P.; Richard, J.-G.; Howe, R.
A Revised Collection of Sunspot Group Numbers
Solar Physics, 291, 9-10, 3061-3074, 2016, DOI: 10.1007/s11207-016-0982-2

48. Vennerstrom, S.; **Lefèvre, L**.; Dumbović, M.; **Crosby, N.B.**; Malandraki, O.; Patsou, I.; **Clette, F.**; Veronig, A.; Vršnak, B.; Leer, K.; Moretto, T.
Extreme Geomagnetic Storms - 1868 - 2010
Solar Physics, 291, 1447-1481, 2016, DOI: 10.1007/s11207-016-0897-y

49. Verhulst, T.G.W.; Sapundjiev, D.; Stankov, S.M.
High-resolution ionospheric observations and modeling over Belgium during the solar eclipse of 20 March 2015 including first results of ionospheric tilt and plasma drift measurements
Advances in Space Research, 57, 11, 2407-2419, DOI: 10.1016/j.asr.2016.03.009

50. Voiculescu, M.; Nygren, T.; Aikio, A.; Vanhamaki, H.; **Pierrard, V.**
Post midnight troughs at high latitudes in summer
Journal of Geophysical Research: Space Physics, 121, 12, 12171-12185, 2016, DOI: 10.1002/2016JA02336

51. Voitenko, Y.; De Keyser, J.
MHD-Kinetic Transition in Imbalanced Alfvénic Turbulence
The Astrophysical Journal Letters, 832, L20, 2016, DOI: 10.3847/2041-8205/832/2/L20

52. Wauters, L. ; Dominique, M.; Dammasch, I.E.
LYRA Mid-Term Periodicities
Solar Physics, 291, 2135–2144, 2016, DOI: 10.1007/s11207-016-0960-8

53. Zhao, J.S.; **Voitenko, Y.**; Wu, D.J.; Yu, M.Y.
Kinetic Alfvén turbulence below and above ion cyclotron frequency
Journal of Geophysical Research: Space Physics, 121, 5-18, 2016, DOI: 10.1002/2015JA021959

Presentations and posters at conferences

1. Attié, R.; De Visscher, R.; Delouille, V.
Characterization of active regions' time evolution in view of solar flare prediction
ESWW13, Oostende, Belgium, 14-18 November 2016

2. Baire Q.; Bergeot N.; Bruyninx C.; Chevalier J.-M.; Legrand J.; Pottiaux E.; Voet P.; De Doncker F.
National Report of Belgium
EUREF Symposium, San Sebastian, Spain, 25-27 May 2016

3. Berckmans, J.; Pottiaux, E.; Van Malderen, R.; Hamdi, R.
Evaluation of the atmospheric water vapor in the regional climate model ALARO coupled to the land surface scheme SURFEX using GNSS observations
COST ES1206 GNSS4SWEC Summer School/Workshop, Potsdam, Germany, 29 August-2 September 2016

4. Bergeot N.; Darrouzet F.; Rasson J.; Tsagouri I.; Lichtenberger J.; Marqué C.; Chevalier J.-M.; Martinez A.; Katsiyannis A.C.; Bruyninx C.; Ranvier S.; Lamy H.; Tétard C.; de Keyser J.; Bracke S.; Gonsette A.; Belehaki A.
GNSS and Space Weather in East Antarctica around the Princess Elisabeth Belgian base
SCAR 2016 Conference, Kuala Lumpur, Malaysia, 20-30 August 2016

5. Bergeot N.; Witasse O.; Kofman W.; Grima C.; Mouginot J.; Peter K.; Pätzold M.; Dehant V.
Study of the Total Electron Content in Mars ionosphere from MARSIS data set
EGU General Assembly 2016, Vienna, Austria, 17-22 April 2016

6. Bergeot N.; Chevalier J.-M.; Bruyninx C.; Denis G.; Camelbeeck T.; van Dam T.; Francis O.
Study of Space Weather Imparc on Antarctica Ionosphere from GNSS Data
BNCGG - BNCAR symposium, Brussels, Belgium, 29 April 2016

7. Berghmans, D.; Rochus, P.
Status EUI development following mini-consortium meeting 2016 Sept 19
Solar Orbiter - Science Working Team, London, UK, 21 September 2016 (invited talk)

8. Berghmans, D.
Tracing back Space Weather data from real-time to the distant past
Space Climate School 6, Levi, Finland, 30 March-3 April 2016 (invited talk)

9. Berghmans, D.; Verbeeck, C.
Observing CMEs with Solar Orbiter (during remote sensing)
2nd Solar Orbiter SAP meeting, Alcala, Spain, 13 April 2016 (invited talk)

10. Berghmans, D.; Zender, J.
PROBA2, Confirmation 2017+2018 and Extension 2019+2020
Joint meeting of the ESA SSEWG and AWG committees, ESTEC, Noordwijk, The Netherlands, 12 October 2016 (invited talk)

11. Berghmans, D.
Coronal EUV imagers: a sunny view thanks to PRODEX
PRODEX 30 years, ESTEC, Noordwijk, The Netherlands, 5-6 September 2016 (invited talk)

12. Boler F.; Brown N.; Fraser R.; Noll C.; Squibb M.; Bradke M.; Bruyninx C.; Wiesensarter E.; Romero I.
Collaborative Development of a Standards-Based XML System for IGS Site Log Metadata Management and Dissemination
IGS Workshop, Sydney, Australia, 8-12 February 2016

13. Bourgoignie, B.; Bogdan N.; Verstringe, F.; Berghmans, D.
JHelioviewer
ESWW13, Oostende, Belgium, 14-18 November 2016 (poster)

14. Brenot, H. et al.
Simulations of delays and gradients: test of improvements and visualization tools in the frame of the Benchmark campaign
COST ES1206 - GNSS4SWEC: 4th Workshop, Reykjavik, Iceland, 08-10 March 2016

15. Bruyninx C.; Baire Q.; Legrand J.; Pottiaux E.; Roosbeek F.
Twenty Years of EPN: Network Challenges Ahead
EUREF Symposium, San Sebastian, Spain, 25-27 May 2016

16. Bruyninx C.
EPN Central Bureau Upgrades in Support of Evolving EUREF Priorities
IGS Workshop, Sydney, Australia, 8-12 February 2016

17. Bruyninx C.
Sharing Geodetic GNSS Data
RDA Europe Science Workshop, Paris, France, 19-20 April 2016

18. Bruyninx C.; Bergeot N.; Camelbeeck T.; van Dam T.; Francis O.; Tabibi S.

High-precision GNSS Infrastructure Around the Princess Elisabeth Base
BNCGG - BNCAR symposium, Brussels, Belgium, 29 April 2016

19. Chevalier J.-M.; Bergeot N.; Marqué C.; Bruyninx C.
Near real-time Detection of Solar Radio Bursts Impacting the GNSS Signal Reception
ESWW13, Oostende, Belgium, 14-18 November 2016

20. Chevalier J.-M., Bergeot N., Marqué C. and Bruyninx C.
Near-real time detection of solar radio burst impacting the GNSS signal reception
ESWW13, Oostende, Belgium, 14-18 November 2016

21. Chevalier J.-M.; Bergeot N.; Marqué C.; Bruyninx C.
Near-real time detection of GNSS signal reception fades due to solar radio bursts
ESWW13, Oostende, Belgium, 14-18 November 2016

22. Chowdhury, P. ; Srivastava, A.K. ; Dolla, L.; Dominique, M.; Moon, Y.-J.; Dwivedi, B.N.
Multi-wavelength Analysis of Quasi-periodic Pulsations in X-rays during a Solar Flare
Dynamic Sun: I. MHD Waves and Confined Transients in the Magnetized Atmosphere, Varanasi, India, 22-26 February 2016 (poster)

23. Chu, X.; Bortnik, J.; Li, W.; Angelopoulos, V.; Thorne, R.M.; Denton, R.E.; Menietti, J.D.; Wang, Y.; Darrouzet, F.
Erosion and refilling of the plasmasphere studied by neural network based three-dimensional plasmaspheric model
4th Joint Cluster-THEMIS Workshop, Palm Springs, California, USA, 7-12 November 2016

24. Crosby, N.B.; Veronig, A.; Rodriguez, L.; Vrsnak, B.; Vennerstrom, S.; Malandraki, O.; Dalla, S.; Srivastava, N.
COMESEP: bridging the gap between the SEP, CME and terrestrial effects scientific communities
EGU General Assembly 2016, Vienna, Austria, 17-22 April 2016 (poster)

25. Dammasch, I.E.; Dominique, M.; Machol, J.
Rescaled PROBA2/LYRA data used as GOES X-ray flux proxy
ESWW13, Proba2 SWT Meeting, Oostende, Belgium, 14-18 November 2016 (poster)

26. Dammasch, I.E.; Dominique, M.; Machol, J.
Rescaled PROBA2/LYRA data used as GOES X-ray flux proxy
XIVth Hvar Astrophysical Colloquium, Hvar, Croatia, 30 September 2016

27. Darrouzet, F.; Lichtenberger, J.; De Keyser, J.
Recent advances in plasmaspheric observation: Ground-based remote sensing (new magnetic VLF antenna in Antarctica) and space based in situ measurement (Cluster and Van Allen Probes data)
7th VERSIM workshop, Western Cape, South Africa, 19-23 September 2016

28. Darrouzet, F.; De Keyser, J.; Decreau, P.; Goldstein, J.; Kurth, W.; De Pascuale, S.; Santolik, O.
Plasmaspheric plume analysis during the 2013 Cluster close separation campaign, augmented with Van Allen Probes data and a plasmapause test particle simulation
4th Joint Cluster-THEMIS Workshop, Palm Springs, California, USA, 7-12 November 2016

29. Darrouzet, F.; Lichtenberger, J.; De Keyser, J.
AWDA in Antarctica: Installation of a magnetic antenna at Princess Elisabeth station during the BELARE 2015-2016 campaign
BNCGG - BNCAR symposium, Brussels, Belgium, 29 April 2016 (poster)

30. de Franceschi G.; Bergeot N. and others
GRAPE "GNSS Research and Application for Polar Environment"
SCAR 2016 Conference, Kuala Lumpur, Malaysia, 20-30 August 2016

31. De Keyser, J.; De Donder, E.; Echim, M.; Crosby, N.B.; Rodriguez, L.; Devos, A.; Berghmans, D.; Poedts, S.; Keil, R.; Jiggens, P.
VSWMC Phase 2 Customer Requirements
ESWW13, Oostende, Belgium, 14-18 November 2016 (poster)

32. De Keyser, J.; Maes, L.; Maggiolo, R.; Haaland, S.
Assessment of possible mechanisms responsible for dawn-dusk asymmetry of the magnetopause: Part of the Status Report on Work Package 2.2
IAP TOPERS annual meeting, ROB, Brussels, 22 January 2016

33. D'Huys, E.; Berghmans, D.; SWAP Team
SWAP Status Update
ESWW13, Proba2 SWT Meeting, Oostende, Belgium, 14-18 November 2016 (invited talk)

34. D'Huys, E.; Berghmans, D.; SWAP Team
SWAP Status Update
PROBA2 SWT, Brussels, Belgium, 28 June 2016 (invited talk)

35. D'Huys, E.; Seaton, D.B.; Poedts, S.; Berghmans, D.
Observing the Unobservable: Identification and Characterisation of Stealth Coronal Mass Ejections (Thesis Talk)
Solar Physics Division Meeting, Boulder, Colorado, USA, 3 June 2016

36. D'Huys, E.; Talpeanu, D. C.; Poedts, S.; Mierla, M.
Numerical and Observational Study of Stealth Coronal Mass Ejections

CHARM meeting, ULB, Brussels, Belgium, 2 May 2016

37. D'Huys, E.
Observing the Unobservable Identification and Characterization of Stealth Coronal Mass Ejections
PhD public defense at KU Leuven, Belgium, 18 January 2016

38. Dolla, L.; Stegen, K.; Zhukov, A.N.
Constraining the radial profiles of temperature and wind velocity with PROBA-3/ASPIICS
Proba-3 SWT5 meeting, Prague, Czech Republic, 28-30 November 2016

39. Dolla, L.
Spectral contributions through the Wide-band filter of PROBA-3/ASPIICS
PROBA-3 SWT4 meeting, Torino, Italy, 18-19 May 2016

40. Dolla, L.
How to model the solar spectrum for the analysis of passbands data of PROBA-3/ASPIICS?
PROBA-3 SWT4 meeting, Torino, Italy, 18-19 May 2016

41. Dolla, L.
Spectral contributions through the green line filter of PROBA-3/ASPIICS
PROBA-3 SWT4 meeting, Torino, Italy, 18-19 May 2016

42. Dominique, M.; Dammasch, I.E.; Katsiyannis, A.C.; Wauters, L.
LYRA status update
ESWW13, Proba2 SWT Meeting, Oostende, Belgium, 14-18 November 2016 (invited talk)

43. Dominique, M.; Dammasch, I.E.; Wauters, L.; Katsiyannis, A.C.
LYRA status update
PROBA2 SWT, Brussels, Belgium, 28 June 2016

44. Dominique, M.; Dolla, L.; Zhukov, A.N.; Lapenta, G.
Multi-instrument observation of sub-minute quasi-periodic pulsations in solar flares
IBUKS 2016, KU Leuven, Leuven, Belgium, 13-17 June 2016

45. Dominique, M.; Zigman, V.
How can LYRA be used to analyze the impact of flares on the ionization rate in the ionospheric D-region?
CHARM meeting, ULB, Brussels, Belgium, 2 May 2016

46. Echim, M. and the STORM team
Solar system plasma turbulence: observations, intermittency and multifractals
2nd THOR Workshop, Barcelona, Spain, 27-29 September 2016 (poster)

47. Fernandes R. and EPOS-IP WP10 team (including Bruyninx C.; Baire Q.)
EPOS-IP WP10: Services and Data Provision for the GNSS Community
EGU General Assembly 2016, Vienna, Austria, 17-22 April 2016

48. García-Rigo A.; … ; Bergeot N. and 23 others
RTIM-WG: IAG's Real Time Ionosphere Monitoring Working Group Current status, outcomes and first results
IAG Commission 4 Positioning and Applications Symposium, Wroclaw, Poland, 4-7 September 2016

49. Grimalsky, V.V.; De Keyser, J.; Krankowski, A.; Parnowski, A.S.; Rapoport, Y.G.; Selivanov, Y.A.; Tkachenko, E.N.; Voitenko, Y.
Advanced Algorithm For The Complex Modeling Seismoionospheric Coupling (SIC) and the Formation of Wave Structures in the Ionosphere
16th Ukrainian Conference on Space Research, Odessa, Ukraine, 22-26 August 2016

50. Haaland, S.; Laundal, K.; Maes, L.; Baddeley, L.; Lybekk, B.
North-south asymmetries in cold ion outflow and lobe density
EGU General Assembly 2016, Vienna, Austria, 17-22 April 2016

51. Haaland, S.; Maes, L.; Laundal, K.; Lybekk, B.; Pedersen, A.
North-south asymmetries in lobe density and cold ion outflow
4th Joint Cluster-THEMIS Workshop, Palm Springs, California, USA, 7-12 November 2016 (poster)

52. Haeffelin, M.; Laffineur, Q.; Bravo-Aranda, J.-A.; Drouin, M.-A.; Casquero-Vera, J.-A.; Dupont, J.-D.; De Backer, H.
PARAFOG: Pre-FOG alert tool based on ceilometer measurements
Journée Scientifique SIRTA 2016, Paris, France, 23 June 2016 (poster)

53. Harrison, R.; Davies, J.; Barnes, C.; Perry, C.; Möstl, C.; Rouillard, A.; Bothmer, V.; Rodriguez, L.; Eastwood, J.; Kilpua, E.; Gallagher, P.; Odstrcil, D.
Highlights and results from the FP7 HELCATS (Heliospheric Cataloguing, Analysis and Techniques Service) project
ESWW13, Oostende, Belgium, 14-18 November 2016

54. Harrison, R.; Davies, J.; Perry, C.; Möstl, C.; Rouillard, A.; Bothmer, V.; Rodriguez, L.; Eastwood, J.; Kilpua, E.; Gallagher, P.
HELCATS - Heliospheric Cataloguing, Analysis and Techniques Service
First VarSITI General Symposium and annual HELCATS meeting, Albena, Bulgaria,6-10 June 2016

55. Katsiyannis, A.C.; Dominique, M.; De Keyser, J.; Berghmans, D.; Kruglanski, M.; Dammasch, I.E.; Borremans, K.; De Donder, E.
The discovery of an electron current at Earth's McIlwain L=6
ESWW13, Oostende, Belgium, 14-18 November 2016 (poster)

56. Katsiyannis, A.C.; Dominique, M.; Berghmans, D.; Dammasch, I.E.
The LYRA Perturbations Project
PROBA2 SWT, Brussels, Belgium, 28 June 2016

57. Katsiyannis, A.C.; Dominique, M.; Pierrard, V.; Borremans, K.; De Keyser, J.; Berghmans, D.; Kruglanski, M.; Dammasch, I.E.; De Donder, E.
The discovery of an electron current at Earth's McIlwain L=6
SDO 2016: Unraveling the Sun's complexity, Burlington, Vermont, USA, 17-21 October 2016

58. Katsiyannis, A.C.; Dominique, M.; Pierrard, V.; Borremans, K.; De Keyser, J.; Berghmans, D.; Kruglanski, M.; Dammasch, I.E.; De Donder, E.
The discovery of an electron current at Earth's McIlwain L=6
SDO 2016: Unraveling the Sun's complexity, Burlington, Vermont, USA, 17-21 October 2016 (poster)

59. Kilpua, E.; Harrison, R.; Davies, J.; Möstl, C.; Bothmer, V.; Eastwood, J.; Gallagher, P.; Rodriguez, L.; Rouillard, A.; Isavnin, A.
Heliospheric Cataloguing, Analysis and Technique Service (HELCATS)
Global modelling of the space weather chain, Espoo, Finland (2016)

60. Klos, A.; Teferle, F.N.; Bock, O.; Pottiaux, E.; Van Malderen, R.; Bogusz, J.
A homogenization of GNSS tropospheric data with autoregressive process
COST ES1206 GNSS4SWEC Summer School/Workshop, Potsdam, Germany, 29 August-2 September 2016

61. Klos, A.; Bock, O.; Pottiaux, E.; Van Malderen, R.; Bogusz, J.
Autoregressive Processes in Homogenization of GNSS Tropospheric Data
AGU Fall Meeting, San Francisco, USA, 12-16 December 2016

62. Kolmasova, I.; Santolik, O.; Darrouzet, F.; Pickett, J.S.; Cornilleau-Wehrlin, N.
Properties of Whistler-Mode Waves in Plasmaspheric Plumes
International Symposium on Recent Observations and Simulations of the Sun-Earth System III (ISROSES-III), Varna, Bulgaria, 11-16 September 2016

63. Kraaikamp, E.; Verbeeck, C.
Solar Demon - automated detection of flares, dimmings and EUV waves in near real-time on SDO/AIA
Modern data-analysis in Solar Physics, RAS, London, UK, 8 January 2016

64. Kraaikamp, E.; Verbeeck, C.
Online demo of Solar Demon
ESWW13, Oostende, Belgium, 14-18 November 2016 (poster)

65. Krupar, V.; Magdalenic, J.; West, M.; D'Huys, E.; Prech, L.; Kruparova, O.
Radio signatures of the shock waves and their association with coronal structures seen by the SWAP and coronagraph observations
ESWW13, Oostende, Belgium, 14-18 November 2016 (poster)

66. Laffineur, Q.; Haeffelin, M.
PARAFOG: a new decision support system for radiation fog forecasting by using ALC
COST ES1303 - TOPROF 6th MC and WG meeting, Varna, Bulgaria, 01-03 June, 2016

67. Laffineur, Q.; Haeffelin, M.; Dupont, J.-C.; Bravo-Aranda, J.A.; Drouin, M.-A.; De Backer, H.
Statistical analysis of parameters computed by PARAFOG: a new pathway to increase knowledge on the early stage of fog formation
7th International Conference on Fog, Fog Collection and Dew, Wroclaw, Poland, 24-29 July 2016 (poster)

68. Laffineur, Q.; Haeffelin, M.; Dupont, J.-C.; Bravo-Aranda, J.A.; Drouin, M.-A.; Casquero-Vera J.A.; De Backer, H.
PARAFOG: A new decision support system for radiation fog forecasting based on analysis of ALC measurements
7th International Conference on Fog, Fog Collection and Dew, Wroclaw, Poland, 24-29 July 2016

69. Lamy, H.; Calders, S.; Gamby, E.; Ranvier, S.; Anciaux, M.; Tétard, C.; De Keyser, J.
BRAMS: a new facility to characterize meteoroids and their interactions with Earth's atmosphere
EGU General Assembly 2016, Vienna, Austria, 17-22 April 2016 (poster)

70. Lazar, M.; Poedts, S.; Fichtner, H.; Pierrard, V.
Suprathermal Kappa populations in the solar wind: from observational evidences to realistic modelling
43rd European Physical Society (EPS) Conference, Leuven, Belgium, 4-8 July 2016

71. Lefèvre, L.; Aparicio, A.; Gallego, M.; Vaquero, J.
Recovering a sunspot catalog for the 1914-1920 period from Madrid

Space Climate School 6, Levi, Finland, 30 March-3 April 2016 (poster)

72. Lefèvre, L.; Dudok de Wit T.; Clette, F.
Uncertainties in the Sunspot Number
Space Climate School 6, Levi, Finland, 30 March-3 April 2016 (poster)

73. Lopez Rosson, G.; Pierrard, V.
The effects of the storm events in 2015 on the radiation belts observed by EPT/PROBA-V
UNITER meeting, UCL, Belgium, 26 February 2016

74. Lopez Rosson, G.; Pierrard, V.
The effects of the storm events in 2015 on the radiation belts observed by EPT/PROBA-V
UNITER meeting, UCL, Belgium, 26 February 2016 (poster)

75. Lopez Rosson, G.; Pierrard, V.
The effects of the storm events in 2015 on the radiation belts observed by EPT/PROBA-V
EGU General Assembly 2016, Vienna, Austria, 17-22 April 2016

76. Lopez Rosson, G.; Pierrard, V.
The effects of the storm events in 2015 on the radiation belts observed by EPT/PROBA-V
7th VERSIM workshop, Western Cape, South Africa, 19-23 September 2016

77. Maes, L.; Maggiolo, R.; André, M.; Li, K.; Eriksson, A.; Haaland, S.
The polar wind: solar illumination, seasonal variations, and north-south asymmetry
EGU General Assembly 2016, Vienna, Austria, 17-22 April 2016 (poster)

78. Maes, L.; Maggiolo, R.; André, M.; Eriksson, A.; Haaland, S.; Li, K.
Solar zenith angle dependency, seasonal variations and N-S asymmetry of the polar wind
4th Joint Cluster-THEMIS Workshop, Palm Springs, California, USA, 7-12 November 2016 (poster)

79. Maes, L.; Maggiolo, R.; De Keyser, J.
Illumination and outflow over the polar caps: Part of the Status Report on Work Package 2.2
IAP TOPERS annual meeting, ROB, Brussels, 22 January 2016

80. Magdalenic, J.
Radio observations and Space Weather Research
The 4th AOSWA Workshop 2016, Jeju, South Korea, 24-27 October 2016 (invited talk)

81. Magdalenic, J.
Radio triangulation - mapping the 3D position of the solar radio emission
EGU General Assembly 2016, Vienna, Austria, 17-22 April 2016 (invited talk)

82. Magdalenic, J.; SIDC SWx Forecasters
Belgian Space Weather services by SIDC
The 4th AOSWA Workshop 2016, Jeju, South Korea, 24-27 October 2016

83. Magdalenic, J.; Marqué, C.; Fallows, R.; Mann, G.; Solar LOFAR KSP, core members
Fine structure of a type II radio burst observed by LOFAR
CESRA 2016, Orléans, France, 13-17 June 2016

84. Maggiolo, R.
Auroral arcs and ion outflows
EGU General Assembly 2016, Vienna, Austria, 17-22 April 2016 (invited)

85. Maggiolo, R.
Auroral arcs and ion outflows
EGU General Assembly 2016, Vienna, Austria, 17-22 April 2016 (poster)

86. Maggiolo, R., Echim, M.; Fear, R.; Fontaine, D.; Hosokawa, K.; Maes, L.
Polar cap arcs and ion outflow
AOGS (Asia Oceanic Geosciences Society) 13th Annual meeting, Beijing, China, 31 July - 5 August 2016 (invited talk)

87. Malisse, V.; Verbeeck, C.
Online demo of the STAFF viewer
ESWW13, Oostende, Belgium, 14-18 November 2016 (poster)

88. Mangold, A.; De Bock, V.; Van Malderen, R.; De Backer, H.; Gielen, C.; Hermans C.
Ozone, UV and aerosol optical depth derived from Brewer spectrophotometer observations at Princess Elisabeth Station, East Antarctica
15th Biennal WMO-GAW Brewer Users Group Meeting, Ponta Delgada, Sao Miguel, Azores, Portugal, 17-20 May 2016

89. Mangold, A.; Laffineur, Q.; Van Malderen, R.;, De Bock, V.; Hermans, C.; Nys, K.; De Backer, H.
Analysis of total ozone and UV radiation and of vertical profile measurements of temperature, humidity and wind data at Princess Elisabeth Station, East Antarctica
BNCGG - BNCAR symposium, Brussels, Belgium, 29 April 2016

90. Marqué, C.
When the Sun impacts air traffic radar operations
ESWW13, Working Meeting: "Which Radio observations and instrumentation for Space Weather?", Oostende, Belgium, 14-18 November 2016

91. Marqué, C.
Can solar radio bursts impact human activities?
Belgian Astronomy Day, Planetarium, Brussels, Belgium, 11 October 2016

92. Marqué, C.; Klein, K.-L.; Monstein, C.; Opgenoorth, H.; Buchert, S.; Pulkkinen, A.; Krucker, S.
The impact of the November 4th 2015 event on air traffic radars
CESRA 2016, Orléans, France, 13-17 June 2016

93. Marqué, C.; Magdalenić, J.; Martinez Picar, A.
Solar observations at the Humain Radio Astronomy Station in Belgium
CESRA 2016, Orléans, France, 13-17 June 2016 (poster)

94. Martinez Picar, A.; Marqué, C; Magdalenic, J.
SPADE: Small Phased Array Demonstrator for Solar Radio Astronomy Observations
CESRA 2016, Orléans, France, 13-17 June 2016 (poster)

95. Martinez Picar, A.; Marqué, C.; Verbeeck, C.; Calders, S.; Ranvier, S.; Gamby, E.; Anciaux, M.; Tetard, C.; Lamy, H.
Numerical simulation of BRAMS interferometer in Humain
International Meteor Conference, Egmond, The Netherlands, 2-5 June 2016 (poster)

96. Mierla, M.; Verdini, A.; Kilpua, E.; Rodriguez, L.; West, M.
Analysis of coronal mass ejections propagating in different solar wind conditions
ESWW13, Oostende, Belgium, 14-18 November 2016

97. Mierla, M.; Verdini, A.; Kilpua, E.; Rodriguez, L.; West, M.
Propagation of coronal mass ejections in different solar wind conditions
First VarSITI General Symposium and annual HELCATS meeting, Albena, Bulgaria, 6-10 June 2016

98. Mierla, M.; Zhukov, A.N.; Inhester, B. ; Koutchmy, S. ; Lamy, P. ; Llebaria, A.
On the calibration of polarised white light images
Proba-3 SWT5 meeting, Prague, Czech Republic, 28-30 November 2016

99. Mierla, M.
On the propagation of coronal mass ejections
CHARM meeting, University of Ghent, Ghent, Belgium, 3-4 October 2016

100. Mierla, M.; Zhukov, A.N.
Calibration of polarized white light images
PROBA-3 SWT4 meeting, Torino, Italy, 18-19 May 2016

101. Moestl, C.; Boakes, P.D.; Isavnin, A.; Kilpua, E.; Bothmer, V.; Davies, J.; Harrison, R.; Perry, C.; Rodriguez, L.; Eastwood, J.P.; Rouillard, A.; Lavraud, B.
Solar coronal mass ejections observed with the Heliophysics System Observatory
First VarSITI General Symposium and annual HELCATS meeting, Albena, Bulgaria,6-10 June 2016

102. Moschou, S.; Pierrard, V.; Keppens, R.; Pomoell, J.
MHD and kinetic aspects in solar wind modelling
43rd European Physical Society (EPS) Conference, Leuven, Belgium, 4-8 July 2016

103. Namaoui, H.; Kahlouche, S.; Belbachir, A.H.; Van Malderen, R.; Brenot, H.; Pottiaux, E.
First results of GPS water vapour and its comparison with radiosondes and ERA-Interim Reanalysis in Algeria
COST ES1206 GNSS4SWEC Summer School/Workshop, Potsdam, Germany, 29 August-2 September 2016

104. Pierrard, V.
Kinetic Aspects in Solar Wind Modelling
ICNS 15th annual international astrophysics conference, Cape Coral, USA, 3-9 April 2016 (invited)

105. Pierrard, V.
Kinetic Models for Space Plasmas: Recent Progress for the Solar Wind and the Earth's Magnetosphere
RGD30, Vancouver, Canada, 10-15 July 2016 (invited talk)

106. Pierrard, V.; Lazar, M.; Poedts, S.
Kinetic Features Observed in the Solar Wind Electron Distributions
AGU Fall Meeting, San Francisco, USA, 12-16 December 2016 (invited talk)

107. Pierrard, V.; Lopez Rosson, G.; Lemaire, J.
The big geomagnetic storm of 17 March 2015: measurements from the EPT/PROBA-V as well as their interpretation
2nd International Conference on Particle Physics and Astrosphysics, Moscow Russia, 10-13 October 2016 (invited talk)

108. Pierrard, V.; Moschou, S.; Lopez Rosson, G.; Borremans, K.
Kinetic models for space weather: from the solar wind to the inner magnetosphere
EGU General Assembly 2016, Vienna, Austria, 17-22 April 2016

109. Pierrard, V.; Moschou, S.; Lopez Rosson, G.; Borremans, K.
Kinetic models for space weather: from the solar wind to the inner magnetosphere
EGU General Assembly 2016, Vienna, Austria, 17-22 April 2016 (poster)

110. Pieroux, D.; Dekemper, E.; Demoulin, P.; Fussen, D.; Vanhellemont, F.; Ranvier, S.; Anciaux , M.; Bonnewijn, S.; Cardoen, P.; De Keyser, J.; Gamby, E.; and 14 others

PIC.A.S.S.O. : atmospheric remote sensing and in situ space science from CubeSats
The 4S Symposium, Valletta, Malta, 31 May-3 June 2016

111. Podladchikova, T.; Van der Linden, R.A.M.
Predictive potential of short-term variations of sunspot number second derivative
Conference "Plasma Phenomena in the Solar System", Space Research Institute, Moscow, Russia, 15-19 February 2016

112. Poedts, S.; and 21 others
Virtual Space Weather Modelling Centre
ESWW13, Oostende, Belgium, 14-18 November 2016 (poster)

113. Pottiaux E.; Bruyninx C.
GNSS-Meteorology and GNSS-Climate Activities at ROB: Contribution to National Projects, E-GVAP and COST Action ES1206 (GNSS4SWEC)
4th E-GVAP III Joint Expert Team meeting, Copenhagen, Denmark, 6-7 December 2016

114. Ranvier, S.; Anciaux, M.; Cardoen, P.; Gamby, E.; Bonnewijn, S.; De Keyser, J.; Pieroux, D.
Use of a Langmuir Probe Instrument on Board a Pico-Satellite
14th Spacecraft Charging Technology Conference, Noordwijk, The Netherlands, 4-8 April 2016

115. Ranvier, S.; Anciaux, M.; Cardoen, P.; Gamby, E.; Bonnewijn, S.; De Keyser, J.; Pieroux, D.
PICASSO-SLP: a Langmuir probe instrument for monitoring the upper ionosphere on board a pico-satellite
EGU General Assembly 2016, Vienna, Austria, 17-22 April 2016 (poster)

116. Ray, L. C.; Gunell, H.; Pokhotelov, D.; Fazakerley, A.N.; Forsyth, C.
Earth's Auroral Acceleration Region: Comparison of Cluster data and Vlasov model results
Chapman conference on currents in geospace and beyond, Dubrovnik, Croatia, 22-27 May 2016

117. Rex, M.; … ; Van Malderen, R.; and 31 others
Arctic ozone loss during the exceptionally cold winter 2015/16 as determined by Match and the ATLAS model
Quadrennial Ozone Symposium, Edinburgh, UK, 4-9 September 2016

118. Rodriguez, L.; Willems, S.; Pant, V.; Mierla, M.; Devos, A.; Housteaux, S.
Automatic detection of CMEs in STEREO-HI data for the FP7 HELCATs project
EGU General Assembly 2016, Vienna, Austria, 17-22 April 2016 (poster)

119. Rodriguez, L.; Masías-Meza, J.J.; Dasso, S.; Demoulin, P.; Zhukov, A.N.; Gulisano, A.M.; Mierla, M.; Kilpua, E.; West, M.; Lacatus, D.; Paraschiv, A.R.; Janvier, M.
Typical profiles and distributions of plasma and magnetic field parameters in magnetic clouds at 1 AU
ESWW13, Oostende, Belgium, 14-18 November 2016

120. Ryan, D.F.; Dominique, M.; Seaton, D.B.; Stegen, K.; White, A.
The Effects of Flare Definitions on the Statistics of Derived Flare Distributions
AAS/SPD 47, Boulder, Colorado, USA, 31 May-03 June 2016

121. Sapundjiev, D.; Stankov, S.M.; Jodogne, J.C.
Present status and modernisation of the Dourbes Cosmic Ray Observatory for improved space weather research and forecasting
ESWW13, Oostende, Belgium, 14-18 November 2016

122. Savage, S.; West, M.; Seaton, D.B.; Kobelski, A.
Observational Signatures of Magnetic Reconnection in the Extended Corona
AAS/SPD 47, Boulder, Colorado, USA, 31 May-03 June 2016

123. Seaton, D.B.; Darnel, J.; West, M.J.; Rachmeler, L.; D'Huys, E.
SWAP, SUVI, and a new view of the Solar Corona
Boulder Solar Day, Boulder, Colorado, USA, 14 March 2016

124. Seaton, D.B.; Darnel, J.; West, M.J.; D'Huys, E.; Rachmeler, L.
The Solar Ultraviolet Imager on GOES-R: Science and Space Weather
Solar Physics Division Meeting, Boulder, Colorado, USA, 2 June 2016

125. Shestov, S.; Zhukov, A.N.; Dolla, L.
Calibration of ASPIICS using stars
Proba-3 SWT5 meeting, Prague, Czech Republic, 28-30 November 2016

126. Shestov, S.; Zhukov, A.N.
Straylight and Vignetting: Comparing ASPIICS with other Coronagraphs
Proba-3 SWT5 meeting, Prague, Czech Republic, 28 November 2016

127. Shestov, S.; Nakariakov, V. M.; Reva, A.; Ulyanov, A.; Kuzin, S.
Nonlinear torsional Alfvén waves in magnetic flux tubes
IBUKS 2016, KU Leuven, Leuven, Belgium, 13-17 June 2016

128. Smit, H.G.J.; Oltmans, S.J.; Braathen, G.; Davies, J.; Deshler, T.; Johnson, B.; Kivi, R.; Van Malderen, R.; Schmidlin, F.; Steinbrecht, W.; Stübi, R.; Tarasick, D.; Thompson, A.M.; Witte, J.

Ozone Data Quality Assessment (O3S-DQA): Resolving inhomogenities in long term ozone sounding records and assessing their uncertainties
Quadrennial Ozone Symposium, Edinburgh, UK, 4-9 September 2016

129. Smit, H.G.J.; Oltmans, S.J. and O3S-DQA Panel
Ozone Data Quality Assessment (O3S-DQA) in a Historical Perspective: Resolving inhomogenities in long term ozone sounding records and assessing their uncertainties
UTLS Observation Workshop, Geneva, Switzerland, 24-27 May 2016

130. Söhne W.; Bruyninx C.; Colucci G.; Neumaier P.; Pacione R.; Pottiaux E.; Wiesensarter E.
EUREF Regional Broadcasters – Redundancy and Monitoring Concepts
IGS Workshop, Sydney, Australia, 8-12 February 2016

131. Stankov, S.M.; Verhulst, T.; Sapundjiev, D.; Nava, B.
Intercomparison of LIEDR and NeQuick ionospheric modeling using radio occultation and ionosonde measurements
International Beacon Satellite Symposium (BSS), Trieste, Italy, 27 June-1 July 2016

132. Stankov, S.M.; Verhulst, T.; Sapundjiev, D.
On the use of IGS TEC maps for ionospheric storm-time specification: scientific user requirements for modelling and service developments
IGS Workshop, Sydney, Australia, 8-12 February 2016

133. Stankov, S.M.; Verhulst, T.; Sapundjiev, D.
High-cadence nowcast of a proxy K-type index of the local magnetic activity for improved space weather monitoring applications
AGU Fall Meeting, San Francisco, USA, 12-16 December 2016

134. Tabibi S.; Van Dam T.; Francis O.; Bruyninx C.; Bergeot N.; Camelbeeck T.
Snow accumulation retrieval in East Antarctica using GNSS-MR
BNCGG - BNCAR symposium, Brussels, Belgium, 29 April 2016

135. Temmer, M.; Dissauer, K.; Thalmann, J.K.; Veronig, A.M.; Rodriguez, L.; Tschernitz, J.; Hinterreiter, J.
Relating CME characteristics from remote-sensing image data to in-situ measurements for Earth-affecting events
ESWW13, Oostende, Belgium, 14-18 November 2016

136. Tétard, C.; Lamy, H.; de Keyser, J.; Anciaux, M.; Calders, S.; Gamby, E.; Martinez Picar, A.; Ranvier, S.; Verbeeck, C.
METRO: reconstruction of the trajectories of meteoroids using the BRAMS interferometer
EGU General Assembly 2016, Vienna, Austria, 17-22 April 2016 (poster)

137. Thompson, B.; Allred, J.C; Kay, C.D.; Kraaikamp, E.; Krista, L.D.; Mason, J.P.; Mays, M.L.; Nieves-Chinchilla, T.; Reinard, A.A.; Verbeeck, C.; Webb, D.F.
Dimmings as a magnetic footprint of coronal mass ejections
ESWW13, Oostende, Belgium, 14-18 November 2016 (poster)

138. Usanova, M.; Mann, I.; Darrouzet, F.
EMIC waves in the Earth's inner magnetosphere
2016 URSI Asia-Pacific Radio Science Conference, Seoul, Korea, 21-25 August 2016

139. Van Malderen R.; Pottiaux E.; Brenot H.; Beirle S.; Wagner T.; De Backer H.; Bruyninx C.
Time variability of IWV datasets retrieved from IGS repro1, GOMESCIA satellite measurements and reanalyses
COST ES1206 - GNSS4SWEC: 4th Workshop, Reykjavik, Iceland, 08-10 March 2016

140. Van Malderen, R.; Allaart M.A.F.; De Backer, H.; Smit H.G.J.; De Muer, D.
On instrumental errors and related correction strategies of ozonesondes: possible effect on calculated ozone trends for the nearby sites Uccle and De Bilt
SPARC Workshop Stratospheric Change and its Role for Climate Prediction (SHARP), Berlin, German, 16-19 February 2016

141. Van Malderen, R.; Allaart, M.A.F.; De Backer, H.; Smit, H.G.J.; De Muer, D.
Testing the SI²N Ozonesonde Data Quality Assessment for the nearby stations Uccle (BE) and De Bilt (NL)
Quadrennial Ozone Symposium, Edinburgh, UK, 4-9 September 2016

142. Van Malderen, R.; Berckmans, J.; De Cruz, L.; De Troch, R.; Van Schaeybroeck, B.
Status and plans of using ground-based GNSS at RMI
4th E-GVAP III Joint Expert Team meeting, Copenhagen, Denmark, 6-7 December 2016

143. Van Malderen, R.; Pateraki, N.; De Backer, H.; Smit, H.G.J.; Thouret, V.
Comparison of tropospheric ozone profiles at Brussels, measured with MOZAIC aircraft and ozonesondes
Quadrennial Ozone Symposium, Edinburgh, UK, 4-9 September 2016

144. Verbanac, G.; Bandic, M.; Moldwin, M.; Pierrard, V.
MLT dependence in the relationship between plasmapause, solar wind and geomagnetic activity based on CRRES: 1990-1991
EGU General Assembly 2016, Vienna, Austria, 17-22 April 2016

145. Verbanac, G.; Bandic, M.; Moldwin, M.; Pierrard, V.
MLT dependence in the relationship between plasmapause, solar wind and geomagnetic activity based on CRRES: 1990-1991
EGU General Assembly 2016, Vienna, Austria, 17-22 April 2016 (poster)

146. Verbeeck, C.; Stegen, K.
EUI campaigns and the onboard science tables
18th EUI Consortium Meeting, CSL, Liège, Belgium, 23-25 November 2016

147. Verbeeck, C.; Berghmans, D.
Observing CMEs with Solar Orbiter (during remote sensing windows)
Remote Sensing Working Group meeting, ESAC, Madrid, Spain, 25 January 2016

148. Verbeeck, C.; Stegen, K.
From Mission Planning to Very Short Term Planning: till when can we still change campaign details?
17th EUI Consortium Meeting, Brussels, Belgium, 25-27 April 2016

149. Verbeeck, C.; Berghmans, D.
Observing CMEs with Solar Orbiter (during remote sensing windows)
8th Solar Orbiter Science Operations Working Group meeting, ESAC, Madrid, Spain, 26-28 January 2016 (invited talk)

150. Verhulst, T.; Sapundjiev, D.; Stankov, S.M.
High time resolution TEC and ionosonde observations at Dourbes, Belgium, during the March 2015 solar eclipse
International Beacon Satellite Symposium (BSS), Trieste, Italy, 27 June-1 July 2016

151. Voitenko, Y.; De Keyser, J.
Strong imbalanced turbulence of kinetic Alfvén waves
AOGS (Asia Oceanic Geosciences Society) 13th Annual meeting, Beijing, China, 31 July - 5 August 2016 (invited talk)

152. Voitenko, Y.
Coronal heating by turbulent cascades
IBUKS 2016, KU Leuven, Leuven, Belgium, 13-17 June 2016

153. Voitenko, Y.; De Keyser, J.; Pierrard, V.
Imbalanced Alfvénic turbulence at ion scales and particle energization in the solar wind
2nd THOR Workshop, Barcelona, Spain, 27-29 September 2016

154. Voitenko, Y.; De Keyser, J.; Pierrard, V.; Zhao, J.S.; Wu, D.J.
MHD-kinetic transition in imbalanced Alfvénic turbulence
7th ISRADYNAMICS Conference "Dynamical processes in space plasmas", Ein Bokek, Israel, 3-11 April 2016 (invited talk)

155. Voitenko, Y.; Melnik, V.; Pierrard, V.; Brazhenko, A.; Frantsuzenko, A.
Narrow-band Bursts of Solar Radio Emission at 15-30 MHz
2016 URSI Asia-Pacific Radio Science Conference, Seoul, Korea, 21-25 August 2016 (invited talk)

156. Voitenko, Y.; Melnik, V.; Pierrard, V.
Kinetic Alfvén model for narrow-band bursts of coronal radio emission at 2-3 solar radii
AOGS (Asia Oceanic Geosciences Society) 13th Annual meeting, Beijing, China, 31 July - 5 August 2016

157. Voitenko, Y.; Pierrard, V.
MLT dependence of the plasmapause from satellite observations and quasi-interchange instability mechanism
2016 URSI Asia-Pacific Radio Science Conference, Seoul, Korea, 21-25 August 2016 (invited talk)

158. Von der Gathen, P.; Rex, M.; Wohltmann, I. and the MATCH team
Arctic ozone loss during the exceptionally cold winter 2015/16 as determined by Match and the ATLAS model
POLSTRACC Science Workshop, Klingenmünster, Germany, 9-10 October 2016

159. Wauters, L.; Dominique, M.; Dammasch, I.E.
LYRA Mid-Term Periodicities
ESWW13, Oostende, Belgium, 14-18 November 2016 (poster)

160. Wauters, L.; Dominique, M.; Dammasch, I.E.
LYRA mid-term periodicities
ESWW13, Proba2 science Meeting, Oostende, Belgium, 14-18 November 2016

161. West, M.; Seaton, D.B.; Savage, S.; Bryans, P.
Post Flare Giant Arches and Run-Away Reconnection
AAS/SPD 47, Boulder, Colorado, USA, 31 May-03 June 2016

162. West, M.; D'Huys, E.; Bonte, K.; Dominique, M.; Mierla, M.; Vansintjan, R.; Seaton, D.
PROBA2: Science Mission and Space Weather Tool
ESWW13, Oostende, Belgium, 14-18 November 2016

163. West, M.
Coronal Fans workshop - EUV Observations
Coronal Fans Workshop, ESAC, Madrid, Spain, 29 November 2016 (invited talk)

164. West, M.
PROBA2 SWT Science Center status Report
ESWW13, Proba2 SWT Meeting, Oostende, Belgium, 14-18 November 2016 (invited talk)

165. West, M.
The SWAP EUV Imager Onboard PROBA2 6 Years of Observations
AOGS (Asia Oceanic Geosciences Society) 13th Annual meeting, Beijing, China, 31 July - 5 August 2016 (poster)

166. West, M.
PROBA2 SWT Guest Investigator Report
ESWW13, Proba2 SWT Meeting, Oostende, Belgium, 14-18 November 2016

167. West, M.
PROBA2 SWT Welcome
ESWW13, Proba2 SWT Meeting, Oostende, Belgium, 14-18 November 2016

168. West, M.; Seaton, D.; Savage, S.; Bryans, P.; Dennis, B.; Feng, L.; Lu, L.
SWAP observations of Post Flare Giant Arches & evidence of Run-Away Reconnection
AGU Fall Meeting, San Francisco, USA, 12-16 December 2016

169. West, M.; Seaton, D.; Savage, S.; Bryans, P.
Post Flare Giant Arches and Run-Away Reconnection
AOGS (Asia Oceanic Geosciences Society) 13th Annual meeting, Beijing, China, 31 July - 5 August 2016

Public Outreach: Talks and publications for the general public

1. Berghmans, D.; Clette, F.; Gissot, S.; Zhukov, A.N.
Operational Directorate 4 "Solar Physics and Space Weather"
Presentation during visit of the Auditing Committee reviewing the Scientific Activities of ROB, Brussels, 24 May 2016

2. Berghmans, D.
Space Weather Services Centers at RMI, ROB and BISA
Trilateral Annual Benelux Meeting of Meteorological Services, ROB, Brussels, 19 October 2016

3. Bourgoignie, B.; Lemaitre, O.; Vanlommel, P.
Regisseer je eigen zonnefilm
Wetenschapsweek, Planetarium, Brussels, 25 & 27 October 2016

4. Darrouzet, F.; De Keyser, J.
Installation d'une antenne magnétique à la station Princesse Elisabeth en Antarctique afin de détecter des ondes radios naturelles
Ciel et Terre, 132, 4, 106-111, July 2016

5. Darrouzet, F.; De Keyser, J.; De Keyser, P.
Installatie van een magnetische antenne op de Prinses Elisabethbasis in Antarctica om natuurlijke radiogolven te detecteren
Heelal, 66, 293-297, September 2016

6. Darrouzet F.; De Keyser, J.
Détection d'ondes radio naturelles à la station Princesse Elisabeth en Antarctique: Installation d'une antenne magnétique durant la campagne 2015-2016
Science Connection, 52, 8-10, November-December 2016

7. Darrouzet F.; De Keyser, J.
Waarneming van radiogolven van natuurlijke oorsprong op de Prinses Elisabeth basis in Antarctica : Installatie van een magnetische antenne tijdens de campagne 2015-2016
Science Connection, 52, 8-10, November-December 2016

8. D'Huys, E. and the PROBA2 team
PROBA2: Ontwikkeling, lancering en data
PROBA2@school sessions for high school students, Klein-Seminarie, Hoogstraten, 24 March 2016

9. D'Huys, E.
De Zon
PROBA2@School Lesson series at Ingenium school, Tervuren, 13 April 2016

10. D'Huys, E.
De Zon en het weer in de ruimte
PROBA2@School Lesson series at Ingenium school, Tervuren, 20 April 2016

11. D'Huys, E.
Ruimtevaart
PROBA2@School Lesson series at Ingenium school, Tervuren, 11 May 2016

12. D'Huys, E. and the PROBA2 team
PROBA2: Satellite, Instrument and Science
ESWW13 (stand), Oostende, Belgium, 14-18 November 2016

13. Fussen, D.; Dekemper, E.; Demoulin, P.; Pieroux, D.; Vanhellemont, F.; Ranvier, S.; Anciaux, M.; Bonnewijn, S.; Cardoen, P.; Gamby E.; De Keyser, J.
PICASSO: Etude de l'atmosphère et de l'ionosphère par un CubeSat
Science Connection, 52, 28-32, November-December 2016

14. Fussen, D.; Dekemper, E.; Demoulin, P.; Pieroux, D.; Vanhellemont, F.; Ranvier, S.; Anciaux, M.; Bonnewijn, S.; Cardoen, P.; Gamby E.; De Keyser, J.
PICASSO: Studie van de atmosfeer en de ionosfeer door een CubeSat
Science Connection, 52, 28-32, November-December 2016

15. Janssens, J.
Het voorspellen van zonnevlammen
PROBA2@school sessions for high school students, Klein-Seminarie, Hoogstraten, 24 March 2016

16. Janssens, J.
De Zon
MIRA Public Observatory, Grimbergen, 13 April 2016

17. Janssens, J.
Het Solar Indices Data analysis Center: De voorspelling van het Ruimteweer
VVS/WG Zon, Grimbergen, Brussels, 4 Juni 2016

18. Janssens, J.
Het nieuwe zonnevlekkengetal: Een kleine samenvatting van een grote verandering
VVS/WG Zon, Grimbergen, Brussels, 4 Juni 2016

19. Janssens, J.
Zonnekijkdag
"Interne Keuken", Radio 1 interview, Hove, 25 June 2016

20. Janssens, J.
Zonneactiviteit en ruimteweer tijdens zonnecyclus 24
VVS / De Sterrenjutters, Koksijde, 2 September 2016

21. Janssens, J.
An introduction to Space Weather
Trilateral Annual Benelux Meeting of Meteorological Services, ROB, Brussels, 19 October 2016

22. Lefever, K.
Evolutie van de atmosfeer in een veranderend klimaat
Science Connection, 50, 6-7, March-April 2016

23. Lefever, K.
L'évolution de l'atmosphère dans un climat qui change
Science Connection, 50, 6-7, March-April 2016

24. Lefèvre, L.
150 ans de tempêtes géomagnétiques
CCT ENV - Atelier "Evènements Solaires Extrêmes", CNES, Toulouse, France, 5 December 2016

25. Marqué, C.
When the Sun impact Air traffic radar operations
Trilateral Annual Benelux Meeting of Meteorological Services, ROB, Brussels, 19 October 2016

26. Marqué, C.
Le Soleil et la Radio astronomie solaire
Amateur organisation Jeunesse et Science, Modave, 19 November 2016

27. Muller, C.
Le Soleil et le climat
Science Connection, 50, 8, March-April 2016

28. Muller, C.
Zon en klimaat
Science Connection, 50, 8, March-April 2016

29. Pierrard V.
Les colères du Soleil
Académie Royale de Belgique, Ed. L'Académie en poche, 96 pp., ISBN 978-2-8031-0524-3, March 2016

30. Pierrard, V.
Les aurores boréales
Cercle d'Astronomes amateurs du Pays de Charleroi (CAAPC), Parentville, Charleroi, 15 April 2016

31. Vanlommel, P.; Janssens, J.
STCE Newsletter
Weekly newsletter, http://www.stce.be , 2016

32. Vanlommel, P.
Krachtige zonnestorm op komst! Solar orbiter en PROBA-3: nieuwe satellieten onderzoeken het geheim achter zonneuitbarstingen
Junior College sessions, KU Leuven Campus Kortijk and KU Leuven, 5 & 7 January 2016

33. Vanlommel, P.
Mini-ijstijd op komst?
Elcker-Ik, Antwerpen, 26 February 2016

34. Vanlommel, P.
Zonnewind en plasmawolken
PROBA2@school sessions for high school students, Klein-Seminarie, Hoogstraten, 24 March 2016

35. Vanlommel, P.
Raket naar de Zon
PROBA2@school sessions for high school students, Klein-Seminarie, Hoogstraten, 24 March 2016

36. Vanlommel, P.
Naar de zon kijken
HUJO vzw, VUB, Brussels, 4 July 2016

37. Vanlommel, P.
Zonnestorm op komst - nieuwe satellieten onderzoeken het onbekende
Volkssterrenwacht MIRA, Grimbergen, 10 December 2016

38. Verbeeck, C.
Zonnewaarnemingen vanuit de ruimte
Volkssterrenwacht Beisbroek, Brugge, 10 February 2016

List of abbreviations

2D	Two dimensional
3D	Three dimensional
4S	Small Satellites Systems and Services
A	Article
AAS	American Astronomical Society
ACE	Advanced Composition Explorer
AFFECTS	Advanced Forecast For Ensuring Communications Through Space
AGU	American Geophysical Union
AIA	Atmospheric Imaging Assembly (SDO)
AIP	American Institute of Physics
ALC	Automatic LIDAR Ceilometer
AMRVAC	Adaptive Mesh Refinement – Versatile Advection Code
AOGS	Asia Oceania Geosciences Society
AOSWA	Asia Oceania Space Weather Alliance
AR	Active Region
ARCAS	Augmented Resolution Callisto Spectrometer
ASGARD	An educational space programme for schools (no acronym)
ASPIICS	Association of Spacecraft for Polarimetric and Imaging Investigation of the Corona of the Sun (PROBA-3)
AU	Astronomical Unit; about 150 million km
AWDA	Automatic Whistler Detector and Analyzer
AWG	Astronomy Working Group
BE	Belgium
BeiDou	Chinese GNSS
BELARE	Belgian Antarctic Expeditions
BELSPO	Belgian Science Policy Office
BIRA	Belgisch Instituut voor Ruimte-Aëronomie
BISA	Belgian Institute for Space Aeronomy
BNCAR	Belgian National Committee on Antarctic Research
BNCGG	Belgian National Committee on Geodesy and Geophysics
BRAIN-be	Belgian Research Action through Interdisciplinary Networks (BELSPO)
BRAMS	Belgian RAdio Meteor Stations
BSS	(International) Beacon Satellite Symposium
B.USOC	Belgian User Support and Operation Centre
Bz	Component of the IMF perpendicular to the ecliptic ("north-south" component)
C-class flare	Common x-ray flare
Ca II H	A blue line in the solar spectrum at 396.85 nm
Ca II K	A blue line in the solar spectrum at 393.37 nm
CAAPC	Cercle d'Astronomes Amateurs du Pays de Charleroi
CACTus	Computer Aided CME Tracking software
CALLISTO	Compound Astronomical Low frequency Low cost Instrument for Spectroscopy and Transportable Observatory
CB	Central Bureau (EPN)
CCSOM	Constraining CMEs and Shocks by Observations and Modelling throughout the inner heliosphere
CCT	Communautés de Compétences Techniques (CNES)
CESRA	Community of European Solar Radio Astronomers
CH	Coronal Hole
CHARM	Contemporary physical challenges in Heliospheric and AstRophysical Models
Cluster	ESA/NASA mission to study the Earth's magnetosphere (no acronym)
CME	Coronal Mass Ejection
CNES	Centre national d'études spatiales (France)
COMESEP	COronal Mass Ejections and Solar Energetic Particles
COPUOS	COmmittee on the Peaceful Uses of Outer Space (UN)

COR (1/2)	Coronagraph (Inner/Outer) onboard STEREO
CORDEX	COordinated Regional Climate Downscaling Experiment
CORONAS	Complex ORbital Observations Near-Earth of Activity of the Sun (series of Russian satellites)
COSPAR	COmmittee on SPAce Research
COST	(European) COoperation in Science & Technology
CRRES	Combined Release and Radiation Effects Satellite
CSL	Centre Spatial de Liège
CubeSat	A small satellite measuring 10cm x 10cm x 10cm
D2D	Digisonde-to-Digisonde
DIARAD	DIfferential Absolute RADiometer
DN	Digital Number (pixel values not calibrated into physically meaningful units)
DOI	Digital Object Identifier
DSCOVR	Deep Space Climate Observatory
DSLP	Dual Segmented Langmuir Probe (PROBA2)
Dst	Disturbance Storm Time index (geomagnetic)
E	East
E-GVAP	EUMETNET EIG GNSS water VApour Programme
EC	European Commission
ECC	Electrochemical Concentration Cell
ECMWF	European Centre for Medium-range Weather Forecasts
Eds.	Editors
EESC	Equivalent Effective Stratospheric Chlorine
EGU	European Geosciences Union
EIG	Economic Interest Grouping
EISCAT	European Incoherent SCATter scientific association
EIT	Extreme ultraviolet Imaging Telescope (SOHO)
ELF	Extremely Low Frequency
EMIC	ElectroMagnetic Ion Cyclotron
ENLIL	Sumerian god of wind and storms (NOT an acronym)
ENV	Environnement atmosphérique et spatial (CNES)
ENVISAT	Environmental Satellite (ESA)
EPN	EUREF Permanent Network
EPOS-IP	European Plate Observing System – Implementation Phase
EPS	European Physical Society
EPT	Energetic Particle Telescope (PROBA-V)
ERA	ECMWF re-analysis
ES	Earth System (Science and Environmental Management (COST)
ESA	European Space Agency
ESAC	European Space Astronomy Centre
ESC	Expert Service Centre
ESERO	European Space Education Resource Office
ESOC	European Space Operations Centre
ESTEC	European Space Research and Technology Centre
ESWW	European Space Weather Week
ETH	Eidgenössische Technische Hochschule (Zürich)
ETRS	European Terrestrial Reference System
EU	European Union
EUHFORIA	European Heliospheric Forecasting Information Asset
EUI	Extreme-Ultraviolet Imager (Solar Orbiter)
EUMETNET	European Meteorological services Network
EUREF	EUropean Reference Frame
EUV	Extreme Ultraviolet
EUVI	Extreme Ultraviolet Imager (STEREO/SECCHI)
EVE	Extreme ultraviolet Variability Experiment (SDO)
$F_{10.7\ cm}$	Solar radio flux at 10.7 cm wavelength
F_2	Main ionospheric layer
FM	Frequency Modulation
foF2	Critical frequency F2-layer
FOV	Field-Of-View
FP7	Framework Programme 7 (EU)

Galileo	European GNSS
GAMIT	GPS Analysis at MIT
GAW	Global Atmosphere Watch
GeV	Giga electronvolt (10^9 . 1.6 . 10^{-19} Joule)
GFZ	Deutsches GeoForschungsZentrum (German Research Centre for Geosciences)
GHz	Gigahertz (10^9 Hz)
GLONASS	GLObal NAvigation Satellite System (Russia)
GNSS	Global Navigation Satellite System
GNSS4SWEC	Advanced GNSS tropospheric products for the monitoring of Severe Weather Events and Climate
GNSS-MR	GNSS multipath reflectometry
GOES	Geostationary Operational Environmental Satellite
GOME	Global Ozone Monitoring experiment (SCIAMACHY)
GOMESCIA	GOME/SCIAMACHY/GOME-2
GPS	Global Positioning System (USA)
GRAPE	GNSS Research and Application for Polar Environment
GRUAN	GCOS Reference Upper-Air Network
GSFC	Goddard Space Flight Center
H	Hydrogen
H-alpha (Hα)	A red visible spectral line at 656.28 nm created by Hydrogen
HELCATS	HELiospheric Cataloguing, Analysis and Techniques Service
HELIOS	HELmet streamers In the solar corona and their OScillations
HF	High Frequency
HI	Heliospheric Imager (STEREO)
h_mF_2	peak density height of F_2-layer
HMI	Heliospheric and Magnetic Imager (SDO)
HSRS	Humain Solar Radio Spectrograph
HUJO	HUmanistische JOngeren
HuRAS	Humain Radio Astronomy Station
Hz	Hertz (per second)
IAG	International Association of Geodesy
IAP	Interuniversity Attraction Pole
IAS(B)	Institut d'Aéronomie Spatiale de Belgique
IAU	International Astronomical Union
IBUKS	India, Belgium, UK, and Spain
ICME	Interplanetary CME
ICNS	International Conferencing and Networking Solutions
ICT	Information and Communication Technologies
IES	Imaging Electron Spectrometer (Cluster)
IGACO-O_3/UV	Integrated Global Atmospheric Chemistry Observation - O_3/UV
IGS	International GNSS Service
IMF	Interplanetary Magnetic Field
INSPIRE	Infrastructure for spatial information in Europe (EC)
IOC	International Ozone Commission
IPSL	Institut Pierre-Simon Laplace
IR	Infrared
IRI	International Reference Ionosphere
IRIS	Interface Region Imaging Spectrograph
IRM	Institut Royal Météorologique
ISBN	International Standard Book Number
ISROSES	International Symposium on Recent Observations and Simulations of the Sun-Earth System
ISS	International Space Station
ISSN	International Standard Serial Number
IT	Information Technology
IWV	Integrated Water Vapour
jHV	jHelioViewer
JSWSC	Journal of Space Weather and Space Climate
K	(1) Local K-index: A 3-hour geomagnetic index, ranging from 0 (quiet) to 9 (extremely severe storm) ; (2) degrees Kelvin

K*	Local 1-minute resolution K index
KAW	Kinetic Alfvén Waves
kHz	kilo Hertz (10^3 /second)
KMI	Koninklijk Meteorologisch Instituut
K_p	A geomagnetic index, ranging from 0 (quiet) to 9 (extremely severe storm)
KSB	Koninklijke Sterrenwacht van België
KSP	Key Science Project
KU	K unit (geomagnetic)
KUL	Katholieke Universiteit Leuven
kV	kiloVolt (10^3 Volt)
λ	wavelength
L	Letter (manuscript)
l/m^2	Liter per square meter
L	Letter (manuscript)
L*	Set of Earth's magnetic field lines which cross the Earth's magnetic equator at * earth radii from the centre of the Earth (e.g. L = 2)
L1	First Lagrangian point
LASCO	Large Angle Spectrometric Coronagraph (SOHO); small (C2) and wide (C3) field of view
LCS	Low-Coronal Signatures
LDE	Long Duration Event
LEO	Low Earth Orbit
LIDAR	LIght Detection And Radar
LIEDR	Local Ionospheric Electron Density profile Reconstruction
LMSAL	Lockheed Martin Solar and Astrophysics Laboratory
LOC	Local Organising Committee
LOFAR	Low-Frequency Array
LT	Local Time
LYRA	Large Yield Radiometer, formerly called Lyman Alpha Radiometer (PROBA2)
LWS	Living With a Star
μm	micrometer (10^{-6} meter)
M-class	Medium class satellite
M-class flare	Medium x-ray flare
MARSIS	Mars Advanced Radar for Subsurface and Ionosphere Sounding
MB	Megabyte
MC	Management Committee
METRO	MEteors TRajectories and Origins (BRAIN-be)
MeV	Mega electronvolt (10^6 . 1.6 . 10^{-19} Joule)
MHD	Magnetohydrodynamics
MHz	Megahertz (10^6/s)
MIT	Massachusetts Institute of Technology
MLT	Magnetic Local Time
MOZAIC	Measurement of OZone by Airbus In-service airCraft
MPI	Message Passing Interface
ms	millisecond (10^{-3} meter)
N	North
N-S	North-South
NASA	National Aeronautics and Space Administration
NASU	National Academy of Sciences of Ukraine
NDACC	Network for Detection of Atmospheric Composition Change
Ne	Neon
NeQuick	Electron density Quick claculation model (ionospheric model)
Net-TIDE	Pilot Network for Identification of Travelling Ionospheric Disturbances in Europe
NIR	Near IR
NL	The Netherlands
NM	Neutron Monitor
nm	nanometer (10^{-9} meter)
N_mF_2	peak density of F_2-layer
NOAA	National Oceanic and Atmospheric Administration
nT	nano-Tesla (10^{-9} Tesla)
O	Oxygen
O_3	Ozone
O3S-DQA	Ozonesonde Data Quality Assessment
OD	Onderdepartement
ODS	Ozone Depleting Substances
ORB	Observatoire Royal de Belgique
P2SC	PROBA2 Science Center
PARAFOG	Predictive Alert of RAdiation FOG
PFSS	Potential Field Source Surface

pfu	particle (proton) flux unit: the number of particles registered per second, per square cm, and per steradian
PhD	Doctor of Philosophy
PI	Principal Investigator
PICASSO	PICo-satellite for Atmospheric and Space Science Observations
PROBA	PRoject for OnBoard Autonomy
PRODEX	PROgramme for the Development of scientific Experiments
PSF	Point Spread Function
Q&A	Questions and Answers
R&D	Research and Development
R-ESC	Space Radiation ESC
RAPID	Research with Adaptive Particle Imaging Detector (Cluster)
RAS	Royal Astronomical Society
RDA	Range-Doppler Algorithm
RGD	Rarefied Gas Dynamics
RHESSI	Reuven Ramaty High Energy Solar Spectroscopic Imager
RMI(B)	Royal Meteorological Institute (of Belgium)
ROB	Royal Observatory of Belgium
RTIM	Real Time Ionosphere Monitoring
RWC	Regional Warning Center
S	South
SAP	Science Activity Plan
SC24	Solar Cycle 24
SCAR	Scientific Committee on Antarctic Research
SCIAMACHY	SCanning Imaging Absorption spectroMeter for Atmospheric CHartographY (ENVISAT)
SDO	Solar Dynamics Observatory
SECCHI	Sun Earth Connection Coronal and Heliospheric Investigation (STEREO)
SEP	Solar Energetic Particle
SEPEM	SEP Environment Modelling
SFU, sfu	Solar Flux Unit (10^{-22} W m^{-2} Hz^{-1})
SHARP	Stratospheric Change and its Role for Climate Prediction (SPARC)
SI^2N	SPARC, IOC, IGACO-O3/UV and NDACC
SIC	Seismoionospheric Coupling
SIDC	Solar Influences Data analysis Center
SILSO	Sunspot Index and Long-term Solar Observations
SIMBA	Sun-earth IMBAlance radiometer
SIRTA	Site Instrumental de Recherche par Télédétection Atmosphérique (IPSL)
SLP	Sweeping / Segmented / Single/ Split / Spherical Langmuir Probe
SN	Sunspot Number
SN	Space weather and Near-earth objects
SOC	Science Operations Centre
SOHO	SOlar & Heliospheric Observatory
SolO	Solar Orbiter
SOLVAM	SOLar VAriability Monitor
SORCE	Solar Radiation and Climate Experiment
SPARC	Stratosphere-troposphere Processes And their Role in Climate
SPD	Solar Physics Division (AAS)
SPENVIS (-NG)	SPace ENVironment Information System (- Next Generation)
SPM	SWIFF Plasmasphere Model
sr	steradian
S_R	Solar Regular
SREM	Standard Radiation Environment Monitor (Integral, Rosetta)
SSA	Space Situational Awareness
SSCC	SSA Space Weather Coordination Centre
SSEWG	Solar System Exploration Working Group
SSN	SunSpot Number
STAFF	Solar Timelines viewer for AFFECTS
STCE	Solar-Terrestrial Centre of Excellence
STCL	Space Technology & Calibration Laboratories
STEREO	Solar-TErrestrial RElations Observatory

SURFEX	Surface Externalisée (surface model developed by Météo France)
SUVI	Solar Ultraviolet Imager (GOES)
SWAP	Sun Watcher using APS detector and image Processing (PROBA2)
SWAVES	STEREO WAVES
SWE	Space Weather
SWIFF	Space Weather Integrated Forecasting Framework
SWPC	Space Weather Prediction Center (USA)
SWSC	Space Weather and Space Climate journal
SWT	Science Working Team
SWx	Space weather
TEC	Total Electron Content
THEMIS	Time History of Events and Macroscale Interactions during Substorms (NASA mission)
THOR	Turbulence Heating ObserveR
TID	Travelling Ionospheric Disturbance
TIM	Total Irradiance Monitor
TOPERS	Planets: Tracing the Transfer, Origin, Preservation, and Evolution of their ReservoirS
TOPROF	Towards Operational ground based PROFiling with ceilometers, doppler lidars and microwave radiometers for improving weather forecasts
TSI	Total Solar Irradiance
UCL	Université Catholique de Louvain
UHF	Ultra High Frequency
UK	United Kingdom
ULB	Université libre de Bruxelles
UNCOPUOS	United Nations Committee on the Peaceful Use of Outer Space
UNITER	Sciences de l'univers, de l'espace, de la terre et du climat
URAN	Ukrainian Radio Interferometer of NASU
URSI	International Union of Radio Science – Union Radio-Scientifique Internationale
US(A)	United States (of America)
USET	Uccle Solar Equatorial Table
UT(C)	(Coordinated) Universal Time
UTLS	Upper Troposphere-Lower Stratosphere
UTR	Ukrainian T-shaped Radio telescope
UV	Ultraviolet
UVIS	Ultraviolet and Visible
v	Velocity (speed)
V	Volt
VarSITI	Variability of the Sun and Its Terrestrial Impact
VERSIM	VLF/ELF Remote Sensing of Ionospheres and Magnetospheres
VHF	Very High Frequency
VIRGO	Variability of solar IRradiance and Gravity Oscillations
VKI	Von Karman Institute
VLF	Very Low Frequency
VSWMC	Virtual Space Weather Modelling Centre
VUB	Vrije Universiteit Brussel
VUV	Vacuum ultraviolet
VVS	Vereniging Voor Sterrenkunde
W	(1) Watt; (2) West
W/m^2	Watt per square meter
WAVES	Radio and plasma wave investigation (WIND, STEREO)
WDC	World Data Center
WG	Working Group
WMO	World Meteorological Organization
WP	Work Package
WRC	World Radiation Center
WS	Workshop
X-class flare	Extreme x-ray flare
XML	Extensible Markup Language
ZTD	Zenith tropospheric Total Delays